SIZE CHARACTERIZATION OF PARTICLES USING CAPILLARY ELECTROPHORESIS

by

Akram Khodabandehloo

M.Sc., Sharif University of Technology, 2010

B.Sc., Sharif University of Technology, 2008

A THESIS SUBMITTED IN PARTIAL FULLFILMET OF

THE REQUIREMENT FOR THE DEGREE OF

DOCTOR OF PHILOSOPHY

in

THE FACULTY OF GRADUATE AND POSTDOCTORAL STUDIES

(Chemistry)

THE UNIVERSITY OF BRITISH COLUMBIA

(Vancouver)

April 2018

Abstract

Taylor dispersion analysis (TDA) can be used for characterizing size of particles over a wide range. This method is performed on a capillary column and its simplicity and reproducibility offer many advantages over other more commonly used techniques for sizing. In the first part of the thesis, different sizing techniques are reviewed and their advantages and disadvantages are discussed.

In the second part of this thesis, numerical modeling is used to optimize the operating conditions for performing TDA. In addition, the validity of TDA conditions is verified and the optimum conditions for performing TDA are discussed. Also, the effect of electric field on the validity of TDA and its application for a mixture of molecules with different sizes is studied. It is concluded that care must be taken to choose parameters in a way that lead to optimal TDA results. For the mixtures, using electric field is advantageous, because it not only leads to separation of molecules but also gives information on the charge of the molecules.

In addition to numerical modeling, the equations for TDA to be used in the presence of electrophoretic mobility are modified and compared to the diffusion coefficients obtained using classical TDA. In this part of thesis, in addition to pressure, voltage is also applied to separate the components of mixtures and characterize the size of individual species. The results indicate that using the modified equations make the resulting values more consistent with the ones obtained from classical TDA. Our method can be used for mixtures, and in this thesis, a preliminary attempt has been made to characterize the size and charge of a mixture of proteins and peptides and amino acids.

The final part of this thesis discusses the dispersion of proteins and small peptides during electrokinetic migration. Like conventional Taylor dispersion, peak broadening is more

pronounced for particles with smaller diffusion coefficients. The theoretical description of band broadening caused by electroosmotic flow dispersion (EOFD) and the experimental verification of this phenomenon are presented.

Lay summary

This thesis mainly focuses on the development of sizing techniques for a mixture of proteins and peptides. The authors of this thesis have modified the equation, which is used for the estimation of the size of a wide range of molecules. The derived equation, which is verified by experiment and simulation, extends the application of capillary electrophoresis as a sizing technique. The last part of this thesis is devoted to explaining a phenomenon observed for large molecules in the presence of an electric field in capillary tubes.

Preface

This dissertation is ultimately based on the experimental and simulated data for the Taylor dispersion analysis experiment on capillary electrophoresis as implemented in Dr. Chen's research laboratory at The University of British Columbia. The majority of experiments, data analysis, interpretation and writings were done by the author of this thesis. Chapters 2 and 6 were published previously, and they are included in this thesis document with little revision.

Contributions from other researchers

Chapter 2: The statistical data for figure 2.1 were collected by Matthew. S. McLennan. All other material presented, including all measured data and analyses, were carried out entirely by the author of this thesis. Dr. D.Y. Chen directed the work and co-authored the journal articles cited below.

Publications arising from works presented in this dissertation

- Akram Khodabandehloo and David D.Y. Chen. Sizing techniques for proteins and their aggregates. *Bioanalysis* (2017) 89 (15), 7823-7827.

  Material from this article is included in Chapter 2.
- Akram Khodabandehloo and David D.Y Chen. Electroosmotic Flow Dispersion of Large Molecules in Electrokinetic Migration. Analytical Chemistry (2017) 89(15), 78233-7827.

  Material from this article is included in Chapter6.

Table of contents

List of tables

List of figures

List of abbreviations

BGE	Background electrolyte
CE	Capillary electrophoresis
DLS	Dynamic light scattering
EM	Electron microscopy
EOF	Electroosmotic flow
EOFD	Electroosmotic flow dispersion
HPC	Hydroxypropyl cellulose
ID	Internal diameter
MW	Molecular weight
OD	Outer diameter
PEI	Poly ethylene imine
SEC	Size exclusion chromatography
SEM	Scanning electron microscopy
TDA	Taylor dispersion analysis
UV	Ultra violet

Acknowledgements

I would like to express my heartfelt gratitude to my supervisor Dr. David Chen whose expertise, understanding, and patience, added considerably to my graduate experience. David, I am deeply grateful for your thoughtful, wise, and patient guidance during every step in my PhD studies, and giving me every opportunity to grow both professionally and individually. This thesis certainly would not have been possible without your guidance and encouragement. I also would like to thank the other members of my committee for the assistance they provided throughout my PhD.

I have been fortunate to work alongside many exceptional people during my research. Thank you to all of my group mates, past and present, who have shared their ideas and provided a friendly and supportive community in the lab: Cheng, Caitlyn, Matthew, Jess, Lingyu, Kevin, Jianhui Roxana, Sherry, Wenqiang, Zi-Ao. I am also very thankful for my two very special friends, Alexis and Laiel. You made Vancouver a home and UBC a very enjoyable place for me. I would particularly like to acknowledge Jess Risley and Caitlyn Grypma De Jong, for reading my thesis and giving me valuable feedbacks.

Benu and Marianne, getting to know you has proved me that friendship is not about who you've known the longest. It's about who walked into your life, said I'm here for you and proved it. This thesis wouldn't be finished if it was not for your continual support and feedbacks. I can't tell you how grateful I am for having you as my friends now.

I am so grateful to have my lovely husband, Hossein, with me in Vancouver through my study. We came to Vancouver with the dream of pursuing higher education and we have become stronger together.

Finally, I want to thank my family for their endless help, support and encouragement. Thank you for believing in me and encouraging me to follow my own path, even though this path has put us apart. Your endless love and support gives me power to forge ahead and tackle all the difficulties on my way. I feel truly blessed to have such wonderful family. Mom and dad, thank you for your

unconditional love and support have been the strongest things helping me through this process. The pages that follow are filled with my gratitude for having such wonderful parents. Thank you.

To My Parents

Chapter 1: Introduction to capillary electrophoresis and Taylor dispersion analysis for the characterization of proteins and protein aggregates

1.1 Capillary electrophoresis

Capillary electrophoresis (CE) is a separation technique which is based on the differential movement of charged species in an electric field. The principle was introduced by Arnie Tiselius in 1937. He placed the protein mixture in a tube between two buffer solutions and applied an electric field. He found that the proteins migrate in a direction and rate dependent on their charge and mobility. He used electrophoresis to separate human serum into albumin, α-globulin, β-globulin, and γ-globulin. [1] Tiselius was awarded a Nobel prize for his pioneering work in separation science in 1948.

Electrophoresis in free solution, as performed by Tiselius, did not get a lot of attention, due to its low separation efficiency caused by thermal diffusion and convection. Hence, anti-convective media, such as polyacrylamide or agarose gels, were used to eliminate convective transport and thermal diffusion. Gels in the slab or tube format have been used for the separation of biological macromolecules, such as nucleic acids and proteins. However, gel electrophoresis generally suffers from long analysis times, low efficiencies, and difficulty in detection and automation. [2 3]

Since narrow capillaries have a low conductance, only small amounts of heat are generated in narrow capillaries. Therefore, the electrophoretic separation in narrow-bore open tubes or

capillaries is an alternative approach to avoid the thermal diffusion and convection. The principle of capillary electrophoresis was investigated in 1967 by Hjerten and coworkers who for the first time performed zone electrophoresis in linear tubes with a diameter of 1-3 mm. [4] The use of narrow bore capillaries for CE has some advantages over the two-dimensional gel electrophoresis in terms of sensitivity, specificity, and separation speed. Further progress in capillary zone electrophoresis was made by Virtanen, and then Mikkers and Everaerts, who performed electrophoresis in capillaries made from glass and Teflon with an inner diameter of 200 μm. [5]

In 1981, Jorgenson and Lukacs demonstrated the use of open tubular capillaries with an inner diameter of 75 μm as separation column. Jorgenson also clarified the theory and demonstrated the potential of capillary electrophoresis as an analytical technique. [6]

Jorgenson's work brought special attention to the use of this technique, especially after the instrument was made commercially available. In the last few decades, CE has progressed from the research lab into practical applications in many fields such as (bio)pharmaceutical, forensics clinical, food, and environmental chemical and biochemical analysis.

Owing to its high separation efficiency, short analysis time, and minimum sample and buffer consumption, CE has entered the research and industry community.

1.1.1 Instrumentation

The basic instrumental configuration for CE is relatively simple. Figure 1.1 shows a schematic set-up for a generic CE instrument. It consists of a narrow bore capillary tube immersed into two buffer vials. The capillary is usually made of fused silica and the outer surface is coated with polyimide and the inner diameter is usually 25-75 μm. Near the end of the capillary, a small portion of the

polyimide is typically removed to create a transparent light path for optical detection which is called the detection window. The buffer vials also contain the two chemically inert electrodes (e.g. platinum) used to make electrical contact between a high power supply and the capillary. [7]

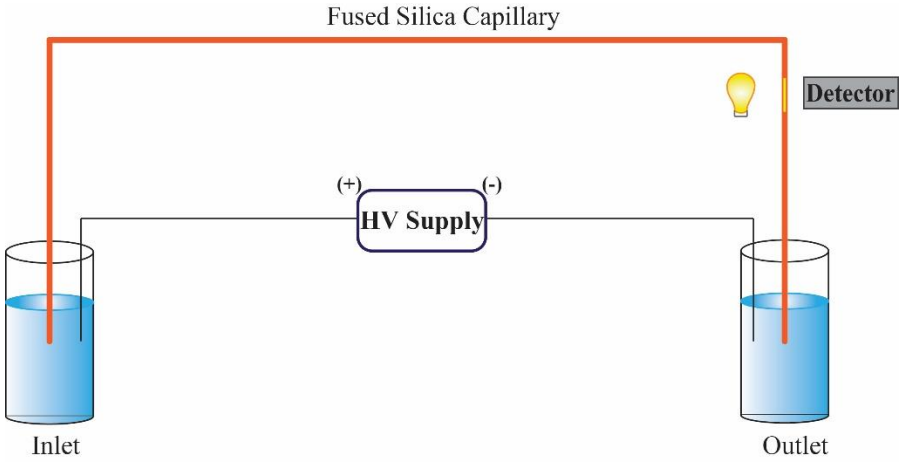

Figure 1.1 Schematic diagram of a capillary electrophoresis instrument with online optical detection.

CE analysis is conducted in several general steps. First, the capillary column is pre-equilibrated by rinsing it with background electrolyte (BGE) prior to sample injection. Then, the sample is introduced either hydrodynamically or electrokinetically by inserting the end of the capillary into the sample solution. The sample plug usually occupies less than 3% of the total capillary column. A very high electric field, often higher than 500 V/cm, is then applied to drive the species towards the CE outlet. The analytes, separated based on their different mobilities in the BGE, pass by the detection window, causing optical absorbance changes at different times. The changes can then be converted into digital signals and recorded by a computer. [8]

1.1.2 Separation principles

In CE, analytes are separated based on their electrophoretic mobility, which is a characteristic of the ion of interest, and it is determined by the charge to size ratio of the analyte. [7] The normal polarity is usually from the anode (inlet) to the cathode (outlet and detector). When high voltage (strong electric field) is applied across the separation capillary, the charged species in the solution accelerate under the electrostatic forces (F_E). Moving in the solution, the charged species also experience drag forces (F_D). These two forces oppose each other so that the ion travels at a constant electrophoretic velocity. The electrophoretic velocity is determined by the ion's net charge, q, the electric field (quotient of the applied voltage and capillary length) in the capillary, E, the hydrated ion radius, R, and the viscosity of the solution, η, as seen in Eq (1-4). Additionally, v is ion velocity, and μ_{ep} is the electrophoretic mobility of the ion.

$$\vec{F}_E = q\vec{E} \qquad (1\text{-}1)$$

$$\vec{F}_D = 6\pi\eta R v \qquad (1\text{-}2)$$

$$q\vec{E} = 6\pi\eta R v \qquad (1\text{-}3)$$

$$v_{ep} = \frac{q\vec{E}}{6\pi\eta R} \qquad (1\text{-}4)$$

.

To describe the electro-migration behavior of ions independent of electric field, the electrophoretic mobility is defined below: [9]

$$\mu_{ep} = \frac{v_{ep}}{\vec{E}} = \frac{q}{6\pi\eta R} \qquad (1\text{-}5)$$

Figure 1.2 shows how molecules with different charges and sizes are separated in CE. It also shows that the negative ions move toward the anode (inlet) and the positive ions move toward the cathode (outlet). It is evident from Eq (1-5) that the neutral species don't move under electric field. Therefore, not all of the species would pass through the detection window. However, under appropriate conditions, all analytes can be detected, indicating that there is another bulk flow that drives the analytes in the separation capillary from the anode to the cathode, which is called electroosmotic flow (EOF). [10]

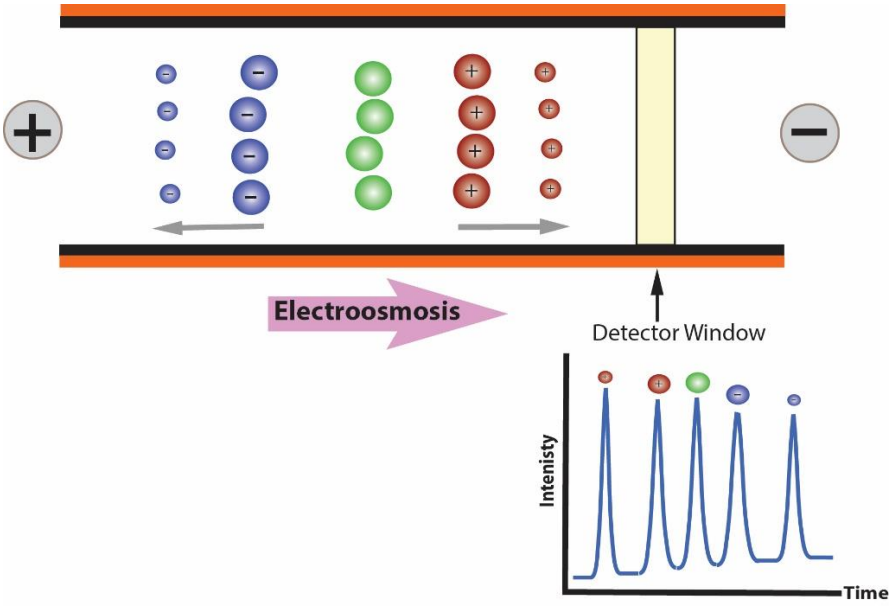

Figure 1.2 Schematic CE separation of molecules with different mobilities: positive species move toward cathode, negative species move toward the anode, and neutral species do not move under electric filed; Electroosmotic bulk flow moves all the species toward the cathode.

1.1.3 Electroosmotic flow: a mode of transport

Electroosmotic flow (EOF) is the bulk flow of solution in the capillary column and exists because of the surface charge on the interior of the capillary wall. EOF assists in transporting the analytes toward the detection window. It is generated when the applied electric field interacts with the ions in the diffuse layer of an electrical double layer. [11] For example, for a bare fused silica capillary, when flushed with a BGE (pH>3), the silanol groups deprotonate and the capillary wall surface is negatively charged. The negatively charged silanol groups on the inner wall attract cationic species from the buffer, and due to strong electrostatic forces between counter ions, the cations form a fixed electrical charged layer (Stern layer). Also, a layer of mobile ions (diffuse layer) is formed because the positively-charged counter ions in the Stern layer are not enough to neutralize all the negative charges on the capillary surface. The Stern layer and diffuse layer form the electrical double layer. The overall charge of the diffuse layer is positive since there is an excess of positive ions. When a voltage is applied, cations in the diffuse layer migrate in the direction of the cathode, carrying hydrating water molecules with them. The hydrogen bonding between the hydrating water molecules and the bulk solution water molecules cause bulk flow towards the cathode. Therefore, EOF is formed with a flat flow profile, which is a unique feature of CE in comparison to High performance liquid chromatography (HPLC). Figure 1.3 depicts the electrical double layer and as illustrated in this figure, the electrical potential decreases linearly with the Stern layer and exponentially within the diffuse later until it approaches zero in the bulk solution. The potential at the interface of the Stern layer and the diffuse layer is called the zeta potential (ζ), and it plays an important role in the determination of EOF. [12]

The magnitude of electroosmotic mobility is determined by Eq (1- 6), where ε is the dielectric constant of the fluid, η is the viscosity of the fluid, and ζ is the zeta potential. [13]

$$\vec{\mu}_{eo} = \frac{\vec{v}_{eo}}{\vec{E}} = \frac{\varepsilon\zeta}{4\pi\eta} \qquad (1-6)$$

The zeta potential is determined by the surface charge on the capillary wall. Since this charge is strongly pH dependent, the magnitude of the EOF varies with pH. At high pH, where the silanol groups are deprotonated, the EOF is significantly greater than at low pH where the silanol groups become protonated.

The apparent mobility of an analyte is the sum of the electroosmotic mobility and the electrophoretic mobility (Eq 1-7). Analytes with different apparent mobilities are separated in CZE as shown in Figure 1.2 EOF makes the analysis of cations, anions, and neutral species possible in one single analysis.

$$\vec{\mu}_{app} = \vec{\mu}_{ep} + \vec{\mu}_{eof} \qquad (1-7)$$

EOF can be controlled by altering the capillary surface charge or buffer viscosity, concentration, and pH. The rate of EOF can be changed by decreasing or increasing the electric field. [14]

EOF can also be controlled by coating the capillary wall. Coatings can increase, decrease, or reverse the surface charge of the inner wall, and therefore affect the EOF.

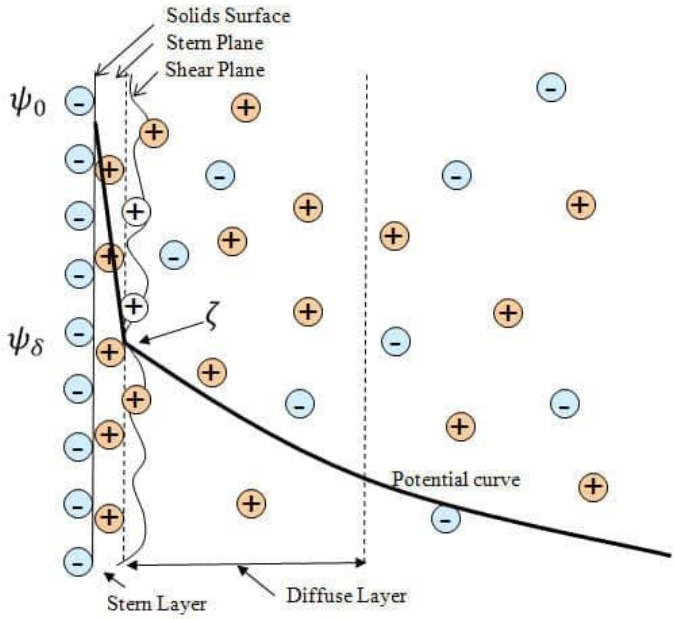

Figure 1.3 Structure of the electrical double layer and resulting EOF due to the deprotonation of the bare-fused silica capillary wall, and potential profile with increasing distance from the wall.

1.1.4 Capillary coating

Bare-fused silica capillaries are commonly used for separating species in CE. The pK_a of the silanol groups on the inner capillary wall is approximately 3.5, and at a pH above 4, the inner surface of the capillary is negatively charged. [15] Due to the charged inner surface of the capillary, charged analyte-capillary wall interactions are unavoidable which may result in a change of EOF and migration time of analytes. [16]

Interactions between analytes and the capillary wall can be partly reduced by using buffers with extreme pH and high ionic strength; however, these conditions may affect the stability of analytes such as proteins. To resolve this issue, coating the inner wall of the capillary is an effective approach, which also facilitates the modification of magnitude and direction of EOF to obtain better separation performance. When choosing the coating for CE, one should consider the coating

stability over time, compatibility with different BGEs and sample matrix components, and the facility of introduction of the coating materials into the capillary column. [17-19]

Capillary wall coatings are either static or dynamic, depending on how the coating is attached to the capillary wall surface. In static coatings, the coating materials are bonded covalently to the capillary wall and they permanently modify the inner wall of the capillary. [20-21] In dynamic coating, there is an adsorptive secondary interaction between the wall and coating material; the dynamic coatings are added to the BGE to minimize analyte adsorption to the capillary wall by competing with the analytes for the silanol binding sites.[19] Hybrid coatings are a combination of dynamic and static coatings, in which one layer is bonded covalently to the capillary wall and the other layer is adsorbed on top of that the first layer.

Static coatings fall into two categories: static-adsorbed (physical adsorption) or static-covalent (chemical reaction) and can be either positive or neutral. Static-adsorbed coatings are preferred over the static-covalent coatings because: (1) the coating procedure is simple, (2) the coating regeneration is straightforward and is performed by using strong acidic or basic solutions, (3) the coating is strongly adsorbed to the wall and is stable, and (4) the coatings are commercially accessible and small volumes of coating material are required. [22-23]

The coatings used in this thesis are both static coatings: a positively-charged coating, Polyethyleneimine (PEI), and a neutral coating, hydroxypropyl cellulose (HPC). The procedure for PEI coating is based on US patent 6923895 B2 in which cationogenic amine groups interact with the negatively-charged silanol groups of the capillary wall through electrostatic interactions. [24] Since this coating forms a cationic layer on the capillary wall, the EOF direction is reversed and therefore the polarity is also reversed to guide the bulk flow toward the detection window.

Neutral coatings are generally covalent and suppress the EOF. In this thesis, HPC-coated capillaries are prepared using the method offered by Shen and Smith. [25] Briefly, HPC is introduced into the capillary via positive pressure, and then heating the capillary results in permanent binding of HPC to the capillary inner wall. This coating is very stable over a wide pH range because hydrogen bonding interactions fix the neutral coating to the capillary wall. Since the inner wall of capillary is neutral, the EOF is negligible and does not play a role in the migration of analytes.

1.2 Taylor dispersion analysis

Taylor dispersion analysis (TDA) dates back to 1953, when Geoffrey Ingram Taylor observed that the axial dispersion of solute occurs when the radial diffusion of the molecules is combined with convection due to the inhomogeneous cross-sectional velocity of the fluid. [26] He used semi-analytical arguments to show the Fickian nature of the mean axial dispersion of a solute undergoing convection by Poiseuille flow and radial diffusion simultaneously in a circular cylindrical tube. [27] He showed that in the long-time limit, the mean axial dispersion obeys a simple one dimensional, convective-diffusive equation. Taylor found that dispersion is caused by the interaction of two independent solute transport mechanisms (inhomogeneous radial velocity field and the diffusion of solute molecules). He also found that this axial dispersion is inversely proportional to the molecule diffusion coefficient which has been repeatedly observed in experiments. [28] This phenomenon was firmly established by Aris in 1956. Aris further generalized Taylor's analysis to include the effects of axial molecular diffusion upon the dispersion process. [29] In the last decade, TDA has been used as an absolute and fast method for the determination of diffusion coefficients and therefore hydrodynamic radii of molecules.

1.2.1 Principles of TDA

When Poiseuille flow is established in a tube, a parabolic velocity profile exists over any cross-section normal to the tube axis so that the fluid at the center of the tube moves at twice the average fluid velocity. [30] Then, a pulse of solute is introduced into the steady flow within a long circular cylindrical capillary, and the solute concentration is recorded at the detection window. As depicted in Fig 1.4, when the sample plug is injected into the solution in the capillary column, radial inhomogeneity occurs initially, in which the sample plug takes a parabolic shape due to the parabolic velocity profile of the hydrodynamic flow. Caused by radial diffusion, molecules move from lower-speed streams in the back of the parabolic sample plug to the higher-speed edges while the reverse occurs at the front of the plug. In short, the molecule's diffusion in radial cross section speeds up the particles at the back of sample plug and slows down particles at front, which results in a compact and homogeneous plug. After a sufficient amount of time, an elongated homogeneous plug would travel along the tube with the mean speed of flow. Because of the combination of convection and radial diffusion, a symmetric distribution of molecules in the sample plug is achieved which follows a normal distribution.

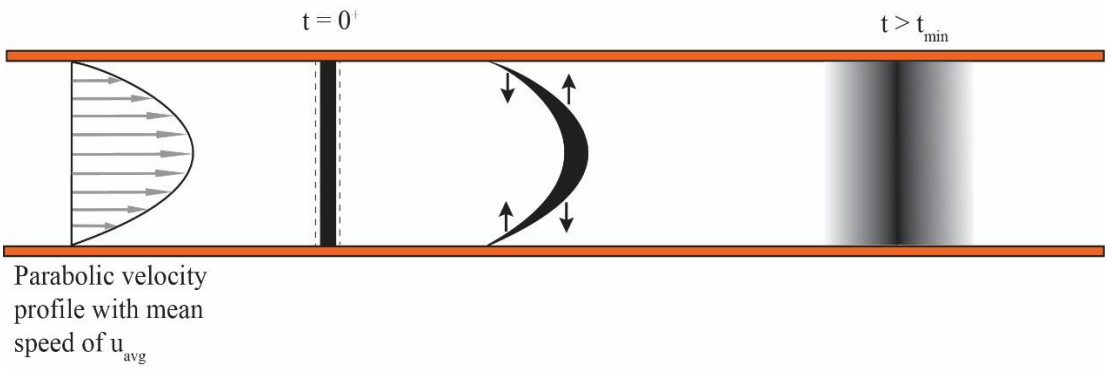

Figure 1.4 Qualitative illustration of Taylor dispersion phenomenon: (1) a small plug of solute is injected and transported through the column, (2) the parabolic velocity profile of the fluid produces a concentration gradient between the center of the capillary and the wall, which causes the solute to diffuse in radial direction, (3) after a certain time, the plug is dispersed uniformly in axial direction.

Taylor derived the equation which describes the axial dispersion of particles as a result of the combined effect of convection and radial diffusion:

$$D^* = D + \frac{R_c^2 \bar{u}^2}{48D} \qquad (1-8)$$

where D is the molecular diffusion coefficient, R_c is the tube radius, and $\bar{u}$ is the average velocity of the flow. Derivation of this equation is shown in chapter 4.

Often, the first term in Eq (1-8) is negligible compared to the second term, so it can be simplified and rearranged to derive the diffusion coefficient. [26, 31]

$$D = \frac{R_c^2 \bar{u}^2}{48D^*} \qquad (1-9)$$

Using the Einstein equation, the diffusion coefficient is related to experimental values such as peak variance and migration time.

$$\sigma_L{}^2 = 2D^* t \qquad (1-10)$$

$$\sigma_L^2 = \sigma_t^2 \times \bar{u}^2 \qquad (1-11)$$

$$D = \frac{R_c^2 t}{24\sigma_t^2} \qquad (1-12)$$

Eq (1-12) is usually used to determine diffusion coefficient of particles experimentally. Finally, the hydrodynamic radius (R_h) is inversely related to the diffusion coefficient via the Einstein-Stokes equation: [32]

$$R_h = \frac{k_B T}{6\pi\eta D} \qquad (1-13)$$

where k_B is the Boltzmann constant, T is the temperature and η is the viscosity of the solvent.

1.2.2 Conditions of TDA

For Eq (1-9) to be valid, two conditions must be met. [31, 33] The first condition requires the migration time to be much greater than the time needed for the particles to diffuse radially across the capillary. As will be discussed in chapter 3, the time, for the particles to diffuse radially, varies with different diameters of capillary column and diffusion coefficient of the particles; therefore, it can be also expressed in terms of a dimensionless residence time, which is the mean analyte residence time to the time required for an analyte to diffuse to a distance equal to the radius of the capillary.

$$\tau = \frac{Dt}{R_c^2} \gg \frac{3}{80\varepsilon} \qquad (1-14)$$

We mentioned that Eq (1-8) can be simplified to Eq (1-9) when the first term is negligible. This assumption is only valid if the axial diffusion of the solute is negligible when compared to its dispersion. This can be expressed with Peclet number (Pe) which is also a dimensionless parameter (Eq 1-15). [34]

$$Pe = \frac{uR_c}{D} \gg \sqrt{\frac{48}{\varepsilon}} \qquad (1-15)$$

Fig 1.4 shows that at the beginning of the injection, there is a small amount of diffusion happening axially (shown with dotted lines). Then, after enough time, the dispersion occurs axially, which is more significant than axial diffusion.

Both the residence time and Peclet number must be greater than a certain value for Eq (1-12) to be valid. The minimum value depends on the relative error (ε) on the determination of D that can be tolerated.

1.2.3 Instrumentation

Taylor set-up

The first set-up for TDA was designed by Taylor to test the proposed equations. Taylor devised the set-up shown in Figure 1.5 and measured the dispersion of permanganate molecules in a long narrow tube. He examined this system with and without the effect of longitudinal diffusion, and with convection only, and with a combination of convection and radial diffusion (Taylor regime). [26] This set-up was not used for decades until the emergence of capillary electrophoresis which offers several advantages for performing TDA.

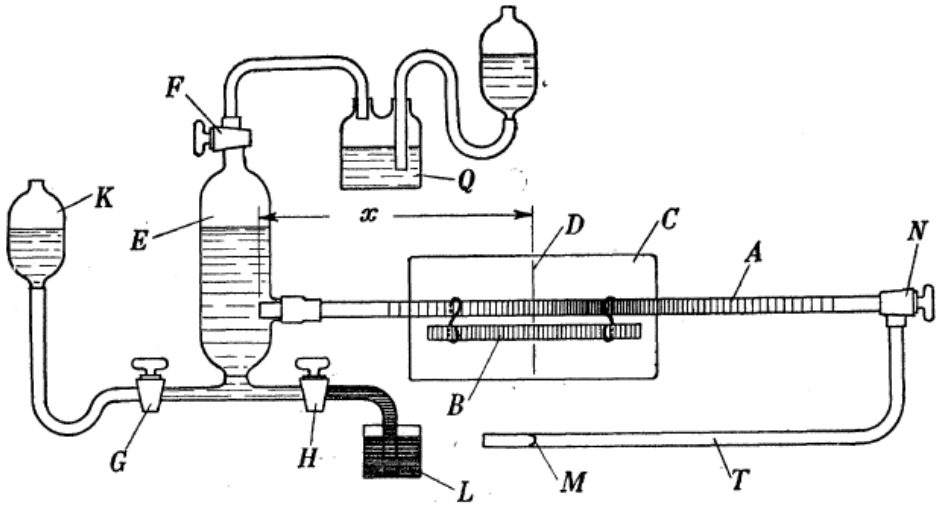

Figure 1.5 Taylor apparatus set up designed by Geoffrey Taylor to study the convection and diffusion of molecules in fluids

In this apparatus, Tube A is filled with a solution of permanganate. Tube B is filled with a different known concentration of permanganate and is used as a reference to determine the concentration of different parts of tube A. Chamber E is filled with a 1% solution of $KMnO_4$ and a pressure is then applied to the liquid in chamber E.

First, Taylor tested if the molecular diffusion in the longitudinal direction is small enough to be negligible. After applying pressure to liquid E, he opened valve N slightly and started a stop watch. When the front of the colored column approached the exit end of the pipe, he closed the needle valve. It was found that, as expected, the molecular diffusion in the longitudinal direction was so small that no appreciable change in color at a fixed spot occurred in several hours after the closing of N.

To calculate the diffusion coefficient of $KMnO_4$, the valve N was opened to allow the solution to flow and the duration of the flow was long compared with $a^2/3.8^2D$ with "a" being the radius of the tube. Then Taylor used the equation derived for the Taylor regime and calculated the diffusion coefficient of permanganate to be 0.8×10^{-5} c.g.c unit. [26]

Capillary electrophoresis

One of the requirements of performing TDA is long narrow tube as well as having a detection and a pumping system. Capillary electrophoresis offers these requirements in addition to its ability to be automated. Therefore, CE is a good candidate and is most often used for TDA experiments. The cartridges in CE can be modified to be used for two detection window TDA, which offers some advantages over the one detection system, such as eliminating the effect of other sources of dispersion. TDA adds another dimension to the application of capillary electrophoresis by enabling it to be used as a size characterization technique.

Malvern instrument

The Malvern Viscosizer system is the commercialized version of TDA which can rapidly determine the hydrodynamic radius of a molecule. It enables the mass-weighted sizing of a mixture of small molecule- and protein-based systems in biological samples using TDA with UV-selective detection. This apparatus is capable of determining size in the range of 0.2-50 nm. A UV light imaging array is used to measure the absorbance of an injected sample as a function of time, as it is driven by pressure through a narrow bore fused-silica capillary with two detection windows. For size measurements, the capillary diameter is approximately 75 mm and the typical run pressure is 140 millibars (2 psi). This combination of capillary diameter and pressure, along with the positions of the two detection windows, assures the validity of the two conditions of TDA for a broad range of typical hydrodynamic radii. To obtain the sizes for each constituent of the sample, an individual fitting is carried out to estimate the radii from the widths and areas of the component taylograms. [35]

1.3 Sizing of proteins and their aggregates

1.3.1 Proteins

Proteins are organic compounds made of amino acids arranged in a linear chain and folded into globular form. The peptide bonds between the carboxyl and amino groups join the amino acids together. The proteins are translated from RNA which is transcribed from DNA. In general, DNA specifies 20 standard amino acids that are used to create proteins. After synthesis, proteins undergo post-translational modifications which adjust their physical and chemical properties, folding, stability, activity, and ultimately, function. Most proteins are typically active as folded monomers

and the shape into which a protein naturally folds is known as its native conformation, which is the most thermodynamically favorable state. The folding process is driven because of the tendency of the hydrophobic parts of the protein to shield themselves from the hydrophilic environment.

The size of a protein is an important physical characteristic that provides useful information including the presence of monomers, dimers and trimers, changes in conformation, aggregation state, and denaturation. [36] Protein-based pharmaceuticals are growing fast for the treatment of autoimmune diseases and various forms of cancer. As a result, more information about the size characterization of proteins is needed to assure the consistency of the protein products. [37]

1.3.2 Aggregation of proteins

Protein aggregation occurs either naturally in living bodies when misfolded proteins aggregate, or in the production of protein-based drugs. The natural aggregation of proteins has been correlated with diseases such as amyloidosis, including Alzheimer's, Parkinson's and prion diseases. [38-39] Generally, the protein structure is stabilized by Van der waals, ionic interactions, or disulfide bonds. When these interactions or bonds change, the proteins are susceptible to misfolding or unfolding. In these cases, if the cell does not assist the protein in refolding or degrade the unfolded protein, unfolded/misfolded proteins may aggregate. Many techniques are available for the analysis of protein aggregates. [40-41] Size is one of the physicochemical properties that changes during protein aggregation; therefore, sizing techniques are important for analyzing protein aggregation. Different sizing methods, such as size exclusion chromatography or Dynamic Light Scattering, can also be used to characterize protein aggregates. Four different sizing techniques are reviewed in chapter 2 of this thesis.

1.4 Research objectives

1.4.1 Numerical modeling of Taylor dispersion analysis

The numerical modeling of classic Taylor dispersion analysis is discussed in chapter 3. Further investigation on TDA in the presence of electric field has be done as well.

All simulations were carried out in COMSOL Multiphysics software in two-dimensional geometry. The diameter of the modelled capillary was kept at 50 µm to remain consistent with the capillary columns used in experiments, but the length was varied to reduce calculation time. Using software to investigate not yet mature methods will give more freedom for changing parameters and analytes.

Chapter 3 is devoted to discussing the parameters affecting the accuracy of Taylor dispersion analysis and investigating the possibility of using voltage alongside pressure in TDA experiments. To the best of our knowledge, no simulation works using COMSOL Multiphysics have been done on TDA and the application of electrophoretic flow.

1.4.2 Modification of equation used in TDA in the presence of electrophoretic flow

As discussed in chapter 3, the application of voltage and electrophoretic field is investigated numerically for TDA. In chapter 5, the TDA experiments are conducted on the particles with different sizes in the presence and absence of electrophoretic flow. In addition, the equations proposed by Taylor are reworked to include the electrophoretic mobility. Further discussion on each new parameter appearing in TDA equations is still needed; however, the modified equations

presented in this thesis lay the ground work. The presented experimental results support the proposed equations.

1.4.3 Investigating band broadening of large molecules in the presence of EOF

In chapter 6, the unusual band broadening of large molecules in CE is investigated. The previously established equations were used and plotted for our system to rationalize the unexpected peak width of the proteins in the presence of electroosmotic field. In this chapter, the conditions for controlling the peak width of electropherogram for proteins are suggested.

1.4.4 Investigating the aggregation of proteins

As mentioned in chapter 2, aggregation is an unwanted phenomenon when dealing with proteins. In chapter 7, proteins are aggregated thermally and their peak width is studied in the presence of Poiseuille flow and electrophoretic flow. In this work, BSA and IgG were heated to above their melting point and then thawed. The electropherograms were collected before heating, heating to temperature before melting point, and heating to the temperature above melting point. This chapter provides the preliminary works but more research is required to investigate this phenomenon in more detail. Further directions are suggested in future work.

Chapter 2: Particle sizing methods for the detection of protein aggregates in biopharmaceuticals

Note: This chapter has been published as a review paper in the journal Bioanalysis, Volume 1, Pages 96-108.

2.1 Introduction

Proteins play essential roles in the human body. They can be major components of cell structure, catalyze biochemical reactions, act as receptors for signaling molecules, and transport molecules within a cell. [42] They naturally require a three-dimensional folded structure to function effectively. [37, 43] The fundamental forces that drive protein folding include van der Waals and hydrophobic interactions, hydrogen bonding, as well as charge-charge interaction, among others. [44] These types of interactions occur between amino acids, the building blocks of proteins, and are critical to maintaining structural integrity. However, these interactions do not only occur between amino acids of the same protein but also occur between amino acids of adjacent proteins. Inter-protein interactions can result in aggregation if the newly synthesized protein does not fold correctly, or if certain chaperone molecules within the cell fail to initiate the degradation or refolding of the faulty protein. Consequently, protein aggregation is an inevitable phenomenon that occurs under certain conditions; [37] mutations, defects in protein biogenesis, environmental stress conditions, and aging can all cause protein aggregation in cells. [45] This aggregation has been identified as the primary cause of neurodegenerative diseases such as Alzheimer's (AD), Parkinson's (PD), and Huntington's disease (HD). [46] Protein aggregation is not only the origin of the diseases as mentioned earlier but also a major concern for pharmaceutical industries.

Pharmaceutical companies are becoming increasingly reliant on proteins for the development of therapeutic drugs. There has been a remarkable increase in the development of protein-based drugs since the approval of insulin as the first recombinant protein-based therapeutic by the US FDA in 1982. [47] Currently, about 250 protein-based therapeutics are commercially available, and they have played a critical role in improving human health during the last decades. They have been successfully used to treat and control some debilitating diseases, such as diabetes and various forms of cancer. [39, 48] The remarkable growth of protein-based drugs has been influenced by the advantages they offer over small molecule drugs, such as lower toxicity and higher specificity towards targets. [49] However, protein aggregation poses a challenge for the development of biological products. Aggregation can adversely affect product quality and efficacy, or potentially induce an immune response in the patient. [50] Regulatory agencies such as the FDA exist for this reason; they certify the safety and efficacy of drugs before they are approved and allowed to enter the market. [51]

Aggregation can occur during the manufacturing of protein-based therapeutics due to variation in solution conditions (pH, ionic strength, and the presence of surfactants), temperature fluctuation, or exposure to light. [52] Even if all of these variables are controlled, there is still a possibility that aggregates will form during production, storage, shipment or delivery to the patient. [53] In this way, the formation of aggregates under various conditions should be investigated to ensure the safety and stability of protein formulations. The early detection and characterization of protein aggregates, including size, morphology, and interactions, is critical in therapeutic products. [54] Moreover, the in vitro and in vivo screening of protein aggregation can advance the understanding of which molecular mechanisms cause the protein aggregation associated with neurodegenerative disease. [55]

The growth of the biotech industry has increased the demand for analytical techniques that can be used to study proteins and their aggregates. Sizing techniques are the workhorse for this field because changes in size are most noticeable when proteins move from monomer to oligomer and then to aggregates. [41] However, the unknown nature of aggregates, as well as their wide size range, from a few nanometers to a few millimeters, makes the analysis of protein aggregates challenging. [56] Each of the available sizing techniques covers a specific range of sizes, so the combination of several techniques is necessary to gain comprehensive knowledge about which types of particles are present in a sample. These techniques are based on different physical principles and hence generate different types of information about the sample. [57]

Previous reviews have described various sizing techniques that can be applied to the study of protein aggregations but have focused on either a particular instrument or a specific particle size. Pryor et al. reviewed a variety of techniques used to study the aggregation of amyloid β protein (Aβ), which plays a significant role in several diseases, such as Alzheimer's disease. They also compared the resolutions, sensitivities, and costs of these techniques for the quantitative detection of aggregates with different sizes. [58] John den Engelsman et al. published a commentary paper with some recommendations from biotech societies about which strategies should be implemented to prevent protein aggregation and therefore, unwanted immunogenicity. [59] Some authors have rather focused on one specific technique, such as dynamic light scattering, presenting its implications for a broad range of particle sizes. [60] Besides, other papers have discussed recent advances in analytical techniques with a focus on biotherapeutic proteins and antibodies. [54] However, to our knowledge, none of these reviews have presented the theory and applications of sizing techniques for protein aggregates in plain and non-technical language. A comprehensive understanding of the instruments, along with the applications and limitations of techniques, will

help pharmaceutical researchers choose the optimal method for their studies with more finesse. In this review paper, we present four analytical techniques that can be used to study protein aggregation. In addition to a discussion about the applications of each technique, the underlying principles and technical concerns are also discussed. Figure 2.1 shows how frequently the four techniques presented in this paper have been used to study proteins and their aggregates over the past 20 years.

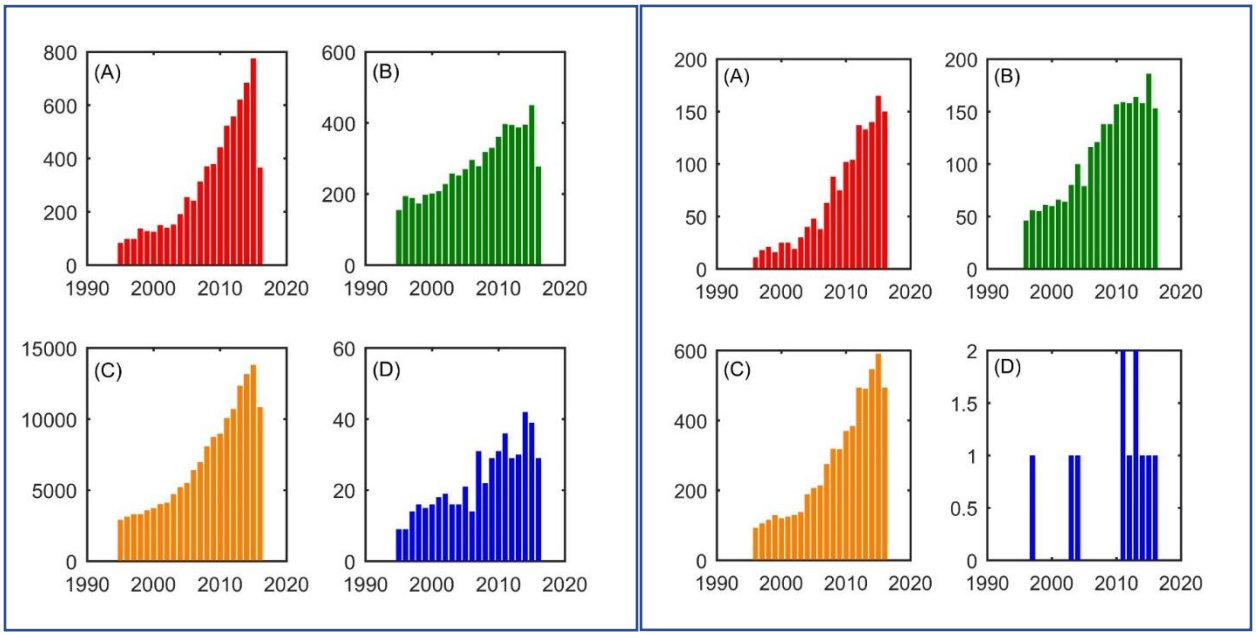

Figure 2. 1 Annual number of articles featuring (A) DLS, (B) SEC, (C) EM, (D) TDA, in the title or abstract between 1995-2015, according to Science Direct (left) for all types of particles, (right) for studying proteins and protein aggregates

2.2 Techniques

2.2.1 Dynamic light scattering

Dynamic light scattering (DLS) is a well-established method and is widely used to measure the size and size distribution of particles. The noninvasive nature of this technique makes it a good candidate for early stages of research that use valuable materials. [59] DLS is an ensemble method that measures all particles at once, as opposed to separation and counting methods. [61] It is used to measure the size of a variety of particles, including proteins, protein aggregates, and polymers. DLS measures particles with a broad range of sizes; it is effective from the nanometer scale, for quantum dots and nanoparticles, to the micrometer scale, for polymers and grains. [62-65] Fast data acquisition, high sensitivity and the reproducibility of this technique have made it a favorable monitoring technique and attracted attention from many pharmaceutical companies. [66]

Dynamic light scattering is based on the scattering of light from particles and their inherent Brownian motion. Scattering occurs when coherent monochromatic light with a wavelength of λ strikes a particle. If the size of the particle is considerably smaller than the wavelength of the incident light (typically less than 1/10 λ), then the scattering will be elastic (Rayleigh scattering), and the intensity of the scattered light is proportional to the sixth power of the particle's radius. [67] The intensity of the scattered light fluctuates over time due to the Brownian motion of the particles, which describes the random movement of particles in a fluid caused by interaction with surrounding molecules. The rate of this Brownian motion depends on the diffusion rate of the particles, which is affected by particle size, viscosity, and temperature. Therefore, the intensity fluctuations recorded during DLS analysis provide time-scale information about the motion of the particles in the medium (Diffusion coefficient). A larger particle will have a smaller diffusion rate,

and therefore, a slower intensity fluctuation.[68-70] A time-domain analysis method, the autocorrelation function, is often used to extract quantitative information from the scattering intensity fluctuations. Hence, DLS is also referred to as photon correlation spectroscopy (PCS). [69] Figure 2.2 shows the intensity fluctuations of scattered light versus time for particles with two different sizes, as well as the subsequent correlation function plot. The correlation decreases over time, and this decay is representative of the diffusion coefficients of the investigated particles. For monodisperse, spherical particles undergoing Brownian diffusion, the autocorrelation function decays exponentially over the delay time τ as follows:

$$g(\tau) = A.\, e^{-Dq^2\tau} + B \qquad (2-1)$$

where D is the translational diffusion coefficient and q is dependent on the scattering angle, the refractive index of the medium, and the wavelength of the laser light. [69]

For spherical particles, the hydrodynamic radius Rh can be obtained from the translational diffusion coefficient (D) using the Stokes−Einstein relationship:

$$D = \frac{k_B T}{6\pi\eta R_h} \qquad (2-2)$$

where k_B represents Boltzmann's constant, η is the solvent viscosity, and T is the absolute temperature. If the particle is non-spherical, then Rh can be used to describe either the apparent hydrodynamic radius or equivalent sphere radius. DLS experiments use these relationships to transform the obtained data into particle size information. [71]

The cumulants method is widely used to derive size distribution information for polydisperse samples. This method assesses the mean size and polydispersity index and it reports the size in terms of intensity-weighed mean diameter (Z average). [69]

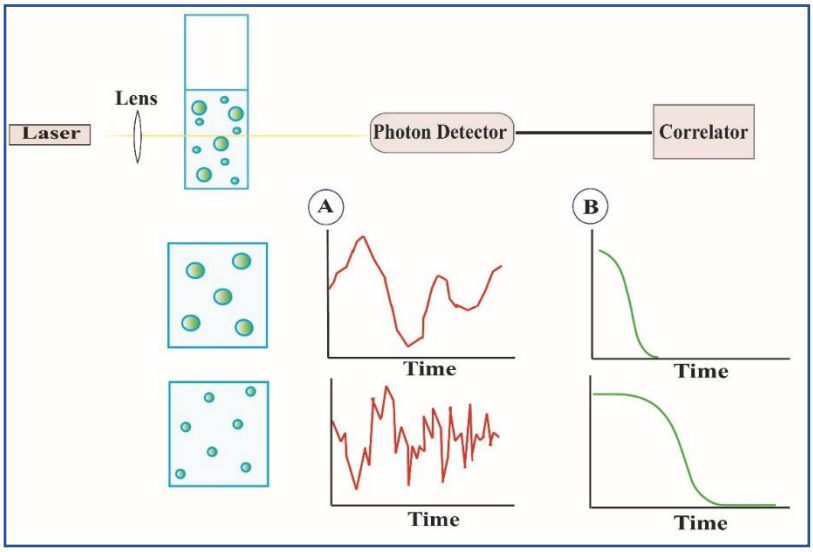

Figure 2. 2 DLS instrumentation and (A) the fluctuation of intensity of scattered light versus time for different sized particles with (B) the subsequent correlation function

DLS measures hydrodynamic size, which is the diameter of a hard sphere that diffuses at the same rate as the particle being measured. The hydrodynamic size not only depends on the particle itself but also on the types of solvation forces that exist in solution, along with surface adsorption. [72] For a non-spherical particle, DLS will give the diameter of a sphere that has a similar average translational diffusion coefficient as the particle of interest, but which also has a higher polydispersity index (PDI). [73]

The precision and repeatability of DLS depend on the measured parameter. For example, the calculation of Z-average is one of the most robust properties of DLS, as it is calculated directly from the decay rate of the intensity correlation function. Since the calculation of the Z-average is mathematically stable, the result is insensitive to noise and therefore a preferred DLS size parameter. [69]

In contrast to some other techniques that require specific temperature, pH, and salt concentration conditions for analysis, DLS performs under normal operating conditions, which allow proteins to maintain their native structure. The fact that proteins maintain their native structure benefits the study of intrinsically disordered proteins (IDPs), which lack a three-dimensional structure. IDPs play a vital role in the pathology of numerous diseases, including cancer, neurodegenerative diseases, and infectious diseases. [74] The investigation of IDPs started during the 1990s, and their unusual behavior soon attracted the attention of many scientists and protein engineers. [75] Static light scattering (SLS) is used along with DLS to characterize the size, molar mass, and intermolecular interactions of IDPs. [76]

The diversity of information provided by DLS makes it applicable to various areas of the protein industry. In addition to information about size, DLS can report the polydispersity index (PDI), which is a good indicator of the homogeneity of a studied product. This parameter can play an important role in crystallography studies. A homogenous solution and pure macromolecules are required to grow the few large, high-quality, and high-performance crystals that will be analyzed through X-ray diffraction. [77] DLS is one of the methods that are routinely used to evaluate protein homogeneity under various conditions and concentrations. The advent of highly-sensitive DLS instruments equipped with plate readers has made this technique easier, faster, and more desirable

for crystallography applications. Another advantage of this method is that the protein is easily recovered for other uses after the measurement. [78]

In an ideal DLS measurement, the reported size is independent of the concentration. However, in reality, there are certain restrictions on the concentration range. At low concentrations, there may not be enough dispersant to scatter the incident light, which will result in a very low signal to noise ratio. At high concentrations, on the other hand, there is a risk of multiple scattering along with changes in viscosity and aggregation. [79-80] Furthermore, measurements of concentrated solutions include a possibility of inter-particle and hydrodynamic interactions, both of which can affect the accuracy and precision of DLS results. However, the adverse effects of these interactions can be eliminated by extrapolating the apparent hydrodynamic radii to a concentration of zero. Takeuchi and et al. used this method to evaluate the size of a set of globular proteins, and the accuracy they reported was comparable to results obtained from more established methods, such as size exclusion chromatography (SEC). [81]

The applicability of DLS to highly concentrated protein solutions appeals to pharmaceutical companies since it enables the analysis of high doses of drugs that are designed for subcutaneous administration. However, high protein concentrations lead to high solution viscosity, which can affect the production, processing, and/or usage of the drug. [82] The rate of diffusion depends on the size of the particle as well as medium viscosity, and this relationship has extended the application of DLS to measuring the viscosity of high concentration protein solutions. The DLS-based results for viscosity are comparable to those obtained through the Cone and Plate method, which is commonly employed in the biopharmaceutical industry to measure the viscosity of protein solutions. DLS measures viscosity based on the light scattering signal from spherical polystyrene beads that are added to a protein solution. These beads are significantly larger than protein

molecules, and the DLS signals originating from the beads can be easily separated from the signals originating from proteins by the time of decay. The utilization of automated plate reader systems has made this method at least five times faster than the Cone and Plate technique. Additionally, the DLS method requires small sample volumes, a characteristic that makes it especially useful for measuring viscosity during the early stages of biopharmaceutical development, a phase when there is often a limited amount of material available for analyses. [79]

The aggregation of proteins poses a challenge for the manufacturing of biological products, but characterization of these aggregates can help control their formation. DLS has proven to be a reliable technique for monitoring and studying protein aggregation, and it can also provide information about the hydrodynamic dimensions of particles to ensure product consistency and help control aggregation. Yu et al. employed DLS to monitor inclusion body (IB) solubilization, protein refolding, and aggregation during the production of recombinant protein-based vaccine candidates and investigated how urea and a reducing reagent affected the unfolding process of the proteins. [83]

Moreover, DLS can be used to study the aggregation of proteins under various conditions, an insight that is crucial for explaining the different behaviors of proteins in the body. For example, Tomar et al. used DLS to study the decapacitating mechanism of the Con A binding fraction of human seminal plasma to understand human fertilization better. They monitored the degree to which Con A proteins aggregate when the pH or concentrations of salt, sugar, and cholesterol change, hypothesizing that the aggregation of these proteins might be required to prevent premature capacitation. [84]

DLS can also be coupled to other techniques to obtain more comprehensive information about biological systems. The nondestructive nature of DLS and its fast analysis enable it to connect to

other sizing techniques or separation instruments. For instance, the coupling of Raman spectroscopy with DLS can provide enough information to determine if protein size has increased due to aggregation or unfolding. Raman spectroscopy provides details about the secondary and tertiary structures of proteins whereas DLS gives information about the size and polydispersity of the sample. Both techniques apply to solutions with high concentrations of proteins, which enables the studying of a protein's physical properties and behaviors in the formulation condition, rather than a diluted sample of the pharmaceutical product. Zhou et al. studied the structure, aggregation, and heat stability of a high concentration formulation of intravenous immunoglobulin (IVIG) using Raman and DLS. While Lewis et al. used the combined DLS and Raman approach to characterize the colloidal and conformational stability of proteins and study the mechanism of lysozyme aggregation as a function of both pH and concentration. [85-86]

DLS has also been coupled with fluorescence to investigate fibril formation in polyglutamine peptides. Thioflavin T fluorescence demonstrates β-sheet fibril content while DLS measures particle size distribution. The combination of these two techniques is used to study complex aggregation kinetics and reveal the multiple stages of amyloid fibril formation. [87] DLS has been coupled to many additional techniques, such as size exclusion chromatography (SEC), and Taylor dispersion analysis (TDA).

Although DLS is considered a popular technique for biopharmaceutical research, it suffers from certain limitations. The main disadvantage is that this technique is highly sensitive to large particles as the intensity of scattered light is proportional to particle size raised to the sixth power. This drawback causes DLS to be more susceptible to contaminants such as dust, requiring an efficient filtration of the solution before measurements. [88]

The other constraint of this technique, which makes it less desirable for polydisperse samples, is its low resolution. DLS will not accurately characterize a polydisperse sample if the size difference is less than a factor of three. Finally, the complicated data analysis procedure and the lack of quantitative results further hinder this technique.

2.2.2 Size exclusion chromatography

Size exclusion chromatography (SEC) is the primary analytical technique that is used to characterize proteins and their aggregates and determine the size distribution of molecules in pharmaceutical products [56]. Molecules pass through the stationary phase of a column and are separated based on size [68]. The stationary phase often consists of heterosporous linked gels that are in equilibrium with a suitable mobile phase [89]. SEC is also called Gel Filtration Chromatography (GFC) when the mobile phase is aqueous and Gel Permeation Chromatography (GPC) when the mobile phase is an organic solvent [90]. SEC is often used to study large molecules, such as polymers as well as proteins and their aggregates [91-92], but it can also be applied to dendrimers, liposomes, and lipid nanoparticles [93-95].

Various mechanisms describe the elution order of a heterogeneous mixture of molecules, but the prevalent mechanism underlying SEC is steric exclusion. This mechanism is based on the idea that beads with pores of a certain size within the gel matrix are available for molecules of different size (30). Figure 2.3 illustrates how three particles of different sizes are separated according to steric exclusion theory.

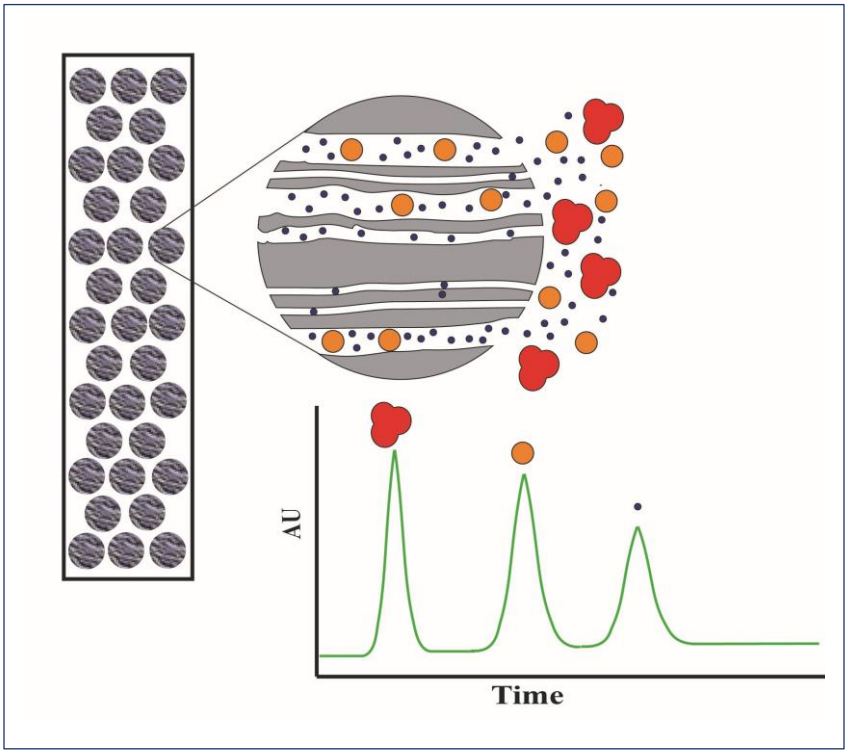

Figure 2. 3 The steric exclusion mechanism for the separation of three molecules of different sizes in SEC packed with porous beads. The larger molecules that are completely excluded from the pores move through space outside of the gel particles and elute first, whereas smaller molecules spend more time inside the bead pores and elute later

The total volume of the column is divided into three parts:

$$V_t = V_g + V_i + V_0 \qquad (2\text{-}3)$$

Where V_g is the volume occupied by the solid matrix of the gel and V_i is the space between the beads of the gel matrix, referred to as the inclusion or internal volume and determined using very small molecules. V_o is the volume outside of the beads and is determined by using a molecule that is larger than the exclusion range for the gel.

$$V_e = V_0 + K_d V_i \quad (2\text{-}4)$$

V_e is the volume required to elute intermediate size molecules and the fraction K_d describes the extent to which molecules can enter the interstices of the gel. In an ideal situation, where the molecules of interest do not interact with the column, this coefficient would be between one and zero. [96] The K_d of molecules that are larger than the pore size is zero and therefore, the elution volume is volume of the solvent outside of the pores. Small particles that can permeate into all pores are eluted with a volume of $V_0 + V_i$.

Ideally, the stationary phase would only minimally interact with the sample, which would retain biomolecular activity [97]. However, the nonspecific adsorption of proteins to the column matrix often affects the accuracy by abnormal elution positions and reduces recovery by the loss of proteins; it also results in an undesirable change in the peak shape and chromatographic resolution [89]. A common approach to reducing these interactions is modifications in the mobile phase. Arakawa et al. (2010) showed that the presence of salt in the mobile phase suppresses undesirable electrostatic interactions and an organic solvent reduces hydrophobic interactions [98].

SEC is commonly utilized during the manufacturing and formulation of pharmaceuticals due to its high speed, reproducibility, and accuracy [99], and is widely used to study protein aggregates and their behaviors. Printz et al. used SEC to study protein aggregation under several conditions, such as the stress caused by pH changes, temperature changes, freezing and thawing, light, and shaking. They showed that each stress factor led to different patterns in the size and degree of unfolding of aggregates. These types of experiments are valuable for biopharmaceutical companies since they provide information that can be used to control and minimize protein aggregation and therefore, increase the stability of the products [52]. Although SEC is mainly applied to so-called soluble aggregates, it can also be used to confirm the presence of large and insoluble aggregates. Barnard

et al. used indirect SEC to study the formation of sub-visible particles during freeze-thawing of an IgG_2 monoclonal antibody (mAb) by comparing the loss of area in the treated sample versus the control sample [100].

Although SEC is a relatively fast and robust high-throughput method, it is still considered a low resolution technique. To improve the resolution, smaller particles are used in the packing of the stationary phase in the column. Fekete et al. evaluated how three different particles sizes for packing influence the ability of SEC to separate protein aggregates. They reported that, on average, sub-2μm particles had 2–5 times lower plate height values than the 3μm and 5μm particles used for column packing. The lower plate height values of the sub-2μm particles represent higher column efficiency. They also demonstrated that, in the practical plate number range, the use of sub-2μm particles reduces the analysis time [101].

SEC is capable of detecting and characterizing a wide range of small aggregates, but sometimes even modifications of the stationary phase and the mobile phase cannot provide adequate resolution. To overcome this limitation, SEC can be combined with other techniques, for instance, Moneeruddin et al. coupled SEC with native Electrospray ionization mass spectrometry (ESI-MS) to characterize the commercial protein samples that were forming small aggregates. The ability of native ESI-MS to resolve different protein assemblies based on their masses helps to overcome the resolution constraint in SEC, and the separative power of SEC eliminates the need for purifying and desalinating the sample before analysis, along with reducing concerns about the co-elution of proteins. Thus, the combination of these two techniques provides a robust and powerful method for the analysis of biopharmaceutical products [102].

SEC can also be complemented by the addition of a variety of detectors, such as those for UV, Fluorescence, light scattering, and refractive index (RI) [99]. These detectors are used to draw more

information from the sample. Printz et al. used SEC to separate monomers from oligomers, a UV detector for their quantification, and fluorescence to observe structural changes in the proteins. Hence, combining SEC with the detection of UV and fluorescence helps to distinguish the different types of particles that form under different stress conditions [52]. SEC can also be coupled to DLS to perform absolute size chromatography (ASEC), which provides rapid and direct measurements of protein size without the need for costly and laborious column calibration. This method can be further combined with multi-angle light scattering (MALS) to investigate the mechanisms of aggregation [103].

2.2.3 Electron microscopy

Electron microscopy (EM) is a powerful technique that provides direct visual information about the size, shape, and aggregation state of a sample. Thus, it has a wide range of applications in studies of protein therapeutics [104]. Electron microscopes are analogous to light microscopes in principle, but the irradiation source differs; the former uses a beam of electrons while the latter uses a light beam. Electrons have a shorter wavelength than visible light, and for this reason, electron microscopes can provide significantly higher resolution images [105]. The instrument consists of an electron gun, an electromagnetic lens, which focuses the electron beam on the specimen, and a detection system, which is normally a fluorescent screen. The entire apparatus is contained in a vacuum to prevent any interactions between electrons and air molecules [106]. Figure 2.4 shows the setup of a conventional electron microscope.

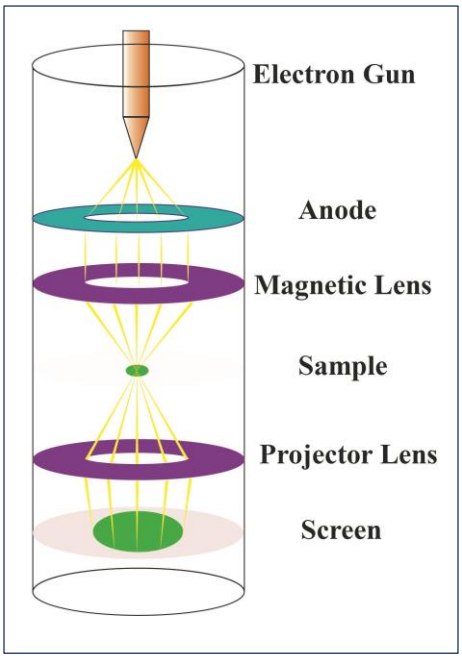

Figure 2. 4 Electron emitted from the electron gun are directed by the anode to the magnetic lens, which focuses the electron beam on the sample. From there, a projector lens projects the passing beam onto a fluorescent screen for detection

The Scanning Electron Microscope (SEM) and the Transmission Electron Microscope (TEM) are two of the most commonly used electron microscopes. TEM was the first developed electron microscope, and it detects the transmitted electrons that pass through a thin sample slice. On the other hand, SEM uses an electron probe to scan the surface of an object, and the scattered electrons are detected to form the image. TEM offers greater magnification and higher resolution, while SEM provides more information about the three-dimensional structure of a particle [107].

Electron microscopes utilize fluorescent planes for the detection of a specimen. Therefore, the sample must be labeled with a fluorescent tag before imaging, a process that might affect the morphology of the particle. For this reason, Valeri et al. evaluated how fluorescent tags affect fibrils grown from both Alzheimer's disease-associated peptides and Parkinson's disease-

associated proteins. Their results showed that, in most cases, the fluorescent tags are compatible with the proteins of interest [108].

Electron microscopes are often used to study biological samples, such as proteins, cells, and viruses, in their native state. However, the interaction between high-energy electrons and the studied molecules may disturb molecular structure, potentially leading to bond breakage, the formation of free radicals, and loss of secondary structure [109]. Proper sample preparation is necessary to alleviate these adverse effects. Negative staining is a commonly used method during of which the particles are coated with a reagent containing heavy atoms. Although this approach prevents the interaction between electrons and the target organic molecule, it may cause other problems, such as the loss of the internal structure information and the presence of artifacts in the final image [110]. Cryo-EM is another sample preparation technique that can be used to prevent the adverse effects of high-energy electrons. In this method, the sample is studied at cryogenic temperatures, usually achieved with either liquid helium or nitrogen, which maintains the natural environment of the sample. [111]

The rapid cooling in cryo-EM traps the macromolecules in their native state and therefore allows the elucidation of their natural conformational distribution and spatial arrangement [112].

Cryo-EM has gained a lot of attention and has been widely used in biological studies. Many researchers have used this technique to obtain information about the size, morphology, and structure of proteins and their aggregates. The application of electron microscopy to studies of amyloid aggregates and the mechanism of their formation is leading the frontier for understanding diseases such as Alzheimer's disease. For example, Wendler and Saibil found cryo-EM to be a promising technique for studying the structure of Hsp100 proteins, which are chaperone proteins that function to reverse the aggregation process, and they have reviewed the application of cryo-

EM to studies of proteins responsible for reversing the aggregation process [113]. Joyce et al. used TEM to study the aggregation process of IgG under freeze-thaw stress, characterizing the size, morphology, and distribution of aggregates, as well as the effect of surfactant on aggregate formation. They also compared the two sample preparation techniques for electron microscopy, negative staining and frozen-hydrated states [104]. Zhao et al. evaluated the shape, size, and structure of HIV-1 capsid protein using 8 Å resolution cryo-EM, which is the basis for research on capsid functions and their assemblies [114]. Cryo-EM also has applications to studies of drug delivery with liposomes or lipid nanoparticles [115]. Fox et al. used cryo-EM to explore the interaction between antigens and an anionic liposome, which forms flattened liposomes consisting of opposing bilayer disks, and they compared these results with those obtained from light scattering techniques [116].

Electron microscopy techniques are still considered the gold standard in the study of different types of materials. They cover a large size range, from nanometer scale to millimeter scale, and can provide high resolution images for the chemical composition of a particle [59, 112]. Although electron microscopy provides an enormous amount of information about specimen shape, atomic structure, composition, and surface features, as well as powerful magnification, this technique still has certain disadvantages that need to be considered. The most notable limitation is the price of the instrument and its maintenance. Furthermore, the microscope requires a large area that is protected from any vibration and sources of unintended influence for the electrons. The sample preparation is also time-consuming and laborious, not to mention that most of the techniques associated with electron microscopy require specialized training [117].

2.2.4 Taylor dispersion analysis

Taylor Dispersion Analysis (TDA) is a rapid and absolute method for determining diffusion coefficients, from which the hydrodynamic radius of a molecule is calculated. The method was first developed by Taylor in 1953 and then modified by Aris in 1956 [118-119]. Taylor dispersion is achieved in a long, narrow capillary tube. For this reason, capillary electrophoresis instruments, which use narrow bore tubes to separate molecules, are particularly suitable for performing TDA. In capillary electrophoresis (CE), only a few nanoliters of the sample is usually injected, which is advantageous for the analyses of samples with low availability, for example, therapeutic proteins or drug delivery systems [120-121]. As a result, TDA has recently gained a lot of attention for studying valuable biological samples. Besides, TDA does not require calibration as it is an absolute method, which makes it more appealing than other sizing techniques, such as SEC. This technique can be used to study a wide variety of particles, such as amino acids, peptides, proteins, macromolecules, polymers, nanoparticles, and liposomes [122-124]. It also applies to non-aqueous solutions, which makes it suitable for the characterization of hydrophobic compounds [125]. Furthermore, TDA can measure a wide range of sizes, from an angstrom to a few hundred nanometers [120].

TDA is based on recording the concentration profile of a solute as a function of time at given positions. This describes the longitudinal dispersion of a small solute plug in a narrow, open tube under Poiseuille laminar flow as a combination of radial diffusion and axial convection. The longitudinal dispersion results in peak broadening, which can be quantified by fitting a Gaussian function to the concentration profile and measuring the temporal variance (σ^2). The diffusion coefficient is estimated using equation 5.

$$D = \frac{R_c^2 t_0}{24\sigma_t^2} \qquad (2\text{-}5)$$

The diffusion coefficient (D) can be accurately determined from measurements in a straight capillary under two conditions: first, longitudinal diffusion is negligible and second, the analyte is well mixed across the capillary of radius R_c during the time of flow [126]. Figure 2.5 depicts the longitudinal dispersion of a sample along the capillary column.

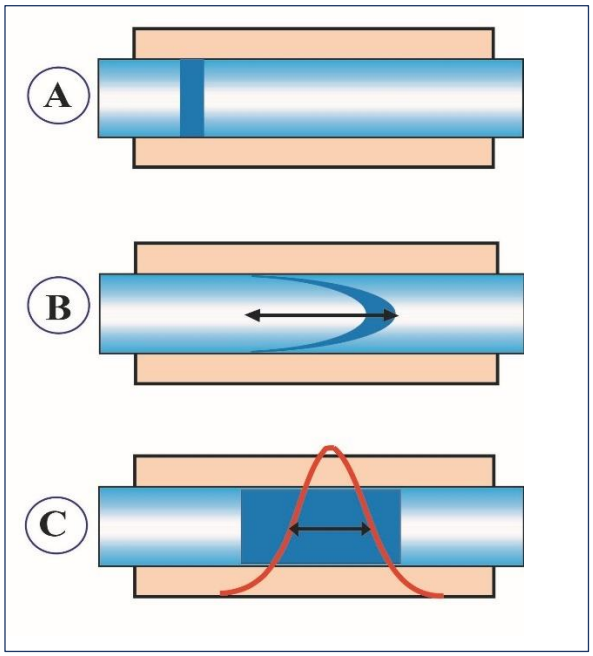

Figure 2. 5 (A) Insert sample. (B) Pressure is applied which forms parabolic flow. (C) The combination of axial convection and radial diffusion leads to longitudinal dispersion

Since this technique is based on measurements of temporal variance of the elution profile, other factors that influence peak variance may affect the accuracy of results. The use of a two-detection window system is an appropriate approach to tackle this problem [127].

The diffusion coefficient can then be used to calculate the hydrodynamic size according to the Einstein-Stokes equation (Eq (2-2)).

The diffusion of drug substances is an essential part of the drug absorption and elimination processes that occur within the body. Over the past ten years, numerous studies have assessed whether TDA can be used to characterize drug diffusivity, size, and charge. Ye et al. studied the

possibility of using TDA to evaluate the diffusion coefficients of three different drugs (Lidocaine, Ibuprofen, and Bupivacaine) in various pharmaceutical solvents. They showed that drug diffusivities decrease as solvent viscosity increases [128]. Likewise, Hulse et al. evaluated the use of TDA in measuring the sizes of therapeutic proteins and small molecules [129]. Jensen et al. used TDA to determine the apparent diffusion coefficient, size, and self-association of insulin over a broad range of concentrations. They took the study one step further and studied the release kinetics of insulin in agarose hydrogel, which mimics the subcutaneous tissue environment. They observed that the diffusivity and transport of insulin changes with pH and/or concentration changes [130].

TDA is also used to characterize the size and charge of drug delivery systems that carry small drugs or therapeutic proteins. These systems maintain a constant drug dose over a long period of time and achieve a controlled release of both hydrophilic and hydrophobic compounds once they reach the target [131]. Ibrahim et al. used TDA and CE to characterize the size and charge of nano-gel based drug delivery systems containing the hydrophobic groups of vitamin E [127]. Oukacine et al. used TDA to measure the hydrodynamic radii of drug-loaded polymeric micelles [132].

TDA has also been involved in the study of protein aggregates, which is critical for the batch-to-batch monitoring of pharmaceutical products [121]. Besides, the immunogenicity assessment of a therapeutic product, for example, evaluates whether aggregates are present at various points of the drug formulation. Lavoisier et al. reported that TDA could be used to monitor the presence of aggregates in a series of antibodies; they showed that this technique is capable of identifying different types of antibodies and aggregates, with applications for evaluations of the consistency of final products [133]. In another study, Hulse and Forbes heat stressed BSA proteins to induce aggregation and then measured the size change using TDA. They showed that this technique is capable of detecting both monomers and aggregates [121]. In further experiments, they monitored the

aggregation process over time and compared the results with DLS [129]. The applicability of this method to both small particles and large molecules makes it a good candidate for evaluating the progress of aggregation when both monomers and oligomers are present in a solution. It can also provide quantitative information about the conversion rate of proteins to aggregates under different conditions. In this way, it is a promising method for monitoring a mixture of proteins and their aggregates. To draw even more information from a mixture, TDA can employ different algorithms to estimate the polydispersity of a solution. The taylogram obtained for polydisperse samples is a convolution of individual Gaussian peaks, each representing a given diffusion coefficient. The cumulants analysis can then be used to extract information about each component, and this method is analogous to the one used in DLS. Cipelletti et al. applied this method to analyze moderately polydisperse polymer samples and the bimodal mixtures of these samples [120]. They also investigated the use of another data processing method, Constrained Regularized Linear Inversion, to evaluate the polydispersity of the samples [134].

2.3 Conclusion

This review describes four sizing techniques that can be used to study proteins and their aggregates. The underlying principles, applications, and disadvantages of each method have been presented clearly and concisely. Additionally, a schematic illustration of each technique has been provided to further demonstrate how the method works. It has also been highlighted that the combination of these technique expands their size range, as well as the amount of extracted information. The summary table gives a general overview of the presented methods and is a tool that can help researchers choose the technique that is most applicable to their studies.

The pharmaceutical industry is shifting towards protein-based therapeutics to battle an array of human diseases. However, the quality of these biopharmaceuticals can be affected by aggregates, which could compromise product safety. In an environment where regulatory agencies require comprehensive information about the safety and efficacy of new pharmaceuticals, sizing techniques are vital in the evaluation and characterization of the protein aggregates in a sample.

Chapter 3: Numerical modeling of Taylor dispersion analysis

3.1. Introduction

Taylor dispersion analysis (TDA) is a novel technique used to determine the diffusion coefficient and size of a variety of particles, such as therapeutic proteins and antibodies, nanoparticles, polymers, and small molecules.[133, 135-137] TDA is becoming more popular due to its simplicity, accuracy, and ability to determine a wide range of molecule sizes without a need for calibration. TDA gives results that are consistent with the more well-established methods like Dynamic Light Scattering (DLS) and Size Exclusion Chromatography (SEC), and offers some advantages over these techniques in terms of sensitivity and simplicity. [138-139] Although, TDA has emerged as a sizing technique during the last few decades, it is still considered a new technique, and more in-depth studies are required to obtain accurate and precise results.

TDA is based on Taylor's work which was extended by Aris. Taylor described the dispersion of a solute plug in an open tube under Poiseuille laminar flow. When a parabolic velocity profile is combined with molecular diffusion, particles redistribute in the cross-section of the capillary, which leads to dispersion. [118-119] Under some specific conditions, molecular diffusion, D, is related to the temporal variance of the electropherogram for an analyte, σ_t^2, the average elution time t_0 and the capillary radius, R_c, of the tube by the following equation. [140]

$$D = \frac{R_c^2 t}{24\sigma^2} \qquad (3\text{-}1)$$

The diffusion coefficient can be converted into the size of particle using the Stokes-Einstein equation.

$$R_h = \frac{KT}{6\pi\eta D} \qquad (3\text{-}2)$$

Where R_h is hydrodynamic diameter, K is Boltzmann's constant, T is temperature, η is viscosity and D is the diffusion coefficient. [32]

TDA is performed in a narrow column tube, and pressure is used as the driving force for the analysis; therefore, capillary electrophoresis (CE) instruments are often used for performing TDA experiments. The elution time and temporal variances of analytes in capillary columns depend on three factors: (i) the applied pressure, (ii) the capillary length, and (iii) the capillary radius. These parameters must be optimized so that the validity of Eq (3-1) is satisfied. Taylor discussed two conditions which need to be fulfilled to perform TDA experiments. [119] The first condition is that the elution time must be much longer than the characteristic time for diffusion of the analyte across the capillary radius.

$$t_0 \geq \frac{3R_c^2}{80D\varepsilon} \qquad (3\text{-}3)$$

Eq (3-3) is used to confirm the validity of the first condition, where R_c is the capillary radius, D is diffusion coefficient, and ε is the relative error on the determination of D that can be tolerated.

The second condition states that longitudinal dispersion must be negligible compared to radial dispersion. To meet this condition, the Peclet number (Pe), which is the ratio of the contributions to mass transport by convection to those by diffusion, must be bigger than a certain value which depends on the desired error percentage of the diffusion coefficient.

$$Pe = \frac{uR_c}{D} \geq \sqrt{\frac{48}{\varepsilon}} \qquad (3\text{-}4)$$

Taylor's two conditions also need to be optimized to minimize the error percentage in the calculation of the diffusion coefficient.

Cottet *et al.* made a substantial contribution in the field of Taylor dispersion analysis by investigating the optimum conditions for performing TDA, and developing methods to analyze mixtures. They used the cumulant method, which is widely used to derive size distribution information for polydisperse samples,[141] to quantify size polydispersity for solutions of polydisperse polymers and polymer mixtures under optimized conditions. [34] Most of the research to date on TDA is carried out by experiments which can be time-consuming and laborious. Fortunately, because the physics of Taylor dispersion is well known, numerical modeling is a reliable complement to experimentation. Simulating Taylor dispersion using numerical methods facilitates the study of different parameters on the performance of TDA and saves time and resources. To the best of our knowledge, no comprehensive modeling has been developed for TDA. In this chapter, we use COMSOL Multiphysics to further study Taylor dispersion in narrow tubes leading to better and faster optimization of the experimental conditions. This study explores the effect of pressure, electric field, diameter and length of column on the TDA conditions and accurately-obtained sizes.

In this work, numerical modeling is used to optimize the operating conditions such as mobilizing pressure, capillary length and capillary radius for molecules having hydrodynamic diameters of 0.5-5 nm. In all cases, the validity of TDA conditions are verified and the optimum condition for performing TDA are discussed. Also, the effect of electric field on the validity and the applicability of TDA for a mixture of molecules with different sizes is studied. We concluded that parameters must be chosen in such a way that Taylor's two TDA conditions are met. For mixtures, using an

electric field is advantageous, because it not only leads to the separation of molecules, but also it gives information about the charge of the molecules.

3.2. Theoretical simulation

The migration of analytes in a two-dimensional capillary tube is calculated using finite-element-scheme simulation software, COMSOL Multiphysics 4.4a (COMSOL Inc., Los Angeles, CA). The modeling procedure with this program includes creating a virtual model with 2D geometry, defining parameters, meshing, solving differential equations, post-processing data. In this study, the molecules are mobilized by the simulated electric field and hydrodynamic flow field. Both electric and fluid fields are calculated in a steady state before solving the mass balance equation, through which the concentration distribution for analytes is calculated in a time-dependent manner. The variance of peaks is calculated by fitting a Gaussian curve to the resulting data. Diffusion coefficients are calculated using Eq (3-1), and the error percentage is calculated by comparing the obtained diffusion coefficient with the input value. The simulations are conducted on a 2, 4, and 8-centimeter length tube with a radius of 25, 50, and 100 μm. In the first section of this paper, TDA with only pressure is investigated and the results are plotted and tabulated. In the second section, voltage is applied along with pressure and the results are compared with classical TDA. In all cases the validity of TDA is confirmed by calculating Peclet number and the characteristic time. To make sure that only diffusion is contributing to band broadening, the injection volume is less than 1% of the column volume.

3.3. Results and discussion

The Taylor dispersion behavior of three particles with different diffusion coefficients in a two-dimensional column is calculated using finite-element-scheme simulation software, COMSOL Multiphysics (COMSOL Inc., Los Angeles, CA). The fluid velocity field of a solution is described by the simplified Navier-Stokes equation $-\nabla p + \eta\nabla^2\vec{v} = 0$, where p is the pressure, η is the viscosity coefficient, and $\vec{v}$ is the fluid velocity vector of any point in the fluid field. [142] The conservation of mass principle gives the relationship of $\nabla.\vec{v} = 0$, which is used in conjunction with the Navier-Stokes equation to solve for the pressure and velocity. The concentration of analytes is determined by numerically solving the mass balance equation $\left(\frac{\partial C}{\partial t}\right) + \vec{v}.\nabla C + \nabla.(-D\nabla C) = 0$, where C is the analyte concentration at a specific location on the column, D is the diffusion coefficient, $\vec{v}$ is obtained from the previous calculation for fluid field. [143] Thus, the analyte concentration and its variation with time at any location is calculated to determine the analyte dispersion along the column.

The purpose of using numerical studies is to investigate the effect of different parameters on the Taylor dispersion of particles such as fluid velocity, capillary diameter and capillary length. Also, the effect of applying voltage on Taylor dispersion is studied here. The parameters should be chosen in such a way that the conditions for the validity of TDA are met.

3.3.1. Dispersion of particles in the presence of Poiseuille flow

TDA uses pressure (Poiseuille flow) to mobilize analytes in a capillary column. In TDA, the particles need to spend enough time in the tube so they redistribute uniformly in the radial direction, but not so long that axial diffusion becomes significant. These criteria are affirmed in the first and second conditions of TDA. To calculate a diffusion coefficient, the elution time and

temporal variance of analytes in the capillary tubes are calculated which depend on three main parameters: (i) applied pressure, (ii) the capillary length, and (iii) the capillary radius. In this section, these variables are investigated. [34]

3.3.1.1. Effect of linear velocity (pressure)

When conducting a TDA experiment, the pressure is adjusted to maintain a constant linear velocity for the bulk flow in the capillary column. Since linear velocity appears in the TDA second condition (Eq (3-4)), we use linear velocity instead of pressure to investigate the effect of the mobilizing pressure on TDA performance. According to Poiseuille's law, Eq (3-5), in a laminar flow the pressure and linear velocity are interchangeable when the viscosity of solution and the radius of the column are constant. [144]

$$v = \frac{PR_c^2}{8\eta L} \qquad (3\text{-}5)$$

In Eq (3-5), v is linear velocity, P is pressure, R_c is capillary radius, η viscosity, and L is the length of the column.

To explore the effect of pressure (or linear velocity) on TDA performance, and on TDA conditions, we used different velocities for this study. Figure 3.1 shows the taylograms for two particles with small and large diffusion coefficients at different linear velocities. For particles with a smaller diffusion coefficient (Figure 3.1A), the taylogram at lower velocity follows a normal distribution as opposed to the higher velocity where more deviation from a normal distribution is observed. This deviation from normal distribution is also evident in Figure 3.2 where for smaller diffusion coefficients, R^2 deviates from 1 as the linear velocity increases. This anomaly in the peak shape affects the accuracy of the diffusion coefficient obtained from Eq (3-1), which leads to a higher error percentage (Figure 3.2).

To explain this divergence, we need to assess the validity of the two TDA conditions at different velocities. Table 3.1 shows the minimum values of Peclet number for fulfilling the TDA second condition and Table 3.2 shows the minimum values of elution time for fulfilling the TDA first condition. As shown in Table 3.2, for a particle with a diffusion coefficient of 5.0E-11 m^2/s to fulfill the TDA first condition, it must spend at least 62.5 seconds in the column. As shown in Table 3.1, at higher velocities, the elution time is shorter than the minimum time; thus, the particles do not have enough time to distribute uniformly in the radial direction. Therefore, the taylogram does not follow a Gaussian function (normal distribution) which leads to a higher error percentage in the evaluation of the diffusion coefficient. On the other hand, to fulfill the TDA second condition, higher velocity is desirable since it gives a higher Peclet number which means less time is available for the axial diffusion of particles in the column. According to Figure (3-1) and Figure (3-2), higher velocity has more of an adverse effect on the first condition than having a favorable effect on the second condition.

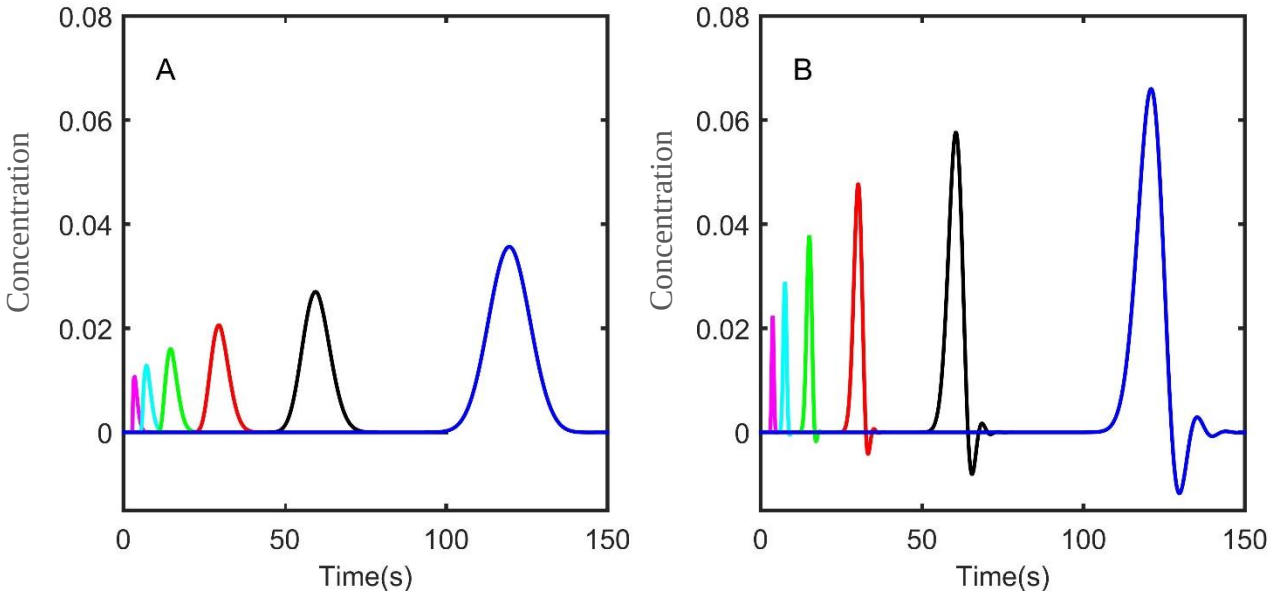

Figure 3. 1 Simulated migration of particles with diffusion coefficient of (A) 5.0× 10^{-11} m^2/s (B) 5.0× 10^{-10} m^2/s at different linear velocities in a column with diameter of 50μm and length of 4 cm.

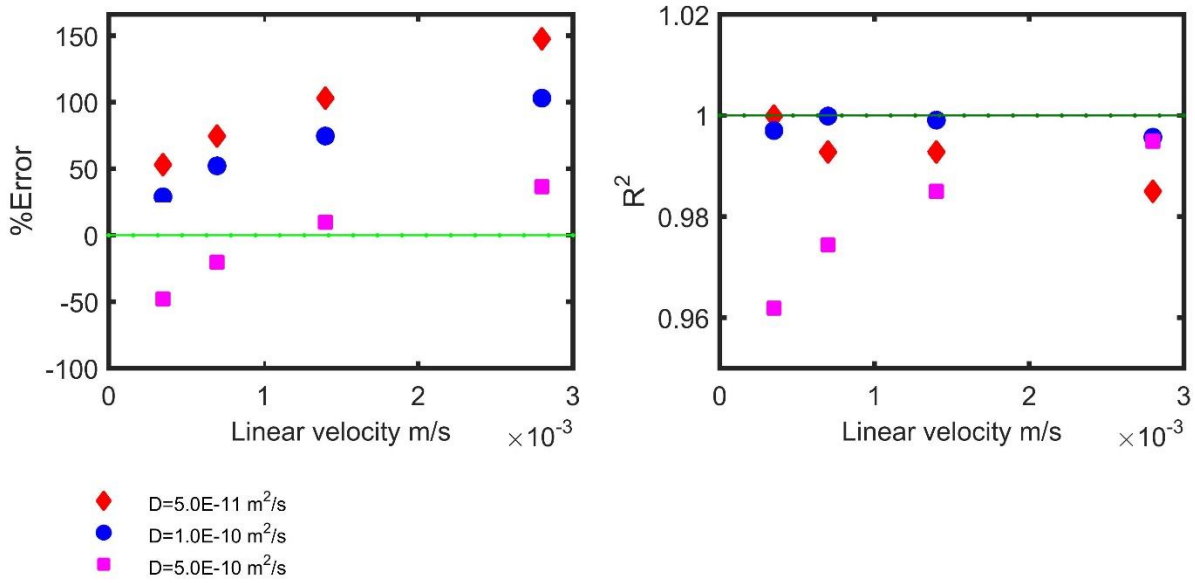

Figure 3. 2 %Error and R^2 for particles of different diffusion coefficient at different velocities

Table 3. 1 Elution time and minimum Peclet number for different linear velocities

D (m^2/s)	5.0E-11		1.0E-10		5.0E-10	
v (m/s)	t	Pe	t	Pe	t	Pe
3.50E-4	120	350	120	175	120	35
7.00E-4	60	700	60	350	60	70
1.40E-3	30	1400	30	700	30	140
2.80E-3	15	2800	15	1400	15	280
5.60E-3	7.5	5600	7.5	2800	7.5	560
1.12E-2	3.7	11200	3.7	5600	3.7	1120

Table 3. 2 The minimum elution time to fulfill the first TDA condition

D (m^2/s)	t_0 (sec)
5.0E-11	62.5
1.0E-10	31.3
5.0E-10	6.3

For a particle with a diffusion coefficient of 5.0E-10 m^2/s, the minimum time to fulfill the first TDA condition is 6.3 seconds. As a result, in addition to the second TDA condition to be valid, the first TDA condition is also valid at higher velocities. Therefore, as shown in Figure 3.2, $\mathbf{R^2}$ becomes closer to 1 as the linear velocity increases.

To summarize, particles with larger diffusion coefficients conform to the TDA conditions and give more accurate results at higher velocities. On the other hand, particles with smaller diffusion

coefficients fulfill the TDA conditions and give more accurate results at smaller velocities. Therefore, to satisfy TDA conditions for a mixture of particles with different diffusion coefficients, an optimum linear velocity is chosen. A velocity of 1.4×10^{-3}m/s is a good compromise between the accuracy and goodness of Gaussian fit. Figure 3.3 shows the taylogram of all three particles at the optimized velocity.

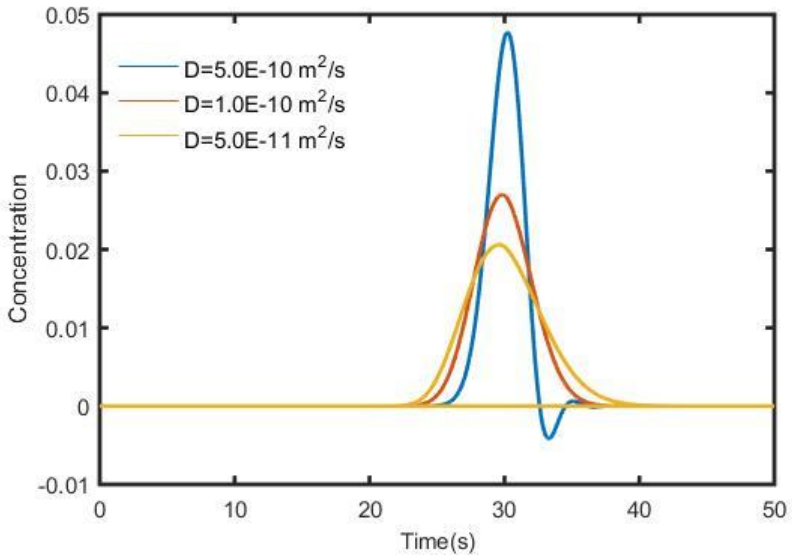

Figure 3. 3 Taylor dispersion of particles with different diffusion coefficient at a linear velocity of $1.4\times 10^{-3}\ m/s$

3.3.1.2. Effect of capillary diameter

Capillary columns are available in different diameters. The inner diameter is typically 25-100 µm and the outer diameter is 200-375 µm. The capillary tubes are coated with a layer of polyimide to enhance their mechanical strength. This section evaluates the effect of column inner diameter on the dispersion of particles and on the validity of the TDA conditions. The diameter of the column affects the minimum time the particles need to spend in the column to meet the first TDA condition. The larger the diameter, the more time it takes for the particles to redistribute across the column; therefore, the minimum time for fulfilling the first TDA condition increases. The minimum time

also increases when the diffusion coefficient decreases, since the rate of diffusion across the column is slower and so more time is needed for the particles to be redistributed. Three columns with the diameter of 25 μm, 50 μm, 100 μm are used here. Table 3.3 shows the minimum time for particles of different diffusion coefficients at different diameters. For larger particles (smaller diffusion coefficients) in larger diameter capillaries the minimum time is 250 seconds, whereas for small particles (larger diffusion coefficients) in smaller diameter capillaries, the minimum time is 1.6 seconds.

According to Eq (3-5), by increasing the capillary diameter, the applied pressure must decrease to maintain a constant linear velocity.

Figure 3.4 is divided into six parts and shows Taylor dispersion of particles with different diffusion coefficients by varying the diameter of the capillary column. We used two opposite extreme linear velocities to explore the two conditions of TDA as well. On the left, A1, B1, C1 show the low velocity extreme and on the right, A2, B2, C2 show the high velocity extreme.

In general, when a higher velocity is used, taylograms deviate from the normal distribution. This deviation becomes even more significant when the column's radius increases. Taylor first condition can explain these anomalies. According to Taylor first condition for performing TDA, the elution time must be larger than the characterization diffusion time of the solute in the capillary cross-section. In Table 3.3, this characterization diffusion time is reported for each particle at each capillary diameter.

When TDA is performed in a diameter of 100μm (C1&C2), the minimum time for the particles to meet the first TDA condition is 25 s, which is longer than the minimum times in smaller diameters (25μm and 50 μm). In capillaries with larger diameter, the minimum time increases because the

particles need to travel longer distances from the wall to the center and vice versa. The increase in minimum time is more significant for particles with smaller diffusion coefficients because of their smaller rate of diffusivity. When a high velocity like 11×10^{-3} m/s is used, the time that particles spend in the column is shorter than the minimum time needed for the particles to redistribute in the column with diameter of 100 µm. Therefore, particles do not have enough time to redistribute radially and form a normal distribution taylogram. In short, the larger the capillary diameter, and the smaller the diffusion coefficient are, the longer the particles must spend in the column to fulfill the first TDA condition. Therefore, to meet the first TDA condition, a smaller linear velocity is preferred when using capillary columns with larger diameters. Besides the first condition of TDA, Taylor's second condition must be fulfilled as well for Eq (3-1) to be valid. The linear velocity should be fast enough so that the axial diffusion can be neglected compared to the Taylor dispersion term. Thus, a higher velocity is favorable to meet the second TDA condition. Yet again, linear velocity or applied pressure must be optimized to meet both conditions.

When TDA is performed in a diameter of 25µm (A1&A2), the minimum time to meet the first TDA condition is 2s for a particle with a smaller diffusion coefficient, and 16s for a particle with a larger diffusion coefficient. At higher velocities in this small diameter column the particles have enough time to diffuse radially. For larger particles, the migration time is smaller than the minimum time, but the time is still close. Therefore, the deviation from the normal distribution is not significant. In summary, as the diameter of the capillary decreases less time is needed for TDA to be valid. Therefore, higher velocities can be used for small diameter capillaries to meet the first TDA condition. Using higher velocities is also advantageous for fulfilling the second TDA condition requirement since there would not be enough time for the axial diffusion of particles. Whereas, at lower velocities, the axial diffusion becomes significant which contradicts Taylor's

second condition. Comparing A1 & A2, at a higher velocity the peak widths are distinctive, while for a smaller velocity they are close to each other. At lower velocity (A1), the particles are spending too much time in the column; thus, the axial diffusion is more significant which is also contributing to the peak width of the taylogram. In this case, more axial diffusion is observed for smaller particles which adds to the peak width and leads to a broader peak.

For capillaries with a diameter of 50µm, higher velocity leads to violating the first TDA condition, which is more significant for particles with smaller diffusion coefficients, leading to taylograms that do not follow a normal distribution. At smaller velocities, the second TDA condition might be disturbed and the axial diffusion would become more significant, especially for particles with bigger diffusion coefficients. Therefore, a medium linear velocity is chosen to meet both TDA conditions.

As the diameter increases, Pe also increases; therefore, the second TDA condition is met even at smaller velocities. Table 3.3 shows the value of the Peclet number for each particle at different diameters. The Peclet number for a 25 µm diameter capillary is small; therefore, to meet the second TDA condition, the linear velocity must be higher than 1.4×10^{-3}m/s to compensate for the small radius of the capillary. By combining minimum time and Peclet number to meet TDA conditions, it is concluded that for smaller diameters, higher linear velocity is needed to increase Pe to meet the second TDA condition which will be in accordance with the first TDA condition. For larger diameters to meet TDA first condition, lower linear velocity is needed to increase the migration time. Since Pe is larger at large diameters, performing TDA at lower velocities does not contradict the second TDA condition. Therefore, it is expected that more accurate results will be obtained at lower velocities.

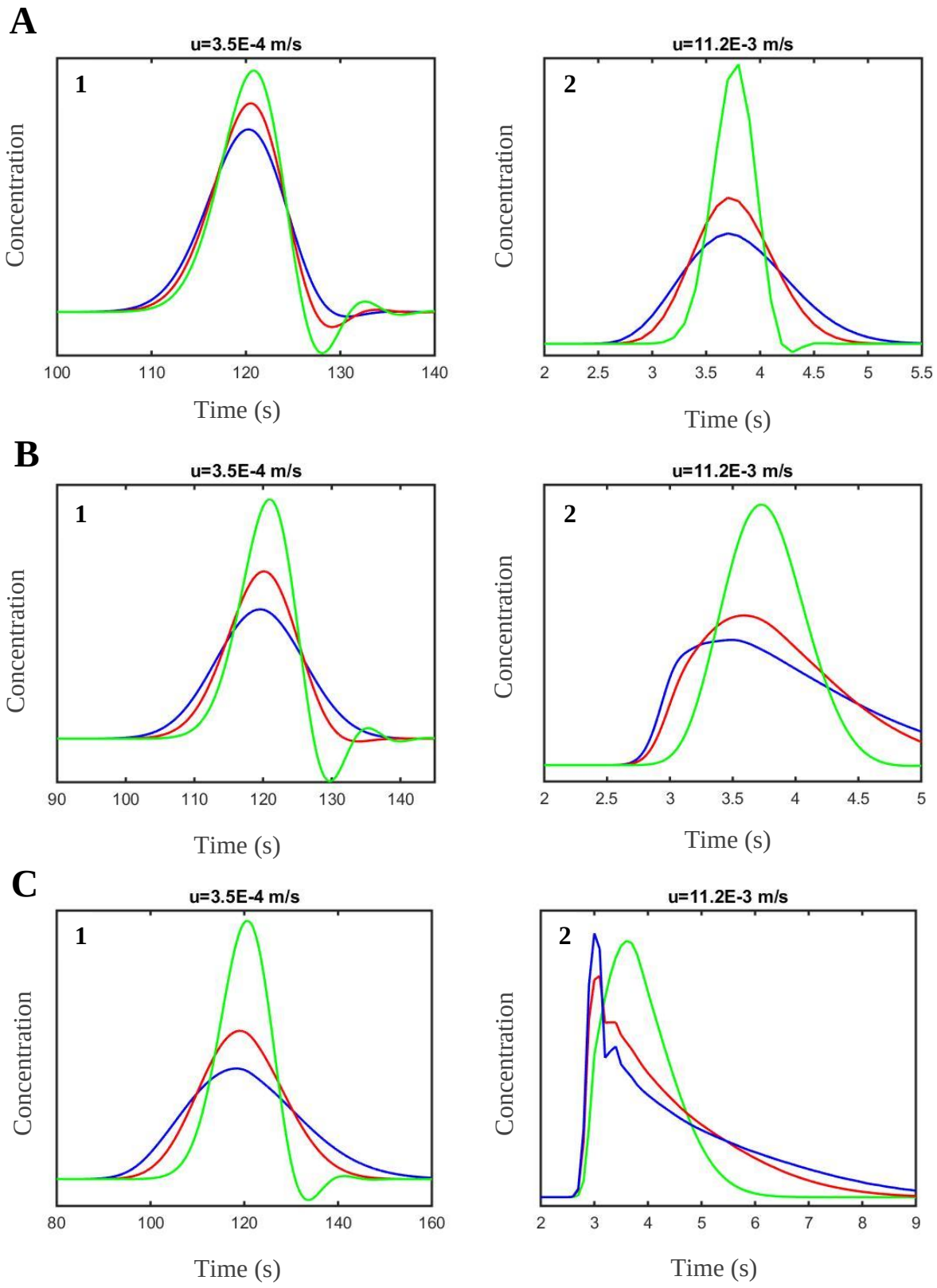

Figure 3. 4 Peak broadening of particles with different diffusion coefficients (Green: D= 5.0× 10^{-10} m^2/s, Red: D= 1.0× 10^{-10} m^2/s, Blue: D= 5.0× 10^{-11} m^2/s) at different diameters (A) 25 μm, (B) 50 μm, (C) 100 μm

Table 3. 3 Minimum time and Peclet number for different capillary diameter at a linear velocity of 1.4×10^{-3} m/s

D (m/s^2)	5.0E-11		1.0E-10		5.0E-10	
R_c(μm)	t_{min}	Pe	t_{min}	Pe	t_{min}	Pe
25	15.6	350	7.8	175	1.6	35
50	62.5	700	31.3	350	6.3	70
100	250	1400	125	700	25	140

Table 3. 4 Minimum time and Peclet number for different capillary diameters at a linear velocity of 11.2×10^{-3} m/s

D (m/s^2)	5.0E-11		1.0E-10		5.0E-10	
R_c(μm)	t_{min}	Pe	t_{min}	Pe	t_{min}	Pe
25	16	5600	8	2800	2	560
50	63	11200	31	5600	6	1120
100	250	22400	125	11200	25	2240

Table 3. 5 Minimum time and Peclet number for different capillary diameters at a linear velocity of 3.5×10^{-4} m/s

D (m/s^2)	5.0E-11		1.0E-10		5.0E-10	
R_c(μm)	t_{min}	Pe	t_{min}	Pe	t_{min}	Pe
25	16	175	8	88	2	18
50	63	350	31	175	6	35
100	250	700	125	350	25	70

Figure 3.5 shows the %Error for the estimation of diffusion coefficient using taylogram and $\mathbf{R^2}$ for goodness of fit of taylogram at different diameters at a velocity of 1.4×10^{-3} m/s. Comparing the combination of %Error and $\mathbf{R^2}$ for the three diameters, it is concluded that a capillary diameter of 50 µm has the best combination of %Error and $\mathbf{R^2}$. For larger diameters, smaller velocities give better result and for smaller diameters, larger velocities are better. Use of all diameters is possible for TDA when velocity is optimized for that specific diameter. However, experimentally, using larger diameters with slower bulk motion is time consuming, and using smaller diameters is always accompanied by column clogging.

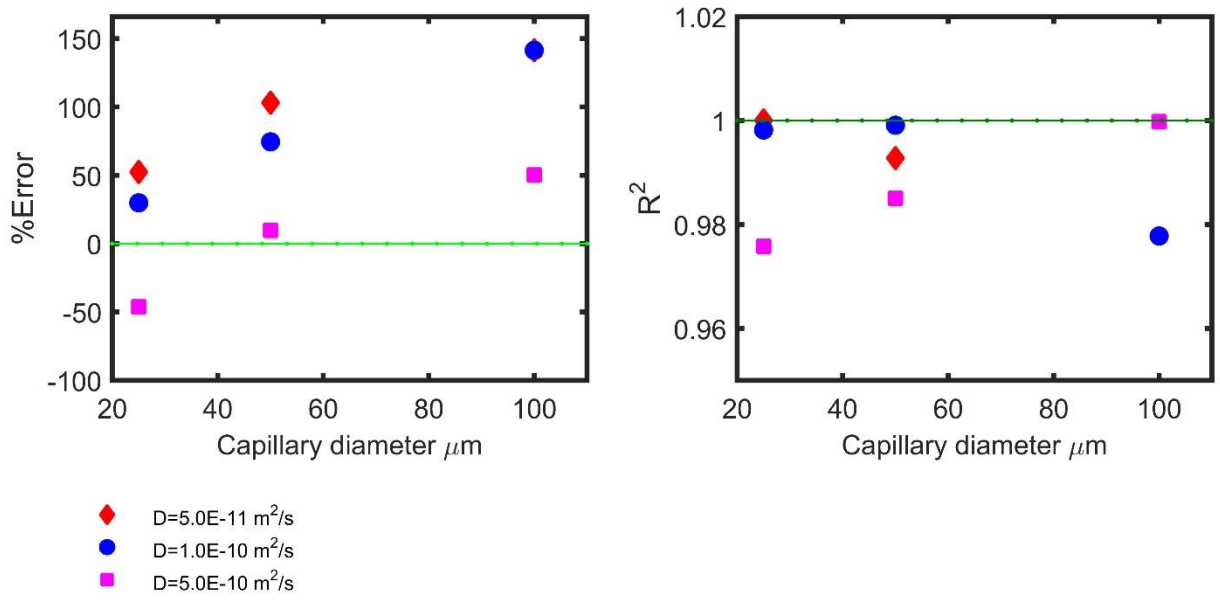

Figure 3. 5 %Error and R^2 for particles of different diffusion coefficient at different capillary diameters (25 µm, 50µm, 100µm) at linear velocity of 1.4×10^{-3} m/s

3.3.1.3. Effect of capillary length

In this section, we used capillary columns with different lengths to study TDA performance and conditions. Capillary length does not directly affect the Peclet number or the minimum time required for particles spend in the column. It does affect the time that the particles spend in the column. For all capillary lengths, the Peclet number decreases as the diffusion coefficient increases. As the Peclet number decreases, the second condition of TDA may be violated, because axial diffusion becomes more significant. As the capillary length increases, to maintain a constant migration time, we need to increase the linear velocity which leads to higher Peclet numbers and favors TDA conditions. At shorter lengths, the velocity must be small to give diffusion enough time to fill the column radially, which is more crucial for particles with smaller diffusion coefficients. However, the decrease in velocity leads to smaller Peclet numbers which is in contrast with the second TDA condition. In general, higher velocities give better results when using longer columns and vice versa when using shorter columns.

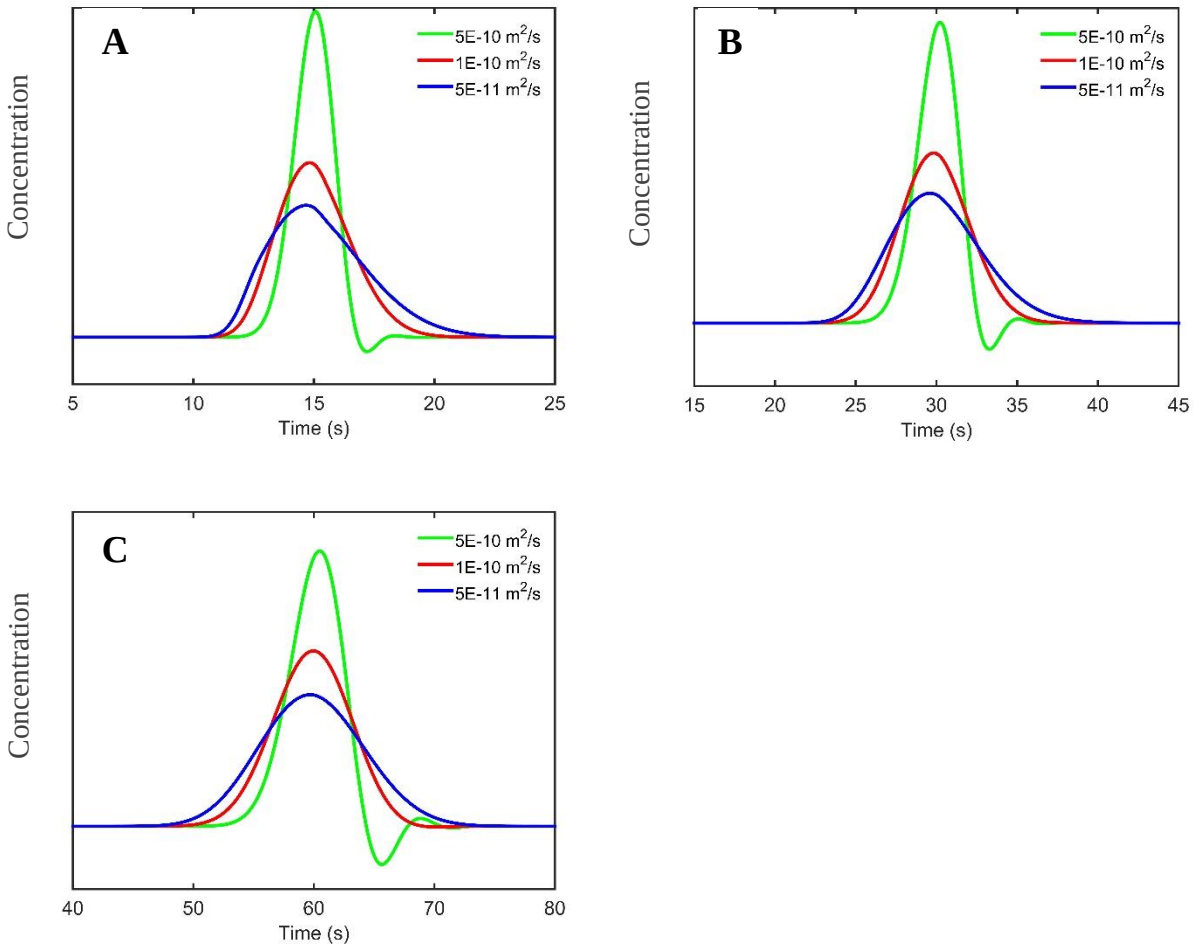

Figure 3. 6 Taylogram of different diffusion coefficient at different capillary lengths (A) 2cm, (B) 4cm, (C) 8cm, at a linear velocity of 1.4×10^{-3} m/s

Figure 3.7 shows %Error for the estimation of diffusion coefficients and the $\mathbf{R^2}$ for the taylograms fitted to Gaussian functions. All these simulations were conducted at a linear velocity of 1.4×10^{-3}

m/s.

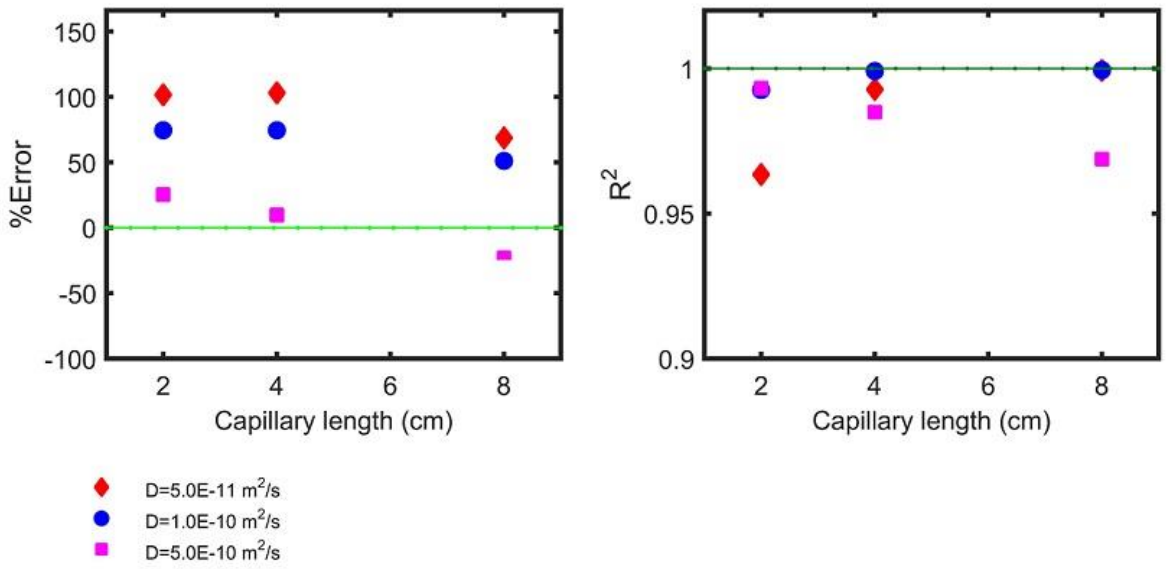

Figure 3. 7 %Error and R^2 for particles of different diffusion coefficient at different capillary lengths (2cm, 4cm, 8cm) at a linear velocity of 1.4×10^{-3}

According to Table 3.4, for capillary columns with a diameter of 50 μm the minimum time for the particles to spend time in the column increases as the diffusion coefficient decreases. Therefore, shorter columns are not suitable for particles with larger diffusion coefficients which is also confirmed in Figure 3.6A. The taylogram for the blue peak deviates from a normal distribution as the column length decreases because the particles do not get enough time to fill the column radially which leads to a smaller $\mathbf{R^2}$ and higher %Error (Figure 3.7).

According to Figure 3.6, as the column length increases, the negative peak becomes more significant. As explained in section 3.3.2.1, this might be due to the effect of axial diffusion happening at the same time and moving the particles in the axial direction very quickly. Since in

longer columns the particles spend more time in the column, so there is more time for the particles to diffuse axially during dispersion.

3.3.2. Dispersion of particles in the presence of electrophoretic flow

TDA offers some advantages in terms of its accuracy, precision, and simplicity. However, in classical TDA, for mixtures all of the particles elute at the same time and as a result, the data analysis for each particle becomes more complicated and inexplicit. Cottet *et al.* established the equations used to calculate the average diffusion coefficient for highly polydisperse samples. [145] Separating the particles in the mixture is an alternative way to study Taylor dispersion of particles. Unlike Poiseuille flow, electrophoresis is a discriminative force that separates particles based on their charge-to-size ratio. In this section, TDA in the presence of electrophoretic flow is studied numerically. TDA evaluates the diffusion coefficients of the particles and therefore their hydrodynamic size. Besides separation, electrophoretic flow gives the charge-to-size ratio of the particles. By calculating particle size from TDA, the average charge of the particles can also be determined.

3.3.2.1. Validity of TDA in the presence of electrophoretic mobility

TDA is conventionally performed under Poiseuille flow, and TDA conditions are investigated accordingly. In classical TDA, two conditions must be fulfilled to be able to estimate the diffusion coefficient of particles using the elution time and the peak variance. These conditions must be revisited when electrophoretic mobility is added to the system.

For our system, we assume that the capillary wall is neutral, and therefore electroosmotic flow does not exist. Thus, when applying voltage and pressure simultaneously the net flow motion only stems from the electrophoretic and Poiseuille flow. In TDA parabolic profile of the flow in the column is a significant factor in the Taylor dispersion of particles. Hence the parabolic flow should not be disturbed while voltage is applied to the system. Applying both pressure and voltage, molecules in the solute move faster due to the presence of electrophoretic mobility of particles, and so a constant forward shift for the flow along the tube is expected. The combination of voltage and pressure results in higher velocities which decrease the amount of time molecules spend in the column. To meet the first TDA condition, the migration time must be long enough so that the molecules spread out radially; therefore, the linear velocity should be smaller than conventional TDA. By adding electrophoretic flow, the second TDA condition is not disturbed because when the net velocity increases, the Peclet number increases, which fulfills the second TDA condition of the negligibility of longitudinal diffusion.

3.3.2.2. Size and charge characterization of mixture

In this section, dispersion is studied under Poiseuille and electrophoretic flow. An electric field is applied with pressure to separate the particles with different charge-to-size ratios. Also, information on the charge-to-size ratio of molecules is achieved. Having collected size information from TDA, the electrophoretic mobility gives the average charge of the particles. Figure 3.8 shows the electropherogram of 3 particles with different diffusion coefficients when pressure and voltage are applied to the system. As opposed to Figure 3.3, particles are being eluted at different times, and are being separated.

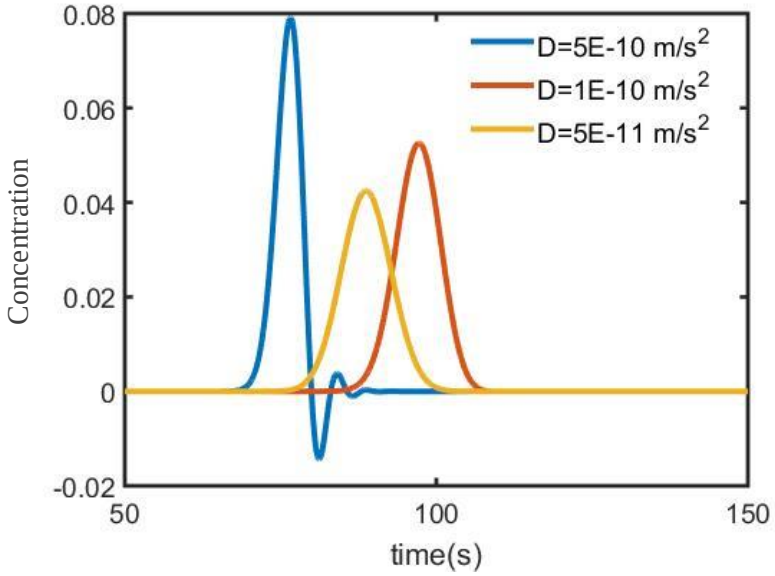

Figure 3. 8 Concentration profile for particles with different size and charge at 3.5× 10^{-4} m/s and 400 volts.

Different combinations of linear velocities and voltages are used and %Error on the estimation of diffusion coefficient is presented in Figure 3.9.

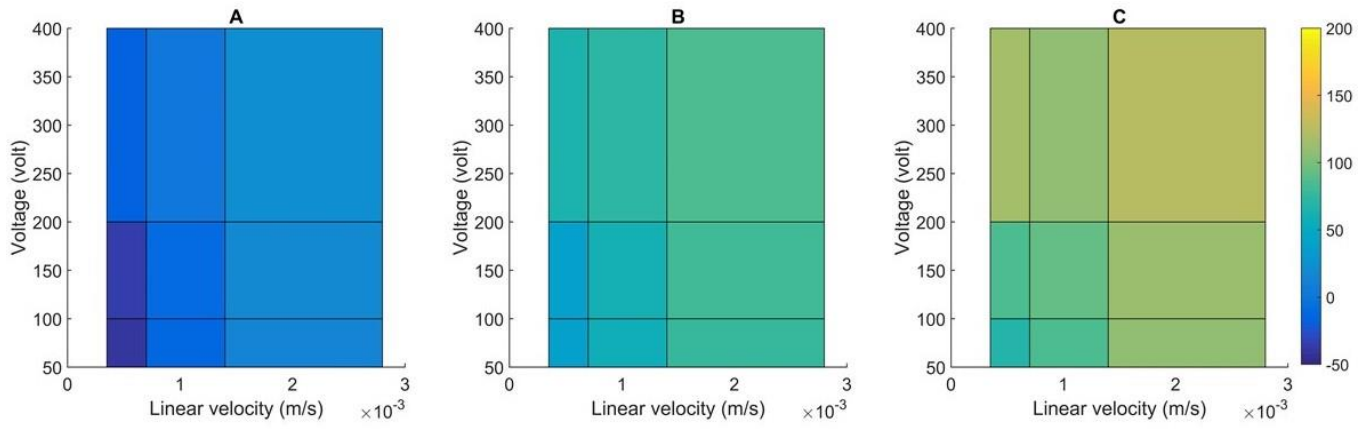

Figure 3. 9 %Error for particles with different diffusion coefficients (A) 5.0× 10^{-11} m^2/s (B) 1.0× $10^{-11}m^2$/s (C) 5.0× $10^{-10}m^2$/s with various combination of velocity and voltage

It is apparent that as the diffusion coefficient increases (smaller size), the %Error increases with the same combination of voltage and velocity. This can be explained in terms of both TDA conditions. Molecules with larger diffusion coefficients have smaller hydrodynamic size and therefore higher electrophoretic mobility. So, molecules might migrate faster in the column and violate the first TDA condition. Also, a higher diffusion coefficient means a smaller Peclet number, which contradicts the second TDA condition.

For each particle, as we increase the voltage and linear velocity, the error increases. Larger voltage means higher electrophoretic velocity and therefore more deviation from classical TDA. %Error increases because we are using the equation derived for classical TDA, even though the particles are not under the same classical TDA conditions. In Chapter 5, the equation for estimation of diffusion coefficients in the presence of electrophoretic flow is modified to include the electrophoretic mobility. Including electrophoretic mobility in the equation lowers the error on the estimation of diffusion coefficients.

Since the voltage increases the net velocity, the linear velocity from pressure must be decreased to give the particles enough time to redistribute radially. By increasing the linear velocity the time particles spend in the column is decreased which violates the first TDA condition, increasing the %Error.

Table 3. 6 Charge of particles calculated with the electrophoretic mobility obtained from COMSOL ($u=1.4\times 10^{-3}$ m/s)

D (m^2/s)	Input charge	Calc-charge-400	Calc- charge'-400	Calc-charge-50	Calc- charge'-50
5.00E-10	1	**1.03**	**0.74**	**0.89**	**0.79**
1.00E-10	2	**2.27**	**1.15**	**3.31**	**1.87**
5.00E-11	6	**6.82**	**2.79**	**10.05**	**4.83**

Table 3.5 shows the charge calculated for 3 particles of different sizes when the linear velocity of 1.4×10^{-3} m/s and two extreme voltages of 400 and 50 volts are used. These charges are derived from the electrophoretic term (Eq (3-6)) with the first column using the input diffusion coefficient and second column using the calculated diffusion coefficient. As the diffusion coefficient decreases the calculated charge deviates more from the input charge. This could be due to smaller electrophoretic velocity of these particles and therefore higher relative error in calculating the value of electrophoretic velocity from the electropherogram. For the same reason, by decreasing voltage, the error in charge evaluation is increased which is again due to the decrease in electrophoretic velocity.

The charge calculated using the calculated diffusion coefficient deviates more from the input charge. This happens because the error in the calculation of diffusion coefficient is also included in the calculation of charge as well.

$$\mu_{ep} = \frac{v_{ep}}{E} = \frac{Q}{6\pi\eta R_h} \qquad (3\text{-}6)$$

In summary, using higher voltage is advantageous in estimating electrophoretic mobility; however, it results in more deviation from classical TDA. By including the electrophoretic term in the estimation of the diffusion coefficient of particles, the diffusion coefficient is estimated correctly. Higher voltage results in higher resolution and higher accuracy in the estimation of average charge.

3.4 Conclusion

In this chapter, the numerical modeling of TDA is used to study the effect of pressure, capillary length and diameter on the evaluation of diffusion coefficient of components of a mixture. The effect of applying voltage on the system is also studied. To estimate the diffusion coefficient of components of a mixture with different sizes accurately, the system parameters need to be optimized. The medium linear velocity and medium capillary radius is used to meet the TDA conditions for large and small particles. Different lengths of capillary column can be used as long as TDA conditions are met. A higher voltage gives larger error because of more deviation from classical TDA. When using voltage and pressure for TDA, the equations must be modified accordingly. This work demonstrates the performance of TDA on a small scale which is advantageous when working with microchips. The applicability of using microchips for TDA offers a rapid and easy way for the characterization of particle size and other parameters.

Chapter 4: Size evaluation of proteins and small molecules using dynamic light scattering, Taylor dispersion analysis, stopped migration CE

4.1. Introduction

The size of protein is an important part of characterizing any protein molecule. Having the knowledge about the size of a protein provides useful information on the presence of monomer, dimer and trimer, as well as the aggregation state, denaturation, and change in conformation. Different methods are currently used to determine protein sizes such as DLS which is a most commonly used technique and a gold standard method. Capillary electrophoresis which is a powerful separation technique has also been used for sizing purposes using different approaches such as stopped migration method and Taylor Dispersion approach. [146]

4.1.1 Dynamic light Scattering

Dynamic light scattering (DLS) is a well stablished method which is often used for particle sizing. DLS is an ideal technique to for characterizing proteins in a variety of conditions and it can be used in early stage of research to provide information about the monodispersity of the sample, aggregation state, stability changes in quaternary structure. [147]

In this method particles undergo a Brownian motion and the average velocity of particles depends on particle size, their thermal energy, and the viscosity of the medium. In DLS, a laser beam is directed into a solution, when it strikes a particle, the light is scattered in all directions. The

scattered light is function of hydrodynamic size of the particles and larger particles scatter more light than smaller molecules at the same concentration. In this method particles undergo a Brownian motion in which the average velocity depends on particle size, their thermal energy, and the viscosity of the medium. Due to Brownian motion, the scattered light fluctuates which is directly related to the rate of diffusion of the molecules in the solution. The correlator measures the decay rate of the scattered light and the measured decay rate is related to the diffusion rate of the particles. The Einstein Stokes equation which was formulated at the beginning of the twenties century is used to correlate the diffusion rate of the particles to the medium and particle hydrodynamic size. [148]

4.1.2 Taylor dispersion analysis

Taylor Dispersion Analysis (TDA) is a recently developed technique that is used for sizing of a variety of small and large molecules such as amino acids, peptides and proteins. In this method, a nanoliter volume of sample is injected into the column containing the buffer under a constant pressure. The sample pulse broadens as it flows along the column due to dispersion which is combination of radial diffusion and axial convection. As the sample plug passes the detection window, the absorbance is plotted as a function of time to produce the taylogram. The width of the taylogram is related to the molecular diffusion coefficient of the solute in the sample. Analysis of this taylogram gives the molecular diffusion coefficient and hence hydrodynamic radius of the molecules. [34, 119] Hydrodynamic radius is then determined using Einstein-Stokes equation. [148] UV absorbance is used to detect target molecules at fixed window positions along the microcapillary.

Eq (4-1) is used for estimation of diffusion coefficient using the characteristics of the peak, where R_c is the radius of the column, t_0 is the migration time, and σ_t^2 is the variance of the peak. Eq (4-2) is Stokes-Einstein equation that is used for calculation of hydrodynamic radius of particle.

$$D = \frac{R_c^2 t_0}{24\sigma_t^2} \qquad (4\text{-}1)$$

$$R_h = \frac{k_B T}{6\pi\eta D} \qquad (4\text{-}2)$$

4.1.3 Stopped migration capillary electrophoresis

Stopped migration is a different approach to estimate the diffusion coefficient of molecules using capillary electrophoresis. Eq (4-3)[149] shows in CE, the variance of the peaks is result of various source of dispersion.

$$\sigma_{\text{total}}^2 = \sigma_{inj}^2 + \sigma_{det}^2 + \sigma_D^2 + \sigma_{\Delta\kappa}^2 + \sigma_{\Delta T}^2 + \sigma_{other}^2 \qquad (4\text{-}3)$$

where σ_{total}^2 is the total variance of the peak and $\sigma_{\text{inj}}^2, \sigma_{\text{det}}^2, \sigma_{\text{D}}^2, \sigma_{\Delta\kappa}^2, \sigma_{\Delta\text{T}}^2, \sigma_{\text{other}}^2$ refers to the variances due to injection plug width, detector zone width, sample diffusion, conductivity effects, Joule heating, and other effects such as analyte-wall interactions, respectively.

Capillary electrophoresis with stopped migration is a method used to measure the diffusion coefficient of molecules. In this method, the electrophoresis run is parted into two sections: first, an electric filed is applied and molecules migrate under electrophoretic and electroosmotic flow. Then, the electric filed is stopped for 2 hours before the molecules reach the detection window.

During this time, diffusion is the only phenomenon occurring. The electric restarted after 2 hours and the molecules migrate toward the detection window. The variance of the eluted peak is measure and compared to when the samples is run under normal condition. Since all variances except diffusion are constant between the runs, the difference in the variance of peaks estimates the diffusion coefficient of the molecule.

$$\sigma_D^2 = \sigma_{t+2hr}^2 - \sigma_t^2 \qquad (4\text{-}4)$$

Where σ_D^2 is the increase in the variance due to diffusion, σ_{t+2hr}^2 is the variance observed with a stopping time of 2 hours, and σ_t^2 is the variance observed without stopping. The diffusion coefficient can then be calculated using the Einstein equation. [149]

$$D = \frac{\sigma^2}{2t} \qquad (4\text{-}5)$$

σ_D^2 in Eq (4-4) is measure in units of time (s^2). To calculate the diffusion coefficient in units of (m^2/s) using Eq (4-5), the spatial variance (σ_l^2) must be calculated using:

$$\sigma_l^2 = \sigma_D^2 (\frac{L_d}{t})^2 \qquad (4\text{-}6)$$

Where σ_l^2 is the spatial variance of the peak, σ_D^2 is the temporal variance of the peak, L_d is the length of the capillary to the detector, and t is the migration time without stopping. [149]

4.2 Experimental section

4.2.1 Chemical and materials

All proteins (Bovine Serum Albumin (BSA), Human Serum Albumin (HSA), ImmunoglobinG (IgG)), peptides (Angiotensin II, Phe-Tyr), and amino acids (Tryptophan) with minimum of 95% purity were purchased from Sigma-Aldrich (St. Louis, MO, U.S.A.). Formic acid (88%) was

purchased form Fisher Scientific (Nepean, ON, Canada). Polyethyleneimine coating reagent of trimethoxysilylpropyl-modified polyethyleneimine, 50% in isopropanol was purchased from Gelest Inc. (Morrisville, PA). Solutions of Proteins and Peptides were prepared in deionized 18 MΩ water and were stored at -20°C unless otherwise stated. All sample solutions and buffers were filtered through 0.22 µm sterile, Nylon syringe filters. All DLS studies were conducted at 25° with 0.5% formic acid solvent as buffer.

4.2.2 Instrumentation

The studies were performed on a P/ACE MDQ capillary electrophoresis system (Beckman Coulter, Brea, CA) with a UV detection. CE studies were carried out on a 50µm inner diameter (I.D.), 365µm outer diameter (O.D.), 60 cm length (L) fused silica capillary (Polymicro Technologies, Phoenix, AZ) coated with cationic Polyethylenimine (*PEI*). DLS studies were performed on a Malvern Zetasizer (Nano-ZS, Malvern 75-01).

4.3 Results and discussion

4.3.1 Size evaluation using dynamic light scattering

Dynamic light scattering (DLS) is a well-established method to measure the hydrodynamic size of particles. in this section, we use DLS to evaluate the size of the proteins and confirm that the proteins have not denatures or aggregated during the preparation. Figure 4.1 shows the results obtained from DLS for BSA, in which data are analyzed with cumulant method.

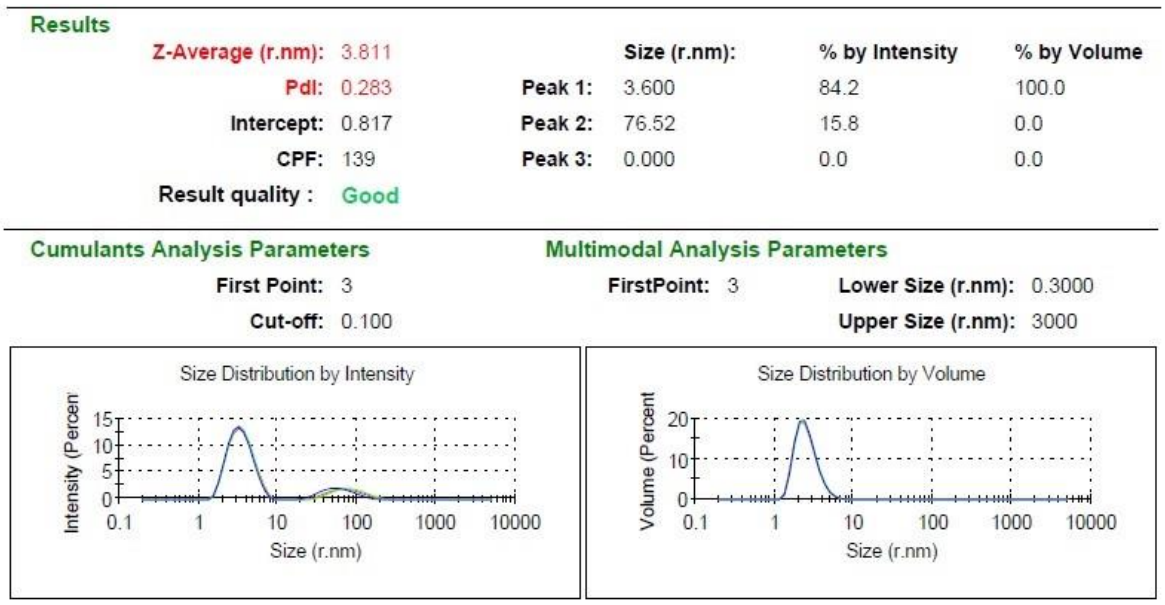

Figure 4. 1 Z-average and polydispersity index (PDI) obtained for BSA using Dynamic Light scattering instrument. Intercept is used to evaluate the signal to noise ratio from a measure sample and is used to judge the data quality. Conditional Probability Function (CPF) evaluates the result quality. Size distribution by intensity (left) is an intensity distribution of particle sizes which is proportional to the square of the molecular weight. Size distribution by volume (right) describes the relative proportion of multiple components in the sample based on their mass or volume rather than based on their intensity.

Table 4.1 shows the hydrodynamic radius for proteins: BSA, HSA, IgG (Human), IgG (Goat), and dimer BSA. DLS was not able to measure the size of the peptides and amino acids, because it is more sensitive to larger particles, therefore gives more accurate results for proteins than for peptides or amino acids.

Size for HSA and BSA (MW≅ 66kDa) are in the same range, 3.049 nm and 3.811 respectively. The hydrodynamic size for the two types of IgG are 11.08 and 13.70 nm. Immunoglobulins (IgG) have higher molecular weight (MW≅ 150kDa), therefore expected to have bigger hydrodynamic size than serum albumins.

DimerBSA is expected to have double size of BSA, but the reported size is 4 times bigger. This can be due to the higher sensitivity of DLS to larger particles or interaction of two dimers together.

Table 4. 1 Size and polydispersity obtained from DLS

Proteins	Hydrodynamic size (nm)	Poly dispersity index (PDI)
BSA	3.811	0.283
HSA	3.049	0.216
IgG (Human)	13.70	0.282
IgG (Goat)	11.08	0.090
Dimer BSA	16.55	0.584

4.3.2 Size and charge evaluation using stopped migration CE

The proteins and peptides are analyzed with stopped migration method here. Figure 4.2 shows the concentration profile for two molecules with different sizes, Tryptophan and IgG (one amino acid and one protein). Each one was stopped in the column for 2 hours and electrophoresed again. Since in CE, EOF is causing the bulk motion, the velocity profile in the column is flat. Therefore, only longitudinal diffusion is happening. Because diffusion coefficient for Tryptophan is bigger than IgG, during 2 hours of waiting in the column, it diffuses

more and therefore the peak becomes broader. However, diffusion coefficient for IgG is very small, and so, the dispersion of this molecule along the column is very small. For such molecules with small diffusion coefficient, the difference in the peak variance is measured with difficulty and

the error percentage will be higher. Therefore, this technique may not be suitable for large molecules.

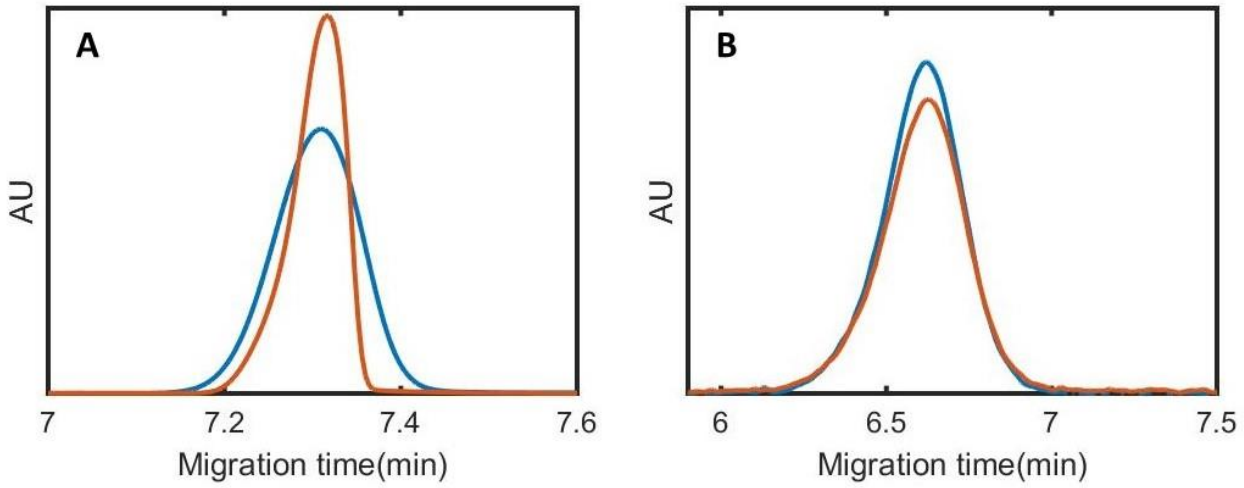

Figure 4. 2 Broadening of the electropherograms observed for (A) tryptophan (B) BSA. Blue: with turning off the electric field for 120 min, Orange: Without turning off the electric field.

Table 4. 2 Calculated diffusion coefficient and size using stopped migration method

	$\sigma_{l,1}^2(m^2)$ *	$\sigma_{l,2}^2(m^2)$**	D (m^2/s)	R_h(nm)
BSA	NA	NA	NA	NA
HSA	NA	NA	NA	NA
Dime BSA	NA	NA	NA	NA
IgG	NA	NA	NA	NA
AngioTensin II	1.55×10^{-6}	9.66×10^{-6}	4.12×10^{-10}	0.41
Phe-Tyr	1.73×10^{-6}	9.55×10^{-6}	4.23×10^{-10}	0.42
Tryptophan	1.24×10^{-6}	1.95×10^{-6}	3.16×10^{-10}	0.32

* spatial variance of orange electropherogram in Figure 4.2.
**spatial variance of blue electropherogram in Figure 4.2.

Table 4.2, shows calculated diffusion coefficient for molecules with a wide range of size using stopped migration method. In this table, the spatial variances for each molecule is calculated in units of length using Eq (4-6). Then Eq (4-5) is used to calculate the diffusion coefficient of each molecule. The difference in peak variance is very small for large particles and it is in the standard deviation range so we could not derive diffusion coefficient for the large particles.

4.3.3 Size evaluation using Taylor dispersion analysis

4.3.3.1 Effect of concentration of size of BSA

Taylor dispersion analysis is an absolute method and does not require calibration. Therefore, no knowledge of concentration is required. In ideal condition, the concentration should not affect the size value but in experimental conditions, lower concentration may not give strong enough signal and higher concentration may lead to undesired interaction between the molecules. In this section, the variation of size for BSA is studied at different concentrations. Figure 4.3 shows the taylogram for BSA using TDA when only pressure or combination of pressure and voltage is applied. There is a negative peak coming out along with BSA that may be due to some impurity or solvent. When only pressure is applied the negative peak is coming out at the same time as BSA peak causing a distortion in the peaks. However, when voltage is applied with pressure, the negative peak is well resolved leading to a well-shaped Gaussian peak. Table 4.3 shows the effect of concentration on the size of BSA. The variation in size is within the standard deviation in the first column of the table where voltage in applied with pressure. But, in the second column where only pressure is applied, the standard deviation between sizes of BSA at different concentration is 0.8 which is

bigger than the standard deviation calculated for each concentration. This might be due to the distortion of peaks in the presence of negative peak which makes Gaussian fitting more complicated. In general, for both columns, the size is increasing as the concentration increases. As the concentration increases, viscosity of the solution can change and aggregation may happen which leads to different sizes.

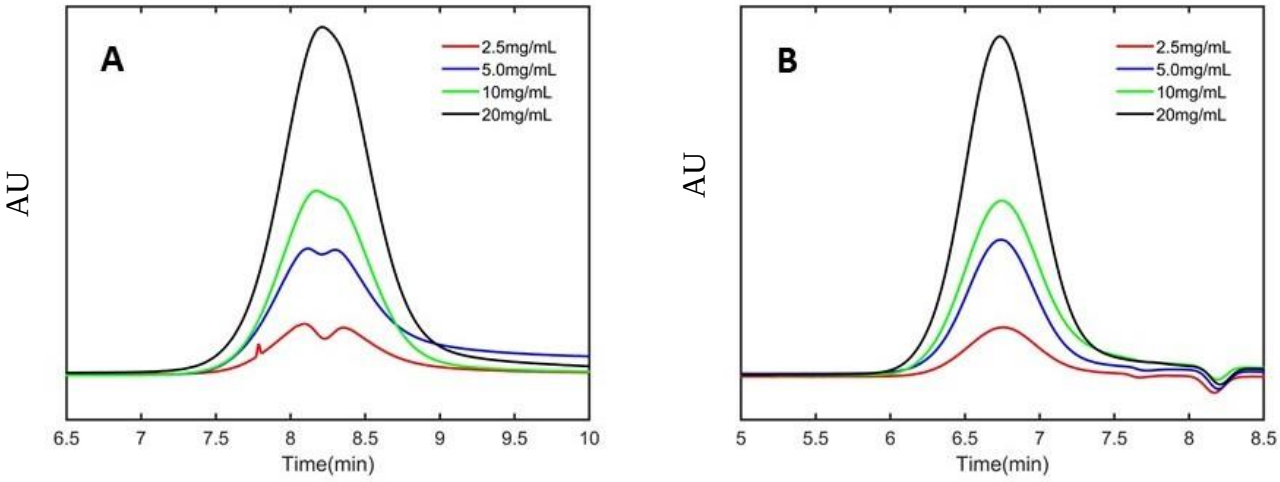

Figure 4. 3 The effect of concentration on the taylogram of BSA with and without applying voltage (A) pressure only: 1psi, (B) pressure and voltage: 1psi+ 10kV

Table 4. 3 Size of BSA at different concentrations

Concentration (mg/mL)	Size (nm) by TDA (P+V)	Size (nm) by TDA (P)
2.5	5.31 ∓ 0.17	7.79 ∓ 0.14
5	5.38 ∓ 0.26	4.62 ∓ 0.09
10	5.40 ∓ 0.38	6.27 ∓ 0.05
20	5.42 ∓ 0.10	6.45 ∓ 0.48

4.3.3.2 Sizing of proteins and peptides using TDA

In this section, the size of proteins and peptides are evaluated with TDA method. All the molecules are separated under the same condition such as similar buffer composition, injection length, mobilizing pressure. The peak width of the electropherograms for each molecule and the migration time is used to estimate the diffusion coefficient. Einstein-Stokes equation is then used for calculating the hydrodynamic size of each molecule. Each run is repeated three time to calculate the standard deviation in calculation of the reported size. As it is shown in the table 4.3 the standard deviation in size is in the acceptable range and relative standard deviation is below 10% for all the proteins and peptides. As opposed to DLS which is more sensitive to larger molecules and Stopped migration method which is more sensitive to smallest molecules, TDA is able to cover a wider range of sizes for proteins, amino acids, and peptides.

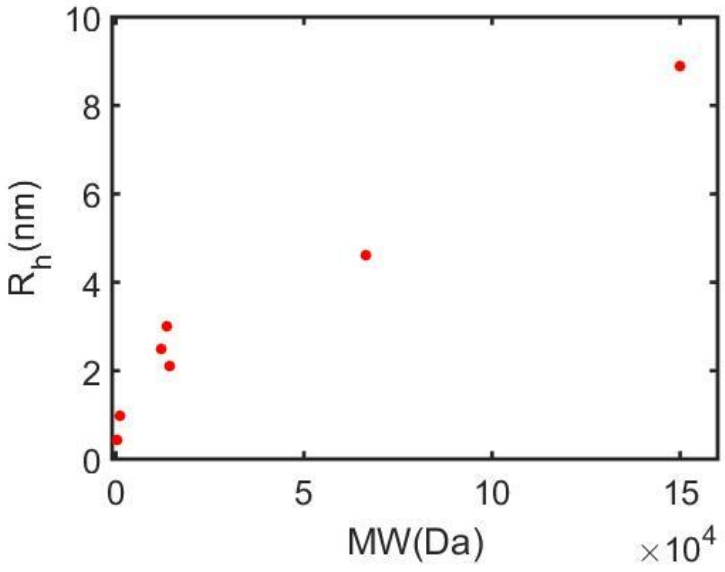

Figure 4. 4 Correlation of molecular weight and calculated hydrodynamic size: as the molecular weight is increasing, the hydrodynamic size is increasing

Figure 4.4 shows, as the molecular weight of proteins and peptides increases, their hydrodynamic size also increases. The hydrodynamic size calculated from diffusion coefficient for a molecule is the size of a hypothetical hard sphere which has the same diffusion coefficient as the molecule of interest. However, In reality, proteins with almost similar molecular weight may not all be spherical and may be solvated slightly differently. [150] This explains why in Figure 4.4, proteins with similar molecular weight have slightly different hydrodynamic size.

Table 4. 4 Size evaluation of proteins and peptides using TDA

	MW (Da)	**Concentration (mg/mL)**	**R_h(nm)***	**%RSD**
IgG (Human)	150000	5.0	8.88 ∓ 0.61	6.87
BSA	66500	5.0	4.62 ∓ 0.09	1.95
Lysozyme	14300	10.0	2.10 ∓ 0.04	1.90
Cytochrome C	12000	4.0	2.50 ∓ 0.04	1.60
RNase A	13700	2.0	3.00 ∓ 0.25	8.33
AngioTensin	1046	2.5	0.97 ∓ 0.05	5.15
Tryptophan	204	3.75	0.44 ∓ 0.03	6.82

4.4 Conclusion

The hydrodynamic size of some proteins and peptides and an amino acid was evaluated using three different methods: DLS, TDA, and Stopped migration CE. DLS was more sensitive to larger molecules such as proteins and was not able to give accurate and precise results for small molecules such as peptides and amino acids. On the other hand, stopped migration CE method gave better results for small molecules than the bigger ones. TDA covered wider size range and it was able to provide reproducible results for small and larger molecules. TDA is a remarkable candidate for study of a mixture of molecules with different sizes.

Chapter 5: Taylor dispersion analysis in the presence of electrophoretic mobility

5.1 Introduction

Taylor dispersion is becoming one of few promising methods to evaluate diffusion coefficient and hydrodynamic size of particles of various sizes such as polymers, proteins, peptides, and small molecules [151-152]. TDA differentiates the particles based on their dispersion coefficient which varies by hydrodynamic radii of species[34, 128]. Therefore, no separation is achieved based on the retention of species which aggravates the application of this technique for mixtures. There have been studies for the use of TDA for the mixture of solutes, most of which calculate average diffusion coefficient and thus average hydrodynamic radius [153]. Cottet et al. formulated equations for the calculation of average diffusion coefficients of particles in the mixture. They showed the average diffusion coefficient value depends on the nature of the detector if it is a mass concentration or molar concentration-sensitive. They also compared values obtained by TDA with the ones achieved by DLS and concluded that for samples with monomodal and relatively low polydispersity, the average diffusion coefficients obtained from both methods are very close. However, for highly polydisperse samples, the difference in the values reported from the two techniques are significant [154]. For characterizing mixtures, other methods are proposed as well, in which, besides the average size, the information about the polydispersity of the mixture is also extracted. For example, Cipelletti et al. deconvoluted taylogram from a mixture into its components to report the average hydrodynamic size and polydispersity index [155]. Cumulant

method is a well-known approach, and it derives polydispersity index from taylogram [156]. Constrained Regularized Linear Inversion (CRLI) is another more recent data processing method to extract the probability density functions of diffusion coefficients from taylogram [157]. Although having polydispersity index beside average size provides useful information about the constituents of the mixture, the size and diffusion coefficient of each component are still undetermined. Also, the data analysis may become more complicated when dealing with particles of similar size. Separating the components of the mixture and then characterizing their size is another approach for dealing with mixtures. Cottet et al. investigated the use of capillary electrophoresis coupled to TDA for the characterization of nanoparticle mixtures. In this method, they used a loop column with three detection window; first, particles are separated under an electric field in CE, and when they pass the first window, the voltage is stopped and particles flow in the column with only pressure (classical TDA). This technique combines the separation power of CE with size characterization of TDA. This method offers comparable results to Dynamic light scattering (DLS) and hydrodynamic chromatography (HPC), but it requires having a column with three detection windows, which is not accessible in all CE instrument [158].

To achieve separation and size characterization using typical CE, we incorporated voltage in TDA, by applying pressure and voltage simultaneously. In this paper, we solved the convection-diffusion equation for system with Poiseuille and electrophoretic flow and derive the modified version of Taylor equation for determination of diffusion coefficient. We also, analyze particles of different sizes (proteins, peptides, amino acids) and compared their size using the equations used for classical TDA and our new equations. In the end, TDA with combination of pressure and voltage is used for size and charge determination of a mixture of BSA, Angiotensin II, and Tryptophan.

5.1.1 TDA theory

This section summarizes the main equations used to derive diffusion coefficient in TDA [159].

Convection-diffusion transfer equation shows how molecular diffusion and convection contributes to the mass transfer of chemical species in a fluid. The convection-diffusion transfer equation [160] for the flow in present case is given by:

$$\frac{\partial C}{\partial t} + U(r)\frac{\partial C}{\partial x} = \frac{D}{r}\frac{\partial}{\partial r}\left(r\frac{\partial C}{\partial r}\right) + D\frac{\partial^2 C}{\partial x^2} \qquad (5-1)$$

In which x and r measures the axial and radial position in a tube of radius R, respectively, and C and D are the concentration and diffusion coefficient of the analyte respectively.

The flow velocity obeys Poiseuille law [161] and is given by:

$$U(r) = 2\bar{U}\left(1 - \frac{r^2}{R^2}\right) \qquad (5-2)$$

In which, $\bar{U}$ is the average velocity of fluid in the tube.

In Taylor dispersion flow, the axial diffusion is assumed to be negligible, therefore $D\frac{\partial^2 C}{\partial x^2}$ is omitted from Eq (5-1).

$$\frac{\partial C}{\partial t} + U(r)\frac{\partial C}{\partial x} = \frac{D}{r}\frac{\partial}{\partial r}\left(r\frac{\partial C}{\partial r}\right) \qquad (5-3)$$

For solving Eq (5-3), it is assumed the process is steady in a reference frame moving with a velocity of $\bar{U}$.

$$\acute{x} = x - \bar{U}t \qquad (5-4)$$

Assuming the steady state condition for the process and combining Eq (5-2), Eq (5-3) and Eq (5-4) gives Eq (5-5).

$$\bar{U}\left(1-\frac{2r^2}{R^2}\right)\frac{\partial C}{\partial \acute{x}}=\frac{D}{r}\frac{\partial}{\partial r}\left(r\frac{\partial C}{\partial r}\right) \qquad (5-5)$$

By the assumption that $\frac{\partial C}{\partial x\prime}$ is independent of r, integration of Eq (5-5) results in Eq (5-6).

$$C(r)=\frac{\bar{U}}{D}\frac{\partial C}{\partial x\prime}\left[\frac{r^2}{4}-\frac{2r^4}{16R^2}\right]+k_1\ln(r)+C_0 \qquad (5-6)$$

In Eq (5-6), k_1 must be zero, otherwise at the center of the tube (r=0) the concentration will be infinite.

$$C(r)=\alpha\left[\frac{r^2}{R^2}-\frac{r^4}{2R^2}\right]+C_0 \qquad (5-7)$$

Where α is $\frac{\bar{U}R^2}{4D}\frac{\partial C}{\partial x\prime}$.

Eq (5-8) is used to obtain the average concentration across the tube.

$$\bar{C}=\frac{1}{A}\int C(r)dA=\frac{1}{\pi R^2}\int_0^R\int_0^{2\pi}C(r)r\,dr\,d\theta \qquad (5-8)$$

Variables r and θ in the integral are independent of each other, so we can integrate each variable independently and multiply the results together.

$$\bar{C}=\frac{2\pi}{\pi R^2}\int_0^R\left(\alpha\left[\frac{r^2}{R^2}-\frac{r^4}{2R^2}\right]+C_0\right)r\,dr \qquad (5-9)$$

$$\bar{C}=C_0+\frac{\alpha}{3} \qquad (5-10)$$

Substituting C_0 from Eq (5-10) in Eq (5-7) leads to Eq (5-11).

$$C(r)=\bar{C}+\alpha\left[-\frac{1}{3}+\frac{r^2}{R^2}-\frac{r^4}{2R^2}\right] \qquad (5-11)$$

To evaluate the extend of dispersion of solute in the column, average mass flux of the solute ($\bar{J}$) in the cross section of the tube is calculated using Eq (5-12).

$$\bar{J} = \frac{1}{\pi R^2} \int_0^R \int_0^{2\pi} MC(r)U(r)d\theta\, r dr \qquad (5-12)$$

Where C(r) is concentration of solute in radial direction with unit of mol/L and M is molar mass of solute with unit of g/mol.

Solving the integration in Eq (5-12) by substituting U(r) from Eq (5-2) and C(r) from Eq (5-11) gives Eq (5-13).

$$\bar{J} = -\frac{1}{12} M\bar{U}\alpha \qquad (5-13)$$

substituting α in Eq (5-13) gives the average mass flux across the capillary column (Eq (5-14)). According to Fick's first law, under assumption of steady state, mass flux and concentration gradient are related by the diffusion coefficient [162]. Because, our system results in a one-dimensional dispersion of the solute, the coefficient has the characteristics of the dispersion. therefore, the dispersion coefficient is obtained using Eq (5-14).

$$\bar{J} = \left(\frac{-R^2\bar{U}^2}{48D}\right)\frac{M\partial C}{\partial x'} \qquad (5-14)$$

Since $\bar{J}$ is the mass flux of solute, the concentration needs to be stated in mass per volume unit. Therefore, Molar Mass (M) is multiplied by Concentration (C) to convert the unit of concentration to g/L.

$$D' = \frac{-Flux}{Gradient} = \frac{R^2\bar{U}^2}{48D} \qquad (5-15)$$

D' is called dispersion coefficient. Eq (5-15) states that effectively solutes with smaller diffusion coefficient disperse faster in axial direction and vice versa.

Dispersion coefficient (D') is measured experimentally by evaluating the variance and migration time of eluted peaks. Einstein equation ($\sigma_l^2 = 2D't$) [165] is used to relate the spatial variance and migration time of the eluted peaks to the dispersion of the solutes.

Eq (5-16) is obtained by substituting Einstein equation in Eq (5-15) and converting spatial variance to temporal variance ($\sigma_l^2 = \bar{U}^2\sigma_t^2$). This equation is used to calculate the diffusion coefficient of solutes using migration time and temporal variance of concentration profile.

$$D = \frac{R^2 t}{24\sigma_t^2} \qquad (5-16)$$

Hydrodynamic size is estimated using Einstein-Stokes equation (Eq (5-17))[163].

$$\frac{k_B T}{6\pi\eta D} \qquad (5-17)$$

5.2 Experimental section

The capillary column was coated with HPC (Hydroxypropyl cellulose) to suppress the electroosmosis flow in the analysis; the column was rinsed with HPC for 20 minutes with 50 psi and then heated in the GC oven for 2.5 hours [164]. The buffer is 25mM ammonium acetate with pH of 3.5-4 to keep the species charged. All the particles (Proteins, peptides, amino acids) were dissolved in buffer with different concentrations (2-5 mg/mL) based on their solubility. The analytes were analyzed under pressure of 1 psi and voltage of 10 kV. The injection was 0.5 psi for 5 seconds. Capillary electrophoresis instrument from Beckman was used for all the analysis. The UV detector at the wavelength of 200 nm was used for detection. All the raw data were analyzed using the program coded in Matlab.

5.3 Results and discussion

Classical TDA uses only pressure for mobilization of bulk flow; therefore, no separation is achieved in this approach. Using voltage along with the pressure in TDA leads to simultaneous separation and size characterization of particles, which is advantageous when dealing with mixtures. However, Eq (5-8) is not accurate for the calculation of diffusion coefficients when voltage is applied besides pressure. In this section, we modify the equation for the calculation of diffusion coefficients for particles of different sizes which are analyzed under the combination of pressure and voltage. Also, we confirm the validity of the TDA when the voltage is applied beside pressure. Finally, the optimized combination of voltage and pressure is used to separate and characterize a mixture of protein, peptide, and amino acid.

5.3.1 Equations for the evaluation of diffusion coefficient in the presence of electrophoretic flow

In TDA technique, when voltage is applied, analytes move faster due to the electrophoretic flow. The net bulk motion is the combination of Poiseuille flow and electrophoretic flow (Eq (5-18)). Thus, the velocity in Eq (5-3) needs to be corrected which gives Eq (5-19). Assumption in Eq (5-4) is also made here that the process is in steady state with a moving frame with speed of $\overline{U}$.

$$U(r) = \bar{U}\left(1 - \frac{2r^2}{R^2}\right) + u_{ep} \qquad (5-18)$$

$$\frac{1}{r}\frac{\partial}{\partial r}\left(r\frac{\partial C}{\partial r}\right) = \left(\frac{\bar{U}}{D}\left(1 - \frac{2r^2}{R^2}\right) + \frac{u_{ep}}{D}\right)\frac{\partial C}{\partial x'} \qquad (5-19)$$

Eq (5-20) and Eq (5-21) are consecutive integration of Eq (5-19) which results in Eq (5-22).

$$r\frac{\partial C}{\partial r} = \frac{\bar{U}}{D}\frac{\partial C}{\partial x'}\left[\frac{r^2}{2} - \frac{2r^4}{4R^2}\right] + \frac{u_{ep}}{D}\frac{\partial C}{\partial x'}\frac{r^2}{2} + h_1 \qquad (5-20)$$

$$\frac{\partial C}{\partial r} = \frac{\bar{U}}{D}\frac{\partial C}{\partial x'}\left[\frac{r^1}{2} - \frac{2r^3}{4R^2}\right] + \frac{u_{ep}}{D}\frac{\partial C}{\partial x'}\frac{r}{2} + \frac{h_1}{r} \qquad (5-21)$$

$$C(r) = \frac{\bar{U}R^2}{4D}\frac{\partial C}{\partial x'}\left[\frac{r^2}{R^2} - \frac{2r^4}{4R^4}\right] + \frac{u_{epR^2}}{4D}\frac{\partial C}{\partial x'}\frac{r^2}{R^2} + h_1 \ln(r) + C_0 \qquad (5-22)$$

In Eq (5-22), h_1 must be zero, otherwise at the center of the tube (r=0) the concentration will be infinite.

$$C(r) = \alpha\left[\frac{r^2}{R^2} - \frac{r^4}{2R^4}\right] + \beta\frac{r^2}{R^2} + C_0 \qquad (5-23)$$

In Eq (5-23), α is $\frac{\bar{U}R^2}{4D}\frac{\partial C}{\partial x'}$ and β is $\frac{u_{ep}R^2}{4D}\frac{\partial C}{\partial x'}$.

To find C_0 in terms of $\bar{C}$ we use Eq (5-24).

$$\bar{C} = \frac{1}{\pi R^2}\int_0^R \int_0^{2\pi} C(r) r\, dr\, d\theta \qquad (5-24)$$

Eq (5-25) is obtained by solving the integration above.

$$\bar{C} = [\alpha\left[\frac{r^4}{2R^4} - \frac{r^6}{6R^6}\right] + \beta\frac{r^4}{2R^4} + \frac{1}{R^2}C_0 r^2]_0^R \qquad (5-25)$$

Using upper and lower limits, C_0 is shown in terms of $\bar{C}$, α, and β.

$$C_0 = \bar{C} - \frac{\alpha}{3} - \frac{\beta}{2} \qquad (5-26)$$

Substituting Eq (5-26) in Eq (5-23) gives Eq (5-27) concentration as a function of r.

$$C(r) = \bar{C} + \alpha\left[\frac{-1}{3} + \frac{r^2}{R^2} - \frac{r^4}{2R^4}\right] + \beta\left[\frac{-1}{2} + \frac{r^2}{R^2}\right] \qquad (5-27)$$

Average mass flux of solute in the cross section is calculated using Eq (5-12) with velocity presented in Eq (5-18).

Mathematica software is used to solve for $\bar{J}$ which is average mass flux of solute in the presence of electrophoretic mobility Eq (5-28).

$$\bar{J} = \left(\frac{-R^2(\bar{U}^2 + 2u_{ep}\bar{U})}{48D}\right)\frac{\partial C}{\partial x'} + u_{ep}\, C(x') \qquad (5-28)$$

Using Fick's first law, dispersion coefficient (D') is derived by dividing the average mass flux ($\bar{J}$) by the concentration gradient ($\frac{\partial C}{\partial x'}$).

$$D' = \frac{R^2\bar{U}^2}{48D} + \frac{R^2(2u_{ep})\bar{U}}{48D} - \frac{u_{ep}C(x')}{\frac{\partial C(x')}{\partial x'}} \qquad (5-29)$$

We introduce γ to simplify Eq (5-29).

$$\gamma = \frac{C(x')}{\frac{\partial C(x')}{\partial x'}} = \frac{\partial x'}{\partial \ln(C(x'))} \qquad (5-30)$$

Eq (5-31) is simplified version of Eq (5-29).

$$D' = \frac{R^2}{48D}\left(\bar{U}^2 + 2u_{ep}\bar{U}\right) - u_{ep}\gamma \qquad (5-31)$$

We use Einstein diffusion equation (Eq (5-32)) [165], to convert the dispersion coefficient to the spatial variance of the concentration profile.

$$\sigma_l^2 = 2D't \rightarrow D' = \frac{\sigma_l^2}{2t} \qquad (5-32)$$

Combining Eq (5-31) and Eq (5-32) gives Eq (5-33).

$$\frac{\sigma_l^2}{2t} = \frac{R^2}{48D}\left(\bar{U}^2 + 2u_{ep}\bar{U}\right) - \frac{D}{D}u_{ep}\gamma \qquad (5-33)$$

By rearranging Eq (5-33), diffusion coefficient is derived as a function of spatial variance, migration time, Poiseuille and electrophoretic velocity (Eq (5-34)).

$$D = \frac{R^2 t}{24\sigma_l^2}\left(\bar{U}^2 + 2u_{ep}\bar{U}\right) - \frac{2Dt}{\sigma_l^2}u_{ep}\gamma \qquad (5-34)$$

Using Eq (5-35), we convert spatial variance to temporal variance, which is easily extracted from the eluted peaks.

$$\sigma_l^2 = \left(\bar{U} + u_{ep}\right)^2 \sigma_t^2 \qquad (5-35)$$

Both σ_l^2 in Eq (5-34) are replaced with the term on the right side of Eq (5-35).

$$D = \frac{R^2 t}{24\sigma_t^2} \frac{\left(\bar{U}^2 + 2u_{ep}\bar{U}\right)}{(\bar{U} + u_{ep})^2} - \frac{2Dt}{\sigma_t^2\left(\bar{U} + u_{ep}\right)^2} u_{ep}\gamma \qquad (5-36)$$

To simplify Eq (5-36) we introduce δ and κ.

$$\delta = \frac{\left(\bar{U}^2 + 2u_{ep}\bar{U}\right)}{(\bar{U} + u_{ep})^2} \qquad (5-37)$$

$$\kappa = \frac{2u_{ep} t\gamma}{\sigma_t^2(\bar{U} + u_{ep})^2} \qquad (5-38)$$

Eq (5-39) is obtained by inserting δ and κ in Eq (5-36).

$$D = \frac{R^2 t}{24\sigma_t^2}\delta - \kappa D \qquad (5-39)$$

Eq (5-39) is rearranged to derive diffusion coefficient.

$$D = \frac{\frac{R^2 t}{24\sigma_t^2}\delta}{1 + \kappa} \qquad (5-40)$$

Eq (5-40) is a used when a voltage is applied in addition to the pressure, and electrophoretic flow is not zero. In classical TDA, δ equals 1 (Eqn (5-37)) and κ becomes zero (Eq (5-38)), therefore, Eq (5-40) equals to Eq (5-16). However, when voltage is applied, δ is smaller than 1, which makes numerator in Eq (5-40) smaller than the one in classical TDA and denominator bigger than 1. Therefore, for TDA with pressure and voltage, if corrections are not made and Eq (5-16) is used for calculation of diffusion coefficients, the obtained values will be bigger than expected which leads to smaller particles size.

5.3.2 Diffusion coefficient of particles in the presence of electrophoretic flow

Table 5.1 shows the values for diffusion coefficients estimated using Eq (5-16) for both classical TDA (D^*) and the one with voltage and pressure (D^{**}). As the electrophoretic velocity increases, %error increases which is due to more deviation from the classical TDA. When we use Eq (5-16) for the calculation of both $D^*$and D^{**}, the results for TDA with voltage are bigger than the ones for classical TDA. Therefore, the modified equation for the calculation of diffusion coefficients must be used (Eq (5-33)). For classical TDA, δ is equal to 1 and κ equals zero which makes this equation equal to Eq (5-16). When a voltage is applied along with pressure, δ becomes smaller than one due to the presence of electrophoretic velocity and κ adds to the denominator, thus, the diffusion coefficients obtained from Eq (5-33) will be smaller than the ones derived from Eq (5-33) which leads to smaller error percentages.

Table 5. 1 Diffusion coefficient with and without applying voltage

Particles	D* (m^2/s)	u_{ep}(m/s)	D**(m^2/s)	%Error
IgG	2.19×10^{-11}	2.7×10^{-04}	3.86×10^{-11}	43.2
BSA	4.21×10^{-11}	2.3×10^{-04}	5.62×10^{-11}	25.0
Lysozyme	9.26×10^{-11}	3.8×10^{-04}	1.77×10^{-10}	47.6
Cytochrome C	7.79×10^{-11}	4.2×10^{-04}	1.60×10^{-10}	51.4

RNase A	6.49×10^{-11}	3.1×10^{-04}	1.05×10^{-10}	38.4
AngioTensin II	2.01×10^{-10}	2.6×10^{-04}	3.46×10^{-10}	41.8
Tryptophan	4.38×10^{-10}	3.4×10^{-05}	4.16×10^{-10}	-5.4

To correct the diffusion coefficients, the values of δ and κ needs to be estimated. Δ is calculated using the electrophoretic and Poiseuille velocity. For κ, we need to have an estimation of γ which is not the goal of this paper and it will be investigated in future work.

5.3.3 Validity of TDA in the presence of electrophoretic flow

For the equations of TDA to be valid, two conditions must be satisfied. The first condition requires the migration time to be much greater than the time required for the solute molecules to diffuse radially across the capillary[119]. The second condition requires the axial diffusion of the solute to be negligible when compared to its dispersion which can be expressed with Peclet number[166]. As the diffusion coefficient of the particle becomes bigger the Peclet number becomes smaller and gets closer to the minimum value. Table 5.2 shows the migration time and Peclet number for particles of different sizes. The minimum values of t_0 and Pe are calculated using the below equations and minimum elution time for each particle is shown in table 5.3.

TDA first condition:

$$t_0 > \frac{1.4R^2}{D}$$

TDA second condition:

$$P_e = \frac{\bar{U}R}{D} > 50$$

Table 5. 2 Peclet number and elution time of particles with and without applying voltage

Particles	t_0(p)	Pe(p)	t_0(p+V)	Pe(p+V)
IgG	493	1158	391	829
BSA	501	593	408	545
Lysozyme	506	267	364	195
Cytochrome C	506	317	355	220
RNase A	505	381	384	310
AngioTenisn	488	127	390	93
Tryptophan	497	57	481	63

Table 5. 3 Minimum elution time for TDA to be valid

Particles	t_0(s)
IgG	22.7
BSA	15.6
Lysozyme	4.9
Cytochrome C	5.5
RNase A	8.3
AngioTenisn	2.5
Tryptophan	2.1

Comparing the values in table 5.2 and table 5.3 for all the particles, the migration times are all longer than the minimum value, therefore, the first condition of TDA is met. Also, all the values for Peclet numbers are bigger than minimum value.

5.3.4 Size and charge characterization of mixture

Using voltage besides pressure gives TDA, a separation power which is advantageous for mixtures. The charge of individual components can be determined as well as the size. Size and charge are fundamental properties of proteins in solution. Amino acids which are constituents of proteins may be positive, negative, neutral, together give a protein its overall charge. At a pH below their pI, proteins carry a net positive charge; above their pI, they carry a net negative charge. The calculation of charge of proteins and peptides is challenging because it requires detailed information about the pH of the surrounding medium and the ionization constant of each amino acid. There are only few works on the estimation of the net charge of peptides and proteins [167-168].

In this section, charge and size of particles of different sizes are estimated. A mixture of a protein, a peptide, and an amino acid is analyzed by applying pressure and voltage at the same time. They are separated by the combination of electrophoretic and Poiseuille flow; electrophoretic velocity is calculated for each particle by calculating the differences between the velocity obtained from combination of pressure and voltage and the one obtained from pressure only. Their diffusion coefficient and hydrodynamic radius are measured using their peak width and migration time using Eq (5-33). Having the electrophoretic velocity of each particle δ is calculated using Eq (5-30). To calculate κ (Eq (5-31)), γ is estimated by comparing the diffusion coefficients obtained from classical TDA and TDA with pressure and voltage.

Figure 5.1 shows the electropherogram for the mixture of BSA, AngioTenisn, and Tryptophan when a pressure of 1psi and voltage of 10 kV is applied. Tryptophan is well separated while AngioTenisn and BSA are migrating close to each other but far enough to analyze each peak separately. Using voltage 20 kV gives better separation but the peaks for BSA and AngioTenisn are still overlapping. We chose voltage of 10kV for this study so that the TDA conditions are met.

The equation describing electrophoretic mobility is [169]:

$$\mu_{ep} = \frac{Q}{6\pi\eta R_h} \qquad (5-41)$$

where Q is charge in coulombs, η is the viscosity of the solution in Pa.s, and R_h is the size estimated using TDA method when pressure and voltage are applied. Eq (5-41) is used to calculate the charge of particles

The charge for proteins is bigger than peptides and bigger than amino acids. All the particles have nonzero charge and it shows pH is below their isoelectric points. BSA carries more charge than the other two which is due to the large surface area.

Table 5. 4 Size and charge measurement of a mixture of BSA, AngioTensin, and Tryptophan at pH 3.5

Particles	R_h(nm)	μ_{ep}(m^2/s.V)	Charge
BSA	5.96 ± 0.14	1.31×10^{-8}	8.2
AngioTenisn	1.03 ± 0.04	1.66×10^{-8}	1.8
Tryptophan	0.47 ± 0.01	9.17×10^{-8}	0.6

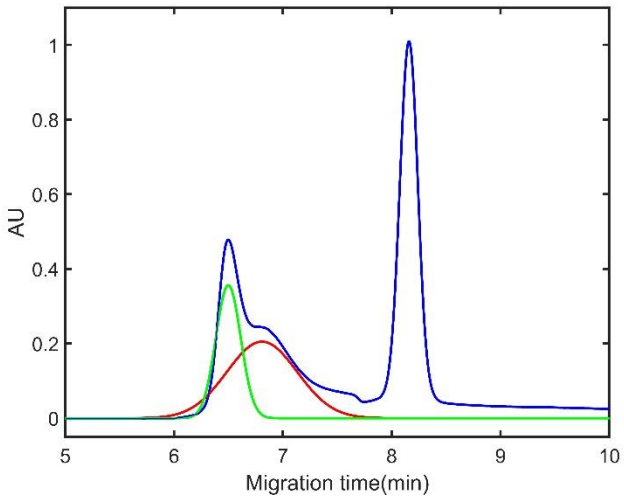

Figure 5. 1 Separation of a mixture of angiotensin (green), BSA(red), tryptophan (blue) at pressure of 1psi and voltage of 10kV with capillary electrophoresis instrument

5.4 Conclusion

In this work, we have demonstrated the modified equations for the estimation of diffusion coefficient in TDA approach when applying the combination of Poiseuille flow and electrophoretic flow. We have also shown that the validity of TDA is retained in our method and the diffusion coefficient is calculated using the temporal variance of the peaks and their migration time as well as the electrophoretic velocity. The resulting equations are consistent with the experimental data obtained for proteins, peptides, and amino acids. The application of this method is investigated for the separation and size characterization of components of the mixture of BSA, AngioTensin, and Tryptophan.

Simultaneous separation and size characterization of molecules in capillary tubes is achieved by applying both voltage and pressure. However, the equations used for classical TDA cannot be used

when voltage is applied. Modifying the equations for TDA in the presence of electrophoretic flow is a valuable work that is done and presented this chapter.

Chapter 6: Electroosmotic flow dispersion of large molecules in electrokinetic migration

6.1 Introduction

Capillary electrophoresis (CE) is one of the separation techniques that can be used to study a variety of molecules, including large biomolecules.[170] In addition to being used for separation and quantification of analytes in complex mixtures, CE has been used for the determination of physicochemical properties such as equilibrium constant [171] and diffusion coefficient. [172] Diffusion is an unavoidable phenomenon in a liquid and is a two-edged sword in CE: it is one of the main components that lead to broadening of peaks and therefore diminishes the resolution of separation but at the same time, it gives some information about the diffusion coefficient, [173-175] or the size, of the particles being separated. [176]

Different sources can contribute to the peak broadening in electropherograms, including the length of sample injection and the width of the detection window, electro migration, wall adsorption, Joule heating and molecular diffusion. There have been several studies on minimizing each one of these sources to achieve high separation efficiency. Sample injection length needs to be short to obtain good resolution. [177-178] Peak asymmetry caused by electro-migration can be reduced by using uniform electrolytes throughout the separation, and wall adsorption can be alleviated by using appropriate coatings.[179-180] Moreover, The effect of Joule heating on resolution of CE has been widely investigated and various approaches have been taken to reduce its effect on band-broadening.[181] Among all of the factors that cause band broadening, diffusion of the molecules in

solution is unavoidable. To control its effect on resolution, and perhaps make use of this phenomenon to better understand the analytes, the phenomenon of diffusion must be understood.

Ghosal[182] reviewed various sources that limit the efficiency of the separation in CE. He investigated the axial dispersion in CE and the factors contributing to the band broadening.[183] Others used the broadening of the peaks to calculate the diffusion coefficient of the molecules.[149] In 1953 Taylor showed that by combining the convection of the fluid in the column with radial diffusion, an "apparent longitudinal diffusion", or dispersion, term is obtained, which is inversely proportional to the diffusion coefficient. These studies led to Taylor dispersion analysis which is used for the determination of diffusion coefficient and also explains the dispersion of molecules under Poiseuille flow. [26] Cottet et al. used this technique to measure the diffusion coefficient of dendrigraft poly-L-lysine by applying pressure to move the sample plug through the capillary and measuring the band broadening of the resulting peaks. [158] They demonstrated that larger molecules with smaller diffusion coefficient give wider peaks.

Although the diffusion of molecules has been extensively studied in narrow tubes under pressure, not enough studies have been done to investigate the dispersive behavior of molecules in electric field driven migration.

In certain conditions, when an electric field is applied to the capillary column, a bulk fluid motion is observed. This motion is called electroosmosis which stems from the electrostatic force on the ions in the electrical double layer, a thin layer of ions that is located near the wall exposed to the solution. The velocity of this motion is determined by the applied electric field, the material used to construct the channel inner wall and the composition of the solution in the channel.[7] The main difference between the pressure driven flow and EOF driven flow is in the shape of the flow profile, which is parabolic in the former and flat in the latter. However, the length of Debye layer varies

with the concentration and the pH of the background electrolyte (BGE) being used. As the Debye length gets larger, there will be a deviation from the flat flow profile and the velocity distribution will be nonuniform. In this case, the dispersion consists of more terms than just the diffusion coefficient. [184]

In this chapter, we described how molecules with different diffusion coefficients behave in the presence of electric field in CE. We also presented how the zeta potential and the Debye layer length affect the dispersion and therefore broadening of the peaks in CE. The results showed that the traditional belief about small peak width for large molecules needs to be revisited. We demonstrated that electroosmotic dispersion must be considered.

6.2 Experimental section

6.2.1 Apparatus

Experiments were performed on a P/ACE MDQ capillary electrophoresis system (Beckman Coulter, Brea, CA) with UV detection at a wavelength of 200 nm. CE studies were carried out with a fused silica capillary (60 cm total length × 50 cm length to detector × 50 μm i.d. × 365 μm o.d.) (Polymicro Technologies, Phoenix, AZ) coated with cationic polyethylenimine (PEI) with the procedure outlined in U.S. Patent 6923895 B2. [185]

Dynamic light scattering (DLS) studies were performed with a Malvern Zetasizer instrument (Nano-ZS, Malvern 75-01).

6.2.2 Reagents

All proteins (bovine serum albumin (BSA), immunoglobinG (IgG)), and peptides (Angiotensin II, Phe-Tyr) with at least 95% purity were purchased from Sigma-Aldrich (St. Louis, MO). Formic

acid (88%) was purchased from Fisher Scientific (Nepean, ON, Canada). Polyethylenimine coating reagent of trimethoxysilylpropyl-modified polyethylenimine, 50% in isopropanol was purchased from Gelest Inc. (Morrisville, PA). Solutions of proteins and peptides were prepared in deionized 18 MΩ water and were stored at -20°C unless otherwise stated. All sample solutions and buffers were filtered through 0.22 µm sterile, Nylon syringe filters. All DLS studies were conducted at 25° with 0.5% formic acid solvent as buffer.

6.2.3 Method for evaluation of dispersion

Proteins and peptides with different sizes were used as analytes, and they were analyzed under different voltages of 10, 15, 20, 25, and 30 kV with three repetitions. Before each injection, the column was rinsed thoroughly with BGE (FA 0.5%) for 5min with a pressure of 30 psi. The samples were injected for 5 s with pressure of 5psi.

6.3 Results and discussion

6.3.1 Size analysis using dynamic light scattering

To study the migration behavior of molecules and particles with different sizes in CE, it is important to know their estimated size. DLS, a well-established method, is used first to estimate the size of the proteins and peptides used in this study. Table 6.1 shows the size of proteins obtained by DLS, and the results are expressed in terms of Z_average which is the intensity weighted mean hydrodynamic size of the ensemble collection of particles measured by DLS. [186] For the proteins (BSA, IgG), the results are reproducible and the Z_average of 3.49 nm and 11.08 nm are obtained, respectively. The sizes for angiotensin II and Tyr-Phe are not reported, because the results did not have good enough quality to be accepted by the instrument. The sensitivity of DLS is higher for

larger particles. The instrument does not give accurate results beyond its dynamic range.[187] IgG protein is shown to be bigger than BSA which agrees with their molecular weight.

Table 6. 1 Molecular size and polydispersity (PDI) of proteins and peptides measured by DLS

	molecular weight (Da)	**Z_average (nm)**	**PDI**
BSA	66500	3.49	0.292
IgG (Goat)	150000	11.08	0.090
Angiotensin II	1046	NA	NA
Tyr-Phe	328	NA	NA

6.3.2 Dispersion of proteins and peptides in CE

To evaluate the effect of molecular size on the peak width in electropherograms, proteins and peptides with different sizes are used for this study (two proteins and two peptides with a wide range of size from 0.1 to 10 nm). Only a few nanoliters of sample were used for each analysis and all the results were obtained within 20 min. No prior sample preparation is needed. Figure 6.1 shows temporal variance of the proteins and peptides under different electric fields which lead to different migration times. IgG has the largest slope and BSA is the next, and then angiotensin II and Tyr-Phe.

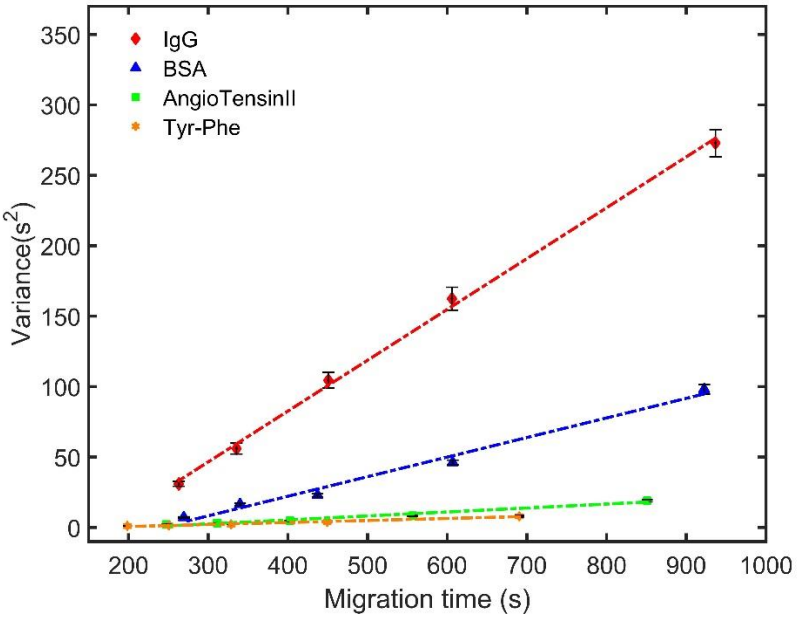

Figure 6. 1 The linear relationship of temporal variance of IgG, BSA, angiotensin II, Tyr-Phe and their migration time

The difference in temporal variance in terms of migration time is not a good indicative of dispersion (spreading) of the analytes in the column since the temporal variance arises from the difference in zone velocity [188]. Therefore, the temporal variance is corrected for the velocity and migration time and the results are represented in terms of spatial variance with units of cm^2.

$$\sigma_L = \sigma_t \times \frac{L}{t_m} \qquad (6\text{-}1)$$

where σ_L is the spatial variance, σ_t is temporal variance, L is the effective capillary length, and $t_m$is the migration time of analytes in the capillary column.

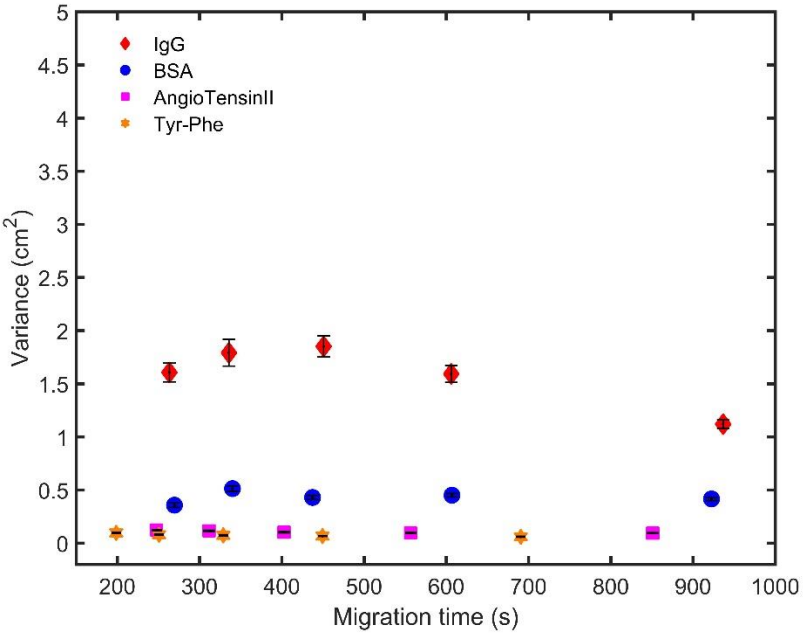

Figure 6. 2 Spatial variance of IgG, BSA, angiotensin II, and Tyr-Phe derived from electropherograms obtained at different voltages

If all the factors (except diffusion) that contribute to the dispersion of the sample plug along the capillary column are negligible, we can use Einstein equation to describe the peak broadening of each particle.

$$\sigma^2 = 2Dt \qquad (6\text{-}2)$$

In our system, we assume dispersion due to injection length and detection length is insignificant. We also used coolant during the separation and kept the temperature constant, therefore, the effect of joule heating is minimized. We used positively charged coating to avoid interaction of protein with the wall of capillary. Because we didn't observe any tailing in the peaks, we assumed the wall interaction is also minimized.

As shown in Figure 6.2, the spatial variance increases as the diffusion coefficient decreases. Therefore, dividing the peak variance of each peak by its migration time, does not give the diffusion coefficient alone and there is another factor that is contributing to broadening of the peak and that factor must be inversely related to the diffusion coefficient. For this reason, we name the ratio of the spatial variance to the migration time, apparent diffusion coefficient or dispersion coefficient.

$$D^A = \frac{\sigma^2}{2t} \qquad (6\text{-}3)$$

D^A is the apparent diffusion (dispersion), σ^2 is spatial variance, and t is migration time.

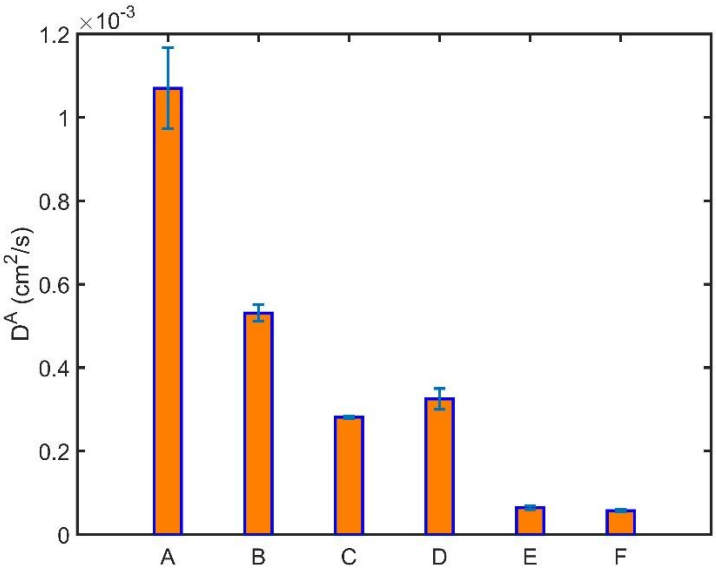

Figure 6. 3 Comparison of dispersion coefficient of (A) IgG, (B) BSA, (C) myoglobin, (D) cytochrome C, (E) angiotensin, (F) Tyr-Phe at 20 kV

This trend is contrary to the common belief that without surface adsorption from the capillary wall, larger molecules should have sharper peaks, but in agreement with the observations in the majority of real experiments.

6.3.3 Theoretical modeling of dispersion in capillary electrophoresis

Other groups have investigated the dispersion of solute due to EOF in a long straight column[182-183]. These analyses used the same approach as the one developed by Taylor[26] (Poiseuille flow in a tube) and extended by Aris.[118] According to the Taylor-Aris theory, after a sufficiently long time, a small solute plug in a narrow open tube is dispersed axially under the combination of diffusion and convection of the solute. For the dispersion of solute in the presence of EOF, the proposed equation contains an apparent diffusion coefficient, D^A, which is referred to as the dispersion coefficient and is given by Eq (6-3).[189]

$$D^A = D(1 + \delta D_{eo}) \qquad (6-4)$$

where D^A is dispersion coefficient, D is diffusion coefficient, and δD_{eo} is the additional dispersion term caused by electroosmotic flow, and is referred to as electroosmotic flow dispersion (EOFD) in this paper. For capillary electrophoresis, where the bulk flow is originated from electroosmotic flow, δD_{eo} is estimated to be: [189]

$$\delta D_{eo} = K(\frac{\epsilon\zeta E}{\eta D\kappa})^2 \, g(\zeta) \qquad (6-5)$$

where ϵ is solution dielectric permittivity, ζ is the zeta potential, E is the magnitude of the electric field, η is the solution viscosity, D is the diffusion coefficient of the particle, and κ^{-1} is the Debye

length. The dimensionless factor, *K*, is defined by the cross-section shape and for circular cross sections is equal to $\frac{1}{2}$. [190] The g(ζ) function depends on the zeta potential in the capillary column and the type of the electrolyte. Eq (6-5) is an empirical interpolation function suggested by Griffiths and Nilson for (Z+: Z-) electrolyte. [189]

$$g_{G-N}(\zeta) = \frac{2592+24(\zeta Z)^2}{2592+96(\zeta Z)^2+(\zeta Z)^4} \qquad (6\text{-}6)$$

where $g_{G\text{-}N}(\zeta)$ is the Griffiths and Nilson approximation for the function g(ζ), Z is the charge on the electrolytes, and ζ is the zeta potential.

Assuming Z = 1 for the electrolyte (0.5% formic acid for BGE), Figure 6.4 is obtained. The zeta potential is calculated to be 1 V in our system using the Helmholtz-Smoluchowski equation,[182] therefore, for our system, g(ζ) is estimated to be 1, as depicted in Figure 6. 4.

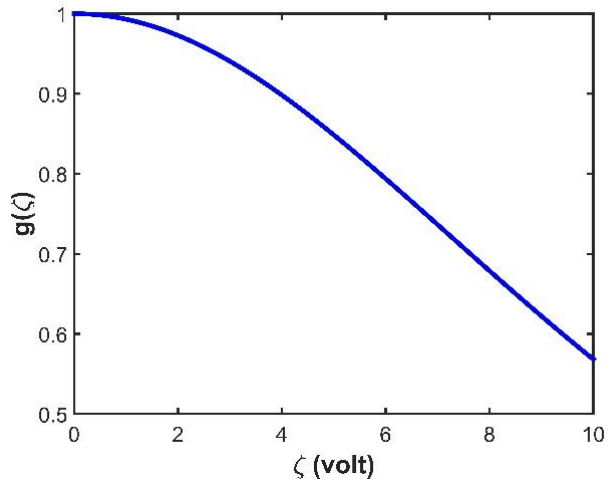

Figure 6. 4 Calculation of g(ζ) at various zeta potentials using empirical interpolation function suggested by Griffiths and Nilson

Eq (6-4) is simplified to Eq (6-6) assuming value of 1 for g(ζ) and K=1/2 (for cylindrical geometry).

$$\delta D_{eo} = \frac{1}{2}\left(\frac{\epsilon \zeta E}{\eta D \kappa}\right)^2 \qquad (6\text{-}7)$$

According to Eq (6-3), in CE, if δD_{eo} is much smaller than 1, then $D^A \cong D$ and the dispersion is limited to diffusion only, but if δD_{eo} is significantly larger than 1, then the dispersion is larger than longitudinal diffusion coefficient. Figure 6. 5 shows how δD_{eo} varies for different values of diffusion coefficient and zeta potential for 3 different Debye layer lengths, 1, 5, and 10 nm, respectively. At a Debye length of 1 nm, δD_{eo} is not significantly larger than 1, but as the length increases, δD_{eo} becomes bigger.

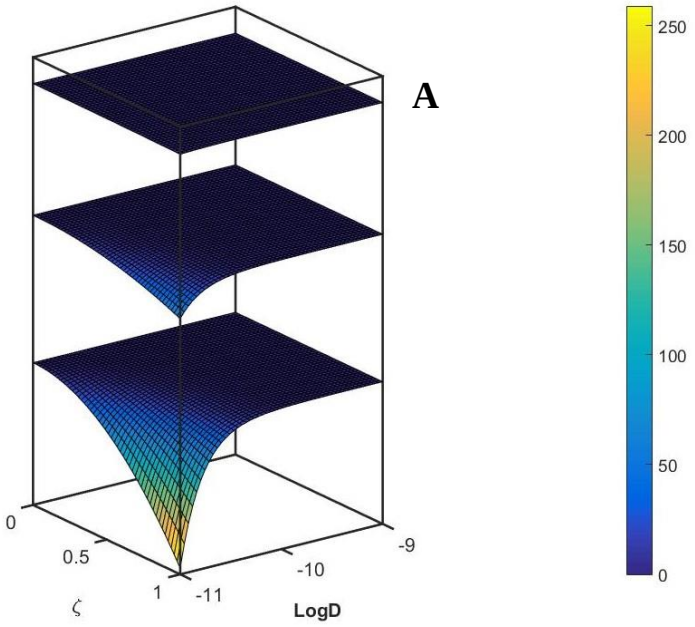

Figure 6. 5 Effect of diffusion coefficient and zeta potential on dispersion term (δD_{eo}) for different Debye lengths.

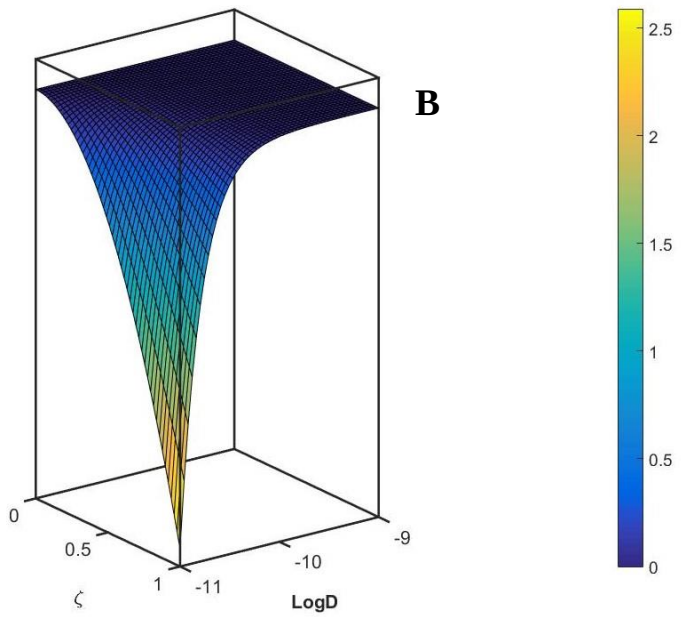

Figure 6. 6 Zoomed view of figure 6.5 for Debye length of 1nm

Figure 6.7 is plotted to better understand the dependence of δD_{eo} on D at a specific zeta potential (zeta=1V for our system). It shows that δD_{eo} becomes bigger for smaller diffusion coefficients. Therefore, it causes more dispersion for large particles with smaller diffusion coefficient. This effect is more apparent when the Debye length is increased. Thus, using different BGE with different ionic strengths, or operating at different temperatures can also result in significant dispersion if the Debye length is significantly increased.

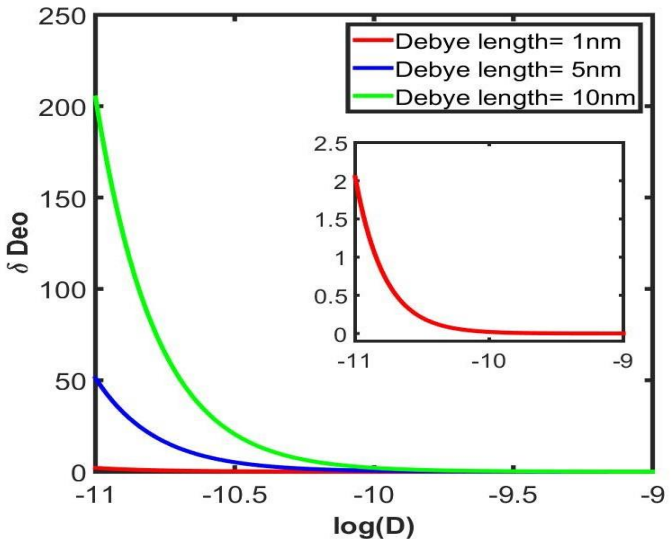

Figure 6. 7 Significance of second term (δD_{eo}) at various Debye lengths at zeta potential =1 V

To evaluate the magnitude of δD_{eo} for our system, we found κ^{-1} to be 1.2 nm using the Debye-Huckel equation(Eq(6-7)).[191]

$$\kappa^{-1} = \left(\frac{\varepsilon k_B T}{\sum_{j=1}^{N} n_j^0 q_j^2}\right)^{1/2} \qquad (6-8)$$

In Eq (6-7), ε is the dielectric constant of buffer, ε_0 is permittivity of vacuum, k_B is Boltzmann constant and n_j^0 is the concentration and q_j is the charge of each ion in the solution.

δD_{eo} for our system approximately follows the red curve in Figure 6.7. The value increases with decreasing diffusion coefficient. For very large particles, D is close to 1.00×10^{-11} m^2/s. δD_{eo} is nearly 4, and therefore D^A is 5 times bigger than the diffusion coefficient. Therefore, more broadening is observed for large particles. However, for small particles where the diffusion coefficient is close to 1.00×10^{-9}, δD_{eo} is almost zero and no extra term need to be added to the variance of the peak.

6.3.4 Comparing theory and experimental results

In the presence of EOF, the extra term δD_{eo} or EOFD leads to the additional dispersion of analytes in the sample plug and therefore more broadening of the peaks is observed. This term is more significant for larger particles with smaller diffusion coefficients and thus EOFD is bigger for proteins. This term depends on ionic strength of the buffer as well. For example, for buffers with lower concentration and singly charged ions, EOFD is larger as opposed to buffers with higher concentrations with multiple charged ions. The EOFD contribution to peak broadening of proteins can be more significant if the buffer has lower ionic strength and larger Debye length.

By using sizes derived for IgG and BSA from DLS and the Einstein-Stokes equation [71], the diffusion coefficient is 2×10^{-11}m^2/s and 6×10^{-11}m^2/s, respectively, and therefore, according to Eq (6-2), their $\sigma^2/2t$ ratio is about 0.3. However, Figure 6.3 shows that $\sigma^2/2t$ is bigger for IgG than BSA. Using Eq (6-4), D^A is 4×10^{-11} m^2/s and 6.6×10^{-11} m^2/s, respectively, and according to Eq (6-3), their $\sigma^2/2t$ ratio is about 0.6. Correcting for EOFD has not resolved the issue completely but has made the ratio closer to the experimental value. For peptides such as angiotensin and Tyr-Phe, EOFD is smaller because their diffusion coefficient is much larger than proteins. Therefore, the axial diffusion becomes significant for these peptides, and Tyr-Phe with a larger diffusion coefficient results in comparable temporal variance to angiotensin (Eq (6-4)).

In summary, EOFD is one of the factors that we believe is causing the extra broadening of peaks for large molecule such as proteins, but it is not the only factor. There are some other factors that are also contributing to the extra broadening, such as heterogeneity of the sample, and they must be investigated thoroughly in the future.

6.4 Conclusion

In this chapter, the source of band broadening for proteins in CE was investigated using commonly used conditions in CE or in microfluidic separations. The experiments showed that proteins experience bigger dispersion than peptides in the presence of EOF. Theoretical models were developed to explain this observation, and it is shown that proteins lead to more band broadening during analyte migration when Debye layer length is bigger. Even though larger molecules have a smaller diffusion coefficient, the apparent dispersion can be more significant if the additional dispersion term caused by EOF is significant which happens when the BGE and/or other conditions used lead to a larger Debye length.

Chapter 7: Concluding remarks and future work

7.1 Concluding remarks

TDA evaluates the diffusion coefficient and the hydrodynamic radius of a wide range of particles and it has become more popular during the last few decades. In TDA, Poiseuille flow (driven by pressure) is a non-discriminative mobilization of the analyte through the column. TDA must meet two conditions to give accurate results on the diffusion coefficient and the hydrodynamic size. TDA conditions assure the axial diffusion to be negligible in comparison to the dispersion, also guarantee the time to be longer than the diffusion characteristics.

The materials presented in this thesis provide a different approach toward the study of Taylor dispersion analysis by investigating the effect of electric field on the dispersion of particles. To be able to use TDA for separation along with the sizing of particles, a combination of voltage and pressure was applied and the results were compared with the results obtained from classical TDA. It was concluded that the equations need to be modified when voltage is added to the system. Electrophoretic mobility was added to Taylor equations and the modified equations were used to explain the difference between the classical TDA results and the ones from TDA with pressure and voltage.

Furthermore, the dispersion of large particles in the presence of the electroosmotic flow was studied and it was used to explain the broader peaks for the large particles in capillary electrophoresis when only voltage is applied. It is shown that EOF contributes to part of broadening of protein in CE.

Also, this thesis described a comprehensive study of TDA in terms of the column dimension, and experimental conditions. Because capillaries are required for performing TDA, their dimensions are important to achieve a successful analysis of diffusion coefficient and so the hydrodynamic size. In chapter 3 of this thesis TDA has been studied numerically to investigate the effect of capillary dimensions on the performance of TDA. It was concluded that for larger diameters, smaller velocities must be used to obtain more precise results and for smaller diameters, using larger velocities give more precise results. Theoretically, we can use columns with different diameters for TDA when the velocity is optimized for that specific diameter. However, in experiments, using larger diameters with slower bulk motion is time consuming and using smaller diameter is often accompanied with clogging of the column. For this reason, columns with a diameter of medium (e.g., 50 μm) are preferred for TDA. For the length of column, to meet TDA conditions, higher velocities give better results when using longer columns and vice versa. The combination of pressure and voltage was also studied numerically to separate particles while they are being dispersed in the column. It was concluded that if we use the equations from classical TDA to estimate the diffusion coefficient, then the voltage must be kept at minimum to obtain more accurate results.

Finally, part of this thesis is devoted to comparing TDA to some other techniques used for size characterization. TDA was conducted on proteins and peptides and amino acids and its application was compared to more established sizing method (DLS) and a CE-based sizing method (stopped-migration). DLS is shown to be more sensitive to the larger particles, whereas the stopped migration method is more sensitive to smaller molecules. TDA could cover sizing of both large and small molecules. Different sizing techniques where reviewed more in detail.

7.2 Future work

7.2.1 Aggregation study of proteins

Proteins in their native state are folded into a three-dimensional conformation which make them thermodynamically stable. The folding happens in a way that the hydrophobic portions of the proteins bury themselves into the interior of the protein which leads to a hydrophilic exterior and a hydrophobic interior. Any disruption occurring in the non-covalent interactions, the proteins may become susceptible to unfolding or misfolding which leads to the aggregation of proteins. Different stress conditions may cause the aggregation of proteins such as pH, temperature, presence of additives in the solution. The aggregation of proteins is an important and critical phenomenon that has been studied for a long time and different instrumentation have assisted with these studies. When protein aggregates, size is an apparent change in the process. Since, TDA is proved to be a sizing technique which covers wide range of sizes, it could be a good candidate for analyzing the aggregation proteins.

We have started investigating the aggregation behavior of proteins using TDA. In this study, we have heated the proteins below and above their melting temperature and then had it cooled down rapidly. Then the untreated protein and the treated ones above and below their melting temperature have been analyzed using TDA. BSA (5mg/ml) solution was heated to 76°C and 60°C in a water bath for 30 min and cooled down to the room temperature. IgG (2mg/ml) solution was heated to 80°C and 50°C in a water bath for 30 min and the cooled down to the room temperature. As it is shown in Figure 7.1 when BSA is treated at 60 °C the taylogram is similar to untreated BSA.

However, when treated at 76 °C, the taylogram is broader even though it is migrating faster which is indicative of larger size.

To better understand the aggregation of proteins and also applicability of using TDA for these types of studies, a lot more work needs to be done. Other types of stresses such as pH and different types of additives must be added to the system to confirm the formation of aggregates and their detection using TDA. Also, the results should be studied with a more established technique such as DLS.

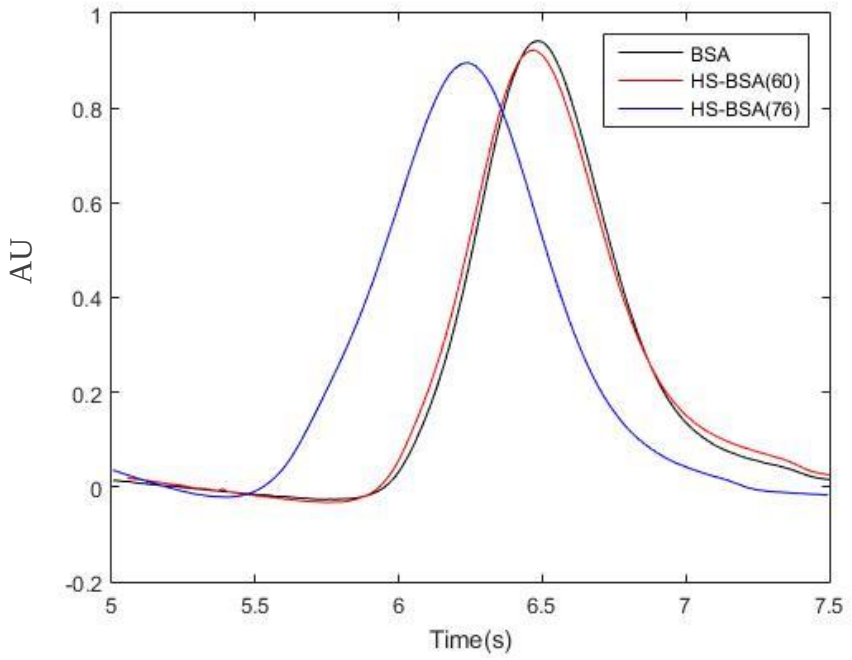

Figure 7. 1 Taylogram of BSA (5mg/mL) (A) untreated, (B) heated at 60°C and 76°C in a neutral coated capillary with 1psi+10kV

7.2.2 Further modification of equation for TDA with voltage

In Chapter 5, the equation for estimation of diffusion coefficient is modified when voltage is applied with pressure in TDA. The modified equation explains the systematic error observed in the comparison of dispersion of the particles when voltage is applied compared to classical pressure driven TDA. The third term in the modified equation needs to be explored more comprehensively to give the equation that can be used for modified TDA. Using the modified equation for size characterization of particle as well as separating them at the same time will be an invaluable tool for studying mixture with wide range of sizes.

7.2.3 Further study on EOF dispersion

In Chapter 6, EOF dispersion is shown to be one of the contributing factors to the band broadening of the large particle. The magnitude of Debye length and zeta potential is a crucial parameter in the significance of the EOF dispersion which can be controlled using buffers with different concentration and pH. Also, the column coating affects the magnitude of zeta potential even if the buffer composition is constant. These conditions were studied by simulating these conditions, and confirming the simulated results via experiments could be a complementary for this study. More investigation and better understanding of this phenomenon can help in optimizing the separation in CE for large particles such as protiens.

Bibliography

1. Tiselius, A., A new apparatus for electrophoretic analysis of colloidal mixtures. *Trans. Faraday Soc* **1937,** *33*, 524-531.
2. Magdeldin, S., *Gel electrophoresis: Principles and basics*. InTech: 2012.
3. Deforce, D. L.; Millecamps, R. E.; Van Hoofstat, D.; Van den Eeckhout, E. G., Comparison of slab gel electrophoresis and capillary electrophoresis for the detection of the fluorescently labeled polymerase chain reaction products of short tandem repeat fragments. *J Chromatogr A* **1998,** *806* (1), 149-55.
4. Hjerten, S., Free zone electrophoresis. *Chromatogr Rev* **1967,** *9* (2), 122-219.
5. Ackermans, M. T., *Electrophoresis in open capillaries : some fundamental aspects*. Technische Universiteit Eindhoven: 1992.
6. Jorgenson, J. W., Zone electrophoresis in open-tubular glass capillaries. *Anal Chem* **1981,** *53*, 1298-1302.
7. Landers, J. P., *Handbook of capillary electrophoresis*. 2nd ed.; CRC Press: Boca Raton, 1997; p 894 p.
8. Skoog, D. A.; Holler, F. J., Principles of Instrumental Analysis. *Nieman, T.A.* **1998**.
9. Weber, R., Concerning theories of electrophoretic separations in porous tube. *Helv. Chim. Acta* **1953,** *36*, 424-.
10. Sazelova, P.; Kasicka, V.; Koval, D.; Prusik, Z.; Fanali, S.; Aturki, Z., Control of EOF in CE by different ways of application of radial electric field. *Electrophoresis* **2007,** *28* (5), 756-66.
11. Shintani, H.; Polonsky, J., *Handbook of Capillary Electrophoresis Applications*. Springer Netherlands: 1996.
12. Cikalo, M. G.; Bartle, K. D.; Robson, M. M.; Myers, P.; Euerby, M. R., Capillary electrochromatography. *Analyst* **1998,** *123*, 87-102.
13. Li, S. F. Y., *Capillary Electrophoresis: Principles, Practice and Applications*. Elsevier: 1992.
14. Marina, M. L.; Torre, M., Capillary electrophoresis. *Talanta* **1994,** *41* (9), 1411-1433.
15. Kalariyaa, P. D.; Namdeva, D.; Srinivasa, R.; Gananadhamu, S., Application of experimental design and response surface technique for selecting the optimum RP-HPLC conditions for the determination of moxifloxacin HCl and ketorolac tromethamine in eye drops. *Journal of Saudi Chemical Society* **2017,** *21*, S373–S382.
16. Horvath, J.; Dolnik, V., Polymer wall coatings for capillary electrophoresis. *Electrophoresis* **2001,** *22* (4), 644-55.
17. Doherty, E. A.; Meagher, R. J.; Albarghouthi, M. N.; Barron, A. E., Microchannel wall coatings for protein separations by capillary and chip electrophoresis. *Electrophoresis* **2003,** *24* (1-2), 34-54.
18. Lucy, C. A.; MacDonald, A. M.; Gulcev, M. D., Non-covalent capillary coatings for protein separations in capillary electrophoresis. *J Chromatogr A* **2008,** *1184* (1-2), 81-105.
19. Righetti, P. G.; Gelfi, C.; Verzola, B.; Castelletti, L., The state of the art of dynamic coatings. *Electrophoresis* **2001,** *22* (4), 603-11.
20. Rutten, G. A. F. M.; Rijks, J. A., Technique for static coating of glass capillary columns. *Journal of separation science* **1978,** *1* (5), 279-280.

21. Goodwin, B. L., Static coating of capillary columns: Some practical considerations. *J Chromatogr A* **1979,** *172* (1), 31-36.
22. Huhn, C.; Ramautar, R.; Wuhrer, M.; Somsen, G., Relevance and use of capillary coatings in capillary electrophoresis-mass spectrometry. *Anal Bioanal Chem* **2010,** *396* (1), 297-314.
23. Dolnik, V., Capillary electrophoresis of proteins 2003-2005. *Electrophoresis* **2006,** *27* (1), 126-41.
24. Ratnayake, C. K.; Flores, I. C. Coated capillary electrophoresis tubes and system 2005.
25. Shen, Y.; Smith, R. D. J., *Microcolumn Sep* **2000,** *12*, 135–141.
26. Taylor, G., Dispersion of Soluble Matter in Solvent Flowing Slowly through a Tube. *Proc R Soc Lon Ser-A* **1953,** *219* (1137), 186-203.
27. Brenner, H., Macrotransport Processes. *Langmuir* **1990,** *6* (12), 1715-1724.
28. Brenner, H.; Edwards, D. A., *Macrotransport processes*. Butterworth-Heinmemann: USA, 1961.
29. Aris, R., Onthe dispersion of a solute in a fluid flowing through a tube. *Proc. Roy. Soc.* **1956,** *235*, 67-77.
30. Peattie, R. A.; Fisher, R. J.; Bronzino, J. D.; Peterson, D. R., *Transport Phenomena in Biomedical Engineering: Principles and Practices*. CRC Press: 2012.
31. Taylor, G., *Proc. R. Soc. London, Ser. A* **1954,** *225*, 473–477.
32. Cottet, H.; Biron, J. P.; Martin, M., Taylor dispersion Analysis of mixtures. *Anal Chem* **2007,** *79* (23), 9066-9073.
33. d'Orlye, F.; Varenn, A.; Gareil, P., Determination of nanoparticle diffusion coefficients by Taylor dispersion analysis using a capillary electrophoresis instrument. *J Chromatogr A* **2008,** *1204*, 226-232.
34. Cottet, H.; Biron, J. P.; Martin, M., On the optimization of operating conditions for Taylor dispersion analysis of mixtures. *Analyst* **2014,** *139* (14), 3552-3562.
35. Taylor Dispersion Analysis (TDA) Introduction and Overview. http://www.azom.com/article.aspx?ArticleID=12173.
36. Walsh, G., *Proteins: Biochemistry and Biotechnology*. 2002; p 547.
37. Roberts, C. J., Protein aggregation and its impact on product quality. *Curr Opin Biotech* **2014,** *30*, 211-217.
38. Uversky, V. N.; Fink, A., Protein Misfolding, Aggregation and Conformational Diseases: Part A: Protein Aggregation and Conformational. *Springer Science & Business Media* **2007**, 419.
39. Wang, W.; Roberts, C. J., Aggregation of Therapeutic Proteins. *John Wiley & Sons* **2010**, 484.
40. HANNS-CHRISTIAN MAHLER, W. F., 2 ULLA GRAUSCHOPF,1 SYLVIA KIESE1, Protein Aggregation: Pathways, Induction Factors and Analysis *JOURNAL OF PHARMACEUTICAL SCIENCES*, **2009,** *98*.
41. Narhi, L. O.; Schmit, J.; Bechtold-Peters, K.; Sharma, D., Classification of protein aggregates. *J Pharm Sci* **2012,** *101* (2), 493-8.
42. Patrick, G., *An Introduction to Medicinal Chemistry*. Oxford University Press: 2013.
43. Tutar , Y., Role of Protein Aggregation in Neurodegenerative Diseases. **2013**.
44. Hong, H., Toward understanding driving forces in membrane protein folding. *Archives of biochemistry and biophysics* **2014,** *564*, 297-313.
45. Tyedmers, J.; Mogk, A.; Bukau, B., Cellular strategies for controlling protein aggregation. *Nat Rev Mol Cell Bio* **2010,** *11* (11), 777-788.

46. Takalo, M.; Salminen, A.; Soininen, H.; Hiltunen, M.; Haapasalo, A., Protein aggregation and degradation mechanisms in neurodegenerative diseases. *American journal of neurodegenerative disease* **2013,** *2* (1), 1-14.
47. J, C. P., Introduction to current and future protein therapeutics: A protein engineering perspective. *Experimental Cell Research* **2011,** *317* (9), 1261–1269.
48. Walsh, G., Biopharmaceutical benchmarks 2014. *Nat. Biotech* **2014**

32, 992-1000.
49. Leader, B.; Baca, Q. J.; Golan, D. E., Protein therapeutics: a summary and pharmacological classification. *Nature reviews. Drug discovery* **2008,** *7* (1), 21-39.
50. Carpenter, J.; Randolph, T.; Jiskoot, W.; Commelin, D.; Russel Middaugh, C.; Winter, G., Potential inaccurate quantitation and sizing of protein aggregates by size exclusion chromatography: Essential need to use orthogonal methods to assure the quality of therapeutic protein products. *Wiley InterScience* **2009,** *99* (5).
51. NG, R., *Drugs from discovery to approval*. Wiley-Blackwell: 2015.
52. Printz, M.; Friess, W., Simultaneous detection and analysis of protein aggregation and protein unfolding by size exclusion chromatography with post column addition of the fluorescent dye BisANS. *J Pharm Sci* **2012,** *101* (2), 826-37.
53. Vazquez-Rey, M.; Lang, D. A., Aggregates in monoclonal antibody manufacturing processes. *Biotechnology and bioengineering* **2011,** *108* (7), 1494-508.
54. Amin, S.; Barnettb, G.; Pathak, J.; Robertsb, C.; Sarangapanic, P., Protein aggregation, particle formation, characterization & rheology. *Current Opinion in Colloid & Interface Science* **2014,** *19* (5), 438-449.
55. Gregoire, S.; Irwin, J.; Kwon, I., Techniques for Monitoring Protein Misfolding and Aggregation in Vitro and in Living Cells. *The Korean journal of chemical engineering* **2012,** *29* (6), 693-702.
56. Philo, J. S., A critical review of methods for size characterization of non-particulate protein aggregates. *Current pharmaceutical biotechnology* **2009,** *10* (4), 359-72.
57. den Engelsman, J.; Garidel, P.; Smulders, R.; Koll, H.; Smith, B.; Bassarab, S.; Seidl, A.; Hainzl, O.; Jiskoot, W., Strategies for the Assessment of Protein Aggregates in Pharmaceutical Biotech Product Development. *Pharm Res-Dordr* **2011,** *28* (4), 920-933.
58. Pryor, N. E.; Moss, M. A.; Hestekin, C. N., Unraveling the Early Events of Amyloid-beta Protein (A beta) Aggregation: Techniques for the Determination of A beta Aggregate Size. *Int J Mol Sci* **2012,** *13* (3), 3038-3072.
59. den Engelsman, J.; Garidel, P.; Smulders, R.; Koll, H.; Smith, B.; Bassarab, S.; Seidl, A.; Hainzl, O.; Jiskoot, W., Strategies for the assessment of protein aggregates in pharmaceutical biotech product development. *Pharm Res* **2011,** *28* (4), 920-33.
60. V, V., Light Scattering as Spectroscopic Tool for the Study of Disperse Systems Useful in Pharmaceutical Sciences. *Wiley InterScience* **2008,** *97* (5), 1703-1730.
61. Couteau, O.; Charoud-Got, J.; Rauscher, H.; Franchini, F.; Rossi, F., A Colloidal Silica Reference Material for Nanoparticle Sizing by Means of Dynamic Light Scattering and Centrifugal Liquid Sedimentation. *Particle & Particle Systems Characterization* **2010,** *27* (3-4), 112-124.
62. Hauck, T. S.; Anderson, R. E.; Fischer, H. C.; Newbigging, S.; Chan, W. C. W., In vivo Quantum-Dot Toxicity Assessment. *Small* **2010,** *6* (1), 138-144.
63. Khlebtsov, B. N.; Khlebtsov, N. G., On the Measurement of Gold Nanoparticle Sizes by the Dynamic Light Scattering Method. *Colloid J+* **2011,** *73* (1), 118-127.

64. Linegar, K. L.; Adeniran, A. E.; Kostko, A. F.; Anisimov, M. A., Hydrodynamic radius of polyethylene glycol in solution obtained by dynamic light scattering. *Colloid J+* **2010,** *72* (2), 279-281.
65. Navarro, F. P.; Berger, M.; Guillermet, S.; Josserand, V.; Guyon, L.; Neumann, E.; Vinet, F.; Texier, I., Lipid Nanoparticle Vectorization of IndoCyanine Green Improves Fluorescence Imaging for Tumor Diagnosis and Lymph Node Resection. *J Biomed Nanotechnol* **2012,** *8* (5), 730-741.
66. Bruce J. Berne, R. P., *Dynamic Light Scattering: With Applications to Chemistry, Biology, and Physics* John Wiley & Sons, Inc.: 1976.
67. Kato, H.; Suzuki, M.; Fujita, K., Reliable size determination of nanoparticles using dynamic light scattering method for in vitro toxicology assessment. *Toxicology in Vitro* **2012,** *23*, 927-934.
68. Podzimek, S., *Light scattering, size exclusion chromatography, and asymmetric flow field flow fractionation : powerful tools for the characterization of polymers, proteins, and nanoparticles*. Wiley: 2010.
69. Hassan, P. A.; Rana, S.; Verma, G., Making Sense of Brownian Motion: Colloid Characterization by Dynamic Light Scattering. *Langmuir* **2015,** *31* (1), 3-12.
70. Lorber, B.; Fischer, F.; Bailly, M.; Roy, H.; Kern, D., Protein analysis by dynamic light scattering: methods and techniques for students. *Biochemistry and molecular biology education : a bimonthly publication of the International Union of Biochemistry and Molecular Biology* **2012,** *40* (6), 372-82.
71. Achuthan, S.; Chung, B. J.; Ghosh, P.; Rangachari, V.; Vaidya, A., A modified Stokes-Einstein equation for Abeta aggregation. *BMC bioinformatics* **2011,** *12 Suppl 10*, S13.
72. Whittaker, G.; Mount, A.; Heal, M., *Instant Notes in Physical Chemistry*. bios scientific publishers: 2000.
73. Lotya, M.; Rakovich, A.; Donegan, J. F.; Coleman, J. N., Measuring the lateral size of liquid-exfoliated nanosheets with dynamic light scattering. *Nanotechnology* **2013,** *24* (26), 265703.
74. N., U. V., The Mysterious Unfoldome: Structureless, Underappreciated, Yet Vital Part of Any Given Proteome. *J Biomed Biotechnol* **2010**.
75. Vladimir N. Uversky, S. L., *Instrumental Analysis of Intrinsically Disordered Proteins*. John Wiley & Sons, Inc.: Hoboken, New Jersey, 2010.
76. Gast, K.; Fiedler, C., Dynamic and static light scattering of intrinsically disordered proteins. *Methods in molecular biology* **2012,** *896*, 137-61.
77. McPherson, A.; Gavira, J. A., Introduction to protein crystallization. *Acta Crystallogr F* **2014,** *70*, 2-20.
78. Proteau, A.; Shi, R.; Cygler, M., Application of dynamic light scattering in protein crystallization. *Current protocols in protein science / editorial board, John E. Coligan ... [et al.]* **2010,** *Chapter 17*, Unit 17 10.
79. He, F.; Becker, G. W.; Litowski, J. R.; Narhi, L. O.; Brems, D. N.; Razinkov, V. I., High-throughput dynamic light scattering method for measuring viscosity of concentrated protein solutions. *Anal Biochem* **2010,** *399* (1), 141-143.
80. Hackley, V., *Measuring the hydrodynamic size of nanoparticles in aqueous media using batch-mode dynamic light scattering*. Methods in molecular biology (Clifton, N.J.): 2011; Vol. 697.

81. Takeuchi, K.; Nakatani, Y.; Hisatomi, O., accuracy of protein size estimation based on light scattering measurement. **2014,** *4* (2), 83-91.
82. Galush, W. J.; Le, L. N.; Moore, J. M., Viscosity behavior of high-concentration protein mixtures. *J Pharm Sci* **2012,** *101* (3), 1012-20.
83. Yu, Z.; Reid, J. C.; Yang, Y. P., Utilizing Dynamic Light Scattering as a Process Analytical Technology for Protein Folding and Aggregation Monitoring in Vaccine Manufacturing. *J Pharm Sci-Us* **2013,** *102* (12), 4284-4290.
84. Tomar, A. K.; Sooch, B. S.; Singh, S.; Yadav, S., Aggregation analysis of Con A binding proteins of human seminal plasma: a dynamic light scattering study. *Int J Biol Macromol* **2013,** *53*, 133-7.
85. Zhou, C.; Qi, W.; Lewis, E. N.; Carpenter, J. F., Concomitant Raman spectroscopy and dynamic light scattering for characterization of therapeutic proteins at high concentrations. *Anal Biochem* **2015,** *472*, 7-20.
86. Lewis, E. N.; Qi, W.; Kidder, L. H.; Amin, S.; Kenyon, S. M.; Blake, S., Combined Dynamic Light Scattering and Raman Spectroscopy Approach for Characterizing the Aggregation of Therapeutic Proteins. *Molecules* **2014,** *19* (12), 20888-20905.
87. Streets, A. M.; Sourigues, Y.; Kopito, R. R.; Melki, R.; Quake, S. R., Simultaneous Measurement of Amyloid Fibril Formation by Dynamic Light Scattering and Fluorescence Reveals Complex Aggregation Kinetics. *Plos One* **2013,** *8* (1).
88. Filipe, V.; Hawe, A.; Jiskoot, W., Critical evaluation of Nanoparticle Tracking Analysis (NTA) by NanoSight for the measurement of nanoparticles and protein aggregates. *Pharm Res* **2010,** *27* (5), 796-810.
89. Fekete, S.; Beck, A.; Veuthey, J. L.; Guillarme, D., Theory and practice of size exclusion chromatography for the analysis of protein aggregates. *J Pharm Biomed Anal* **2014,** *101*, 161-73.
90. André M. Striegel, W. W. Y., Joseph J. Kirkland, Donald D. Bly, *Modern Size-Exclusion Liquid Chromatography: Practice of Gel Permeation and Gel Filtration Chromatography, Second Edition*. John Wiley & Sons, Inc.: 2009.
91. Sullivan, M. A.; Powell, P. O.; Witt, T.; Vilaplana, F.; Roura, E.; Gilbert, R. G., Improving size-exclusion chromatography separation for glycogen. *J Chromatogr A* **2014,** *1332*, 21-9.
92. Gaborieau, M.; Castignolles, P., Size-exclusion chromatography (SEC) of branched polymers and polysaccharides. *Anal Bioanal Chem* **2011,** *399* (4), 1413-23.
93. John F. Carpenter, T. W. R., Wim Jiskoot, Daan J.A. Crommelin, C. Russell Middaugh andGerhard Winter, Potential inaccurate quantitation and sizing of protein aggregates by size exclusion chromatography: Essential need to use orthogonal methods to assure the quality of therapeutic protein products. *J Pharm Sci-Us* **2010,** *99* (5), 2200-2208.
94. Sakai-Kato, K.; Ota, S.; Hyodo, K.; Ishihara, H.; Kikuchi, H.; Kawanishi, T., Size separation and size determination of liposomes. *Journal of separation science* **2011,** *34* (20), 2861-5.
95. Zhang, J. T.; Haas, R. M.; Leone, A. M., Polydispersity Characterization of Lipid Nanoparticles for siRNA Delivery Using Multiple Detection Size-Exclusion Chromatography. *Anal Chem* **2012,** *84* (14), 6088-6096.
96. Patil SV, P. R., and Barge VU, Size-exclusion chromatography in Biotech Industry. *Journal of Microbiology and Biotechnology* **2014,** *3* (4).

97. Kang, D. Y.; Moon, J. M.; Lee, S., Comparison of Size-Exclusion Chromatography and Flow Field-Flow Fractionation for Separation of Whey Proteins. *B Korean Chem Soc* **2011,** *32* (4), 1315-1320.
98. Tsutomu Arakawa, D. E., Tiansheng li, John s. Philo, The Critical Role of Mobile Phase Composition in Size Exclusion Chromatography of Protein Pharmaceuticals. **2010**.
99. Hong, P.; Koza, S.; Bouvier, E. S. P., A Review Size-Exclusion Chromatography for the Analysis of Protein Biotherapeutics and Their Aggregates. *J Liq Chromatogr R T* **2012,** *35* (20), 2923-2950.
100. James G. Barnard, S. S., Theodore W. Randolph andJohn F. Carpenter, Subvisible particle counting provides a sensitive method of detecting and quantifying aggregation of monoclonal antibody caused by freeze-thawing: Insights into the roles of particles in the protein aggregation pathway. *J Pharm Sci-Us* **2011,** *100* (2), 492–503.
101. Fekete, S. S., Critical evaluation of fast size exclusion chromatographic separations of protein aggregates, applying sub-2 μm particles. *J Pharmaceut Biomed* **2013,** *78-79* 141-149.
102. Muneeruddin, K.; Thomas, J. J.; Salinas, P. A.; Kaltashov, I. A., Characterization of Small Protein Aggregates and Oligomers Using Size Exclusion Chromatography with Online Detection by Native Electrospray Ionization Mass Spectrometry. *Anal Chem* **2014,** *86* (21), 10692-10699.
103. Vladimir Voynov, J. A. C., *Therapeutic Proteins Methods and Protocols*. Methods in Molecular Biology: 2012; Vol. 899.
104. Joyce J. Sung, N. N. P., Anke M. Mulder, Sean K. Mulligan, Joel Quispe, Kathy On, Bridget Carragher, Clinton S. Potter, John F. Carpenter, Anette Schneemann, Transmission Electron Microscopy as an Orthogonal Method to Characterize Protein Aggregates. *Pharmaceutical Nanotechnology* **2014,** *104*, 750-759.
105. Leslie Wilson, P. T., *Correlative Light and Electron MIcroscopy*. Academic Press,Elsevier: 2014; Vol. 124.
106. Daisuke Shindo, T. O., Analytical Electron Microscopy for Materials Science. *Springer Tokyo* **2002**, 152.
107. Egerton, R., Physical Principles of Electron Microscopy An Introduction to TEM SEM and AEM. *Springer* **2008**, 211.
108. Webb, V. L. A. a. W. W., Transmission electron microscopy characterization of fluorescently labelled amyloid b 1-40 and a-synuclein aggregates. *BMC Biotechnology* **2011,** *11*.
109. Cosslett, V. E., Radiation damage in the high resolution electron microscopy of biological materials: a review. *Journal of microscopy* **1978,** *113* (2), 113-29.
110. Zhang, L.; Song, J.; Cavigiolio, G.; Ishida, B. Y.; Zhang, S.; Kane, J. P.; Weisgraber, K. H.; Oda, M. N.; Rye, K. A.; Pownall, H. J.; Ren, G., Morphology and structure of lipoproteins revealed by an optimized negative-staining protocol of electron microscopy. *Journal of lipid research* **2011,** *52* (1), 175-84.
111. Khudyakov, Y. E. P., Paul, Viral nanotechnology. *CRC Press* **2016**.
112. Alberto Bartesaghi, D. M., Soojay Banerjee, Alan Merk, and Sriram Subramaniam, Structure of β-galactosidase at 3.2-Å resolution obtained by cryo-electron microscopy. *Proceedings of the National Academy of Sciences of United States of America* **2014,** *111* (32), 11709-11714.
113. Wendler, P.; Saibil, H. R., Cryo electron microscopy structures of Hsp100 proteins: crowbars in or out? *Biochemistry and cell biology = Biochimie et biologie cellulaire* **2010,** *88* (1), 89-96.

114. Gongpu Zhao, J. R. P., Ernest L. Yufenyuy, Xin Meng, BoChen and Jiying Ning, Mature HIV-1 capsid structure by cryo-electron microscopy and all-atom molecular dynamics. *Nat Methods* **2013**.
115. Kuntsche, J.; Horst, J. C.; Bunjes, H., Cryogenic transmission electron microscopy (cryo-TEM) for studying the morphology of colloidal drug delivery systems. *Int J Pharm* **2011,** *417* (1-2), 120-37.
116. Fox, C. B.; Mulligan, S. K.; Sung, J.; Dowling, Q. M.; Fung, H. W. M.; Vedvick, T. S.; Coler, R. N., Cryogenic transmission electron microscopy of recombinant tuberculosis vaccine antigen with anionic liposomes reveals formation of flattened liposomes. *Int J Nanomed* **2014,** *9*, 1367-1377.
117. Wilson, S. M.; Bacic, A., Preparation of plant cells for transmission electron microscopy to optimize immunogold labeling of carbohydrate and protein epitopes. *Nature protocols* **2012,** *7* (9), 1716-27.
118. R, A., On the Dispersion of a Solute in a Fluid Flowing through a Tube. *The Royal Society* **1956,** *235*, 67-77.
119. G, T., Dispersion of soluble matter in solvent flowing slowly through a tube. *The Royal Society* **1953,** *219*, 186-203.
120. Cipelletti, L.; Biron, J. P.; Martin, M.; Cottet, H., Polydispersity Analysis of Taylor Dispersion Data: The Cumulant Method. *Anal Chem* **2014,** *86* (13), 6471-6478.
121. Hulse, W.; Forbes, R., A Taylor dispersion analysis method for the sizing of therapeutic proteins and their aggregates using nanolitre sample quantities. *Int J Pharmaceut* **2011,** *416* (1), 394-397.
122. Ulrik Franzen, C. V., Henrik Jensen,Jesper Østergaard, Physicochemical characterization of a PEGylated liposomal drug formulation using capillary electrophoresis. *Electrophoresis* **2011,** *32*, 738–748.
123. Cottet, H.; Biron, J. P.; Cipelletti, L.; Matmour, R.; Martin, M., Determination of individual diffusion coefficients in evolving binary mixtures by taylor dispersion analysis: application to the monitoring of polymer reaction. *Anal Chem* **2010,** *82* (5), 1793-802.
124. Hulse, W. L.; Forbes, R. T., A nanolitre method to determine the hydrodynamic radius of proteins and small molecules by Taylor dispersion analysis. *Int J Pharmaceut* **2011,** *411* (1-2), 64-68.
125. Wim Th. Kok, A. J. T., Mark Grutters, Andrew G. Shepherd, Characterization of Asphaltenes by Nonaqueous Capillary Electrophoresis. *Energy Fuels* **2011**

25 (1).
126. Lewandrowska, A.; Majcher, A.; Ochab-Marcinek, A.; Tabaka, M.; Holyst, R., Taylor Dispersion Analysis in Coiled Capillaries at High Flow Rates. *Anal Chem* **2013,** *85* (8), 4051-4056.
127. Ibrahim, A.; Meyrueix, R.; Pouliquen, G.; Chan, Y. P.; Cottet, H., Size and charge characterization of polymeric drug delivery systems by Taylor dispersion analysis and capillary electrophoresis. *Anal Bioanal Chem* **2013,** *405* (16), 5369-5379.
128. Ye, F. B.; Jensen, H.; Larsen, S. W.; Yaghmur, A.; Larsen, C.; Ostergaard, J., Measurement of drug diffusivities in pharmaceutical solvents using Taylor dispersion analysis. *J Pharmaceut Biomed* **2012,** *61*, 176-183.
129. Hulse, W. L.; Gray, J.; Forbes, R. T., Evaluating the inter and intra batch variability of protein aggregation behaviour using Taylor dispersion analysis and dynamic light scattering. *Int J Pharmaceut* **2013,** *453* (2), 351-357.

130. Jensen, S. S.; Jensen, H.; Cornett, C.; Moller, E. H.; Ostergaard, J., Insulin diffusion and self-association characterized by real-time UV imaging and Taylor dispersion analysis. *J Pharmaceut Biomed* **2014,** *92*, 203-210.
131. Liechty, W. B.; Kryscio, D. R.; Slaughter, B. V.; Peppas, N. A., Polymers for drug delivery systems. *Annual review of chemical and biomolecular engineering* **2010,** *1*, 149-73.
132. Oukacine, F.; Bernard, S.; Bobe, I.; Cottet, H., Physico-chemical characterization of polymeric micelles loaded with platinum derivatives by capillary electrophoresis and related methods. *Journal of controlled release : official journal of the Controlled Release Society* **2014,** *196*, 139-45.
133. Lavoisier, A.; Schlaeppi, J. M., Early developability screen of therapeutic antibody candidates using Taylor dispersion analysis and UV area imaging detection. *mAbs* **2015,** *7* (1), 77-83.
134. Luca Cipelletti, J.-P. B., Michel Martin, and Hervé Cottet, Measuring Arbitrary Diffusion Coefficient Distributions of Nano-Objects by Taylor Dispersion Analysis. *Anal. Chem* **2015,** *87* (16), 8489–8496.
135. Chamieh, J.; Jannin, V.; Demarne, F.; Cottet, H., Hydrodynamic size characterization of a self-emulsifying lipid pharmaceutical excipient by Taylor dispersion analysis with fluorescent detection. *Int J Pharm* **2016,** *513* (1-2), 262-269.
136. Pyell, U.; Jalil, A. H.; Pfeiffer, C.; Pelaz, B.; Parak, W. J., Characterization of gold nanoparticles with different hydrophilic coatings via capillary electrophoresis and Taylor dispersion analysis. Part I: determination of the zeta potential employing a modified analytic approximation. *J Colloid Interface Sci* **2015,** *450*, 288-300.
137. Laurent Leclercq, S. R., Joseph Chamieh, Markus Döblinger, Ernst Wagner, and Hervé Cottet, Fast Characterization of Polyplexes by Taylor Dispersion Analysis. *Macromolecules* **2015,** *48* (19), 7216-7221.
138. Hawe, A.; Hulse, W. L.; Jiskoot, W.; Forbes, R. T., Taylor Dispersion Analysis Compared to Dynamic Light Scattering for the Size Analysis of Therapeutic Peptides and Proteins and Their Aggregates. *Pharm Res-Dordr* **2011,** *28* (9), 2302-2310.
139. Cottet, H.; Martin, M.; Papillaud, A.; Souaid, E.; Collet, H.; Commeyras, A., Determination of dendrigraft poly-L-lysine diffusion coefficients by taylor dispersion analysis. *Biomacromolecules* **2007,** *8* (10), 3235-43.
140. Alizadeh, A.; Nieto de Castro, C. A.; Wakeham, W. A., The theory of the Taylor dispersion technique for liquid diffusivity measurements. *International Journal of Thermophysics* **1980,** *1* (3), 243-284.
141. Koppel, D. E., Analysis of Macromolecular Polydispersity in Intensity Correlation Spectroscopy: The Method of Cumulants. *J. Chem. Phys* **1972,** *57*, 4814−4820.
142. Acheson, D. J., *Elementary Fluid Dynamics (Oxford Applied Mathematics and Computing Science Series)*. Oxford University Press: Oxford, UK, 1990.
143. Cussler, E. L., *Diffusion: Mass Transfer in Fluid Systems*. Oxford University Press: Oxford, UK, 2009.
144. Hasan, A., *Understanding Mechanical Ventilation: A Practical Handbook*. Springer-Verlag: London, 2010.
145. Cottet, H.; Biron, J. P.; Martin, M., Taylor dispersion analysis of mixtures. *Anal Chem* **2007,** *79* (23), 9066-73.
146. Wei Wang, C. J. R., *Aggregation of Therapeutic Proteins*. 2010.

147. Pecora, R., *Dynamic Light Scattering: Applications of Photon Correlation Spectroscopy*. Springer US: 1985.
148. Eiser, E., *Dynamic Light Scattering, in Multi Length-Scale Characterisation*. John Wiley & Sons, Ltd, Chichester, UK.: 2014.
149. Stellwagen, N. C.; Magnusdottir, S.; Gelfi, C.; Righetti, P. G., Measuring the translational diffusion coefficients of small DNA molecules by capillary electrophoresis. *Biopolymers* **2001,** *58* (4), 390-7.
150. Teraoka, I., *Polymer Solutions: An Introduction to Physical Properties*. John Wiley & Sons: 2002.
151. Hulse, W. L.; Forbes, R. T., A nanolitre method to determine the hydrodynamic radius of proteins and small molecules by Taylor dispersion analysis. *Int J Pharm* **2011,** *411* (1-2), 64-8.
152. Zuo, M.; Chen, Y., Fast determination of protein diffusion coefficient by Taylor dispersion analysis and capillary electrophoresis system. *Chem J Chinese U* **2007,** *28* (10), 1875-1877.
153. Chamieh, J.; Cottet, H., Comparison of single and double detection points Taylor Dispersion Analysis for monodisperse and polydisperse samples. *J Chromatogr A* **2012,** *1241*, 123-127.
154. Cottet, H.; Biron, J. P.; Martin, M., Taylor dispersion analysis of mixtures. *Anal Chem* **2007,** *79* (23), 9066-9073.
155. Luca Cipelletti, J.-P. B., Michel Martin, and Hervé Cottet, Measuring arbitrary diffusion coefficient distributions of nano-objects by Taylor dispersion analysis. *Anal Chem* **2015,** *87* (16), 8489-8496.
156. Cipelletti, L.; Biron, J. P.; Martin, M.; Cottet, H., Polydispersity analysis of Taylor dispersion data: the cumulant method. *Anal Chem* **2014,** *86* (13), 6471-8.
157. Chamieh, J.; Biron, J. P.; Cipelletti, L.; Cottet, H., Monitoring Biopolymer Degradation by Taylor Dispersion Analysis. *Biomacromolecules* **2015,** *16* (12), 3945-51.
158. Cottet, H.; Martin, M.; Papillaud, A.; Souaid, E.; Collet, H.; Commeyras, A., Determination of dendrigraft poly-L-lysine diffusion coefficients by taylor dispersion analysis. *Biomacromolecules* **2007,** *8* (10), 3235-3243.
159. Taylor dispersion. http://ocw.mit.edu (accessed April 29).
160. L, C. E., *Mass transfer in fluid systems: Diffusion*. Cambridge University Press: New York, 2009.
161. Kirby, B. J., *Micro- and nanoscale fluid mechanics : transport in microfluidic devices*. Cambridge University Press: New York, 2010; p xxiii, 512 p.
162. Smith W F, H. J., *Foundations of Materials Science and Engineering*. 4 ed.; McGraw-Hill Higher Education: Boston, 2006.
163. Sirkar, K. K., *Separation of Molecules, Macromolecules and Particles: Principles, Phenomena and Processes*. Cambridge University Press: New York, 2014.
164. Giovannoli C, A. L., Tozzi C, Giraudi G, Vanni A., DNA separation by capillary electrophoresis with hydrophilic substituted celluloses as coating and sieving polymers. Application to the analysis of genetically modified meals. *Journal of separation science* **2004,** *27* (17-18), 1551-1556.
165. Vitha, M. F., *Chromatography: principles and instrumentation*. John Wiley & Sons: Hoboken, New Jersey, 2016.
166. Taylor, G., Conditions under Which Dispersion of a Solute in a Stream of Solvent can be Used to Measure Molecular Diffusion. *Proc. R. Soc* **1954,** *225*, 473-477.

167. Gao, J.; Gomez, F. A.; Harter, R.; Whitesides, G. M., Determination of the effective charge of a protein in solution by capillary electrophoresis. *Proc Natl Acad Sci U S A* **1994,** *91* (25), 12027-30.
168. Menon, M. K.; Zyndey, A. L., Measurement of protein charge and ion binding using capillary electrophoresis. *Anal Chem* **1998,** *70* (8), 1581–1584.
169. Frazier, R. A. J., M. A. Harry E.N., *Capillary Electrophoresis for Food Analysis: Method Development*. Royal Society of Chemistry: Cambridge, 2000.
170. Volpi, N.; Maccari, F., *Capillary Electrophoresis of Biomolecules: Methods and Protocols*. Humana Press: New York, 2013; Vol. 984, p 358.
171. Rundlett, K. L.; Armstrong, D. W., Methods for the determination of binding constants by capillary electrophoresis. *Electrophoresis* **2001,** *22* (7), 1419-1427.
172. d'Orlye, F.; Varenne, A.; Gareil, P., Determination of nanoparticle diffusion coefficients by Taylor dispersion analysis using a capillary electrophoresis instrument. *J Chromatogr A* **2008,** *1204* (2), 226-232.
173. Yao, Y. J.; Li, S. F. Y., Determination of Diffusion-Coefficients by Capillary Zone Electrophoresis. *J Chromatogr Sci* **1994,** *32* (4), 117-120.
174. Zhang, H. Y.; Song, X. R.; Shi, Z. H.; Yang, G. L.; Hu, Z. D., Capillary zone electrophoresis for the determination of average hydrodynamic velocity and diffusion coefficient. *Fresen J Anal Chem* **1999,** *365* (6), 499-503.
175. Zuo, M.; Han, Y. L.; Qi, L.; Chen, Y., Fast and accurate measurement of diffusion coefficient by Taylor's dispersion analysis. *Chinese Sci Bull* **2007,** *52* (24), 3325-3332.
176. Khodabandehloo, A.; Chen, D. D. Y., Particle sizing methods for the detection of protein aggregates in biopharmaceuticals. *Bioanalysis* **2017,** *9* (3), 313-326.
177. Grushka. E, M. R. M., Zone broadening due to sample injection in capillary zone electrophoresis. *Journal of chromatography* **1989,** *471*, 421-428.
178. Peng. X, C. D., Variance contributed by pressure induced injection in capillary electrophoresis. *J Chromatogr A* **1997,** *767* (1-2), 205-216.
179. Cordova, E. G., JM; Whitesides, GM, Noncovalent polycationic coatings for capillaries in capillary electrophoresis of proteins. *Anal Chem* **1997,** *69* (7), 1370-1379.
180. Bekri, S.; Leclercq, L.; Cottet, H., Polyelectrolyte multilayer coatings for the separation of proteins by capillary electrophoresis: Influence of polyelectrolyte nature and multilayer crosslinking. *J Chromatogr A* **2015,** *1399*, 80-7.
181. Xuan. X, L. D., Joule heating effects on peak broadening in capillary zone electrophoresis. *Journal of Micromechanics and Microengineering* **2004,** *14* (8), 1171-1180.
182. Ghosal, S., Fluid mechanics of electroosmotic flow and its effect on band broadening in capillary electrophoresis. *Electrophoresis* **2004,** *25* (2), 214-28.
183. Ghosal, S., Electrokinetic flow and dispersion in capillary electrophoresis. *Annu Rev Fluid Mech* **2006,** *38*, 309-338.
184. Hayes, M. A.; Kheterpal, I.; Ewing, A. G., Effects of buffer pH on electroosmotic flow control by an applied radial voltage for capillary zone electrophoresis. *Analytical Chemistry* **1993,** *65* (1), 27-31.
185. Ratnayake, C. K.; Flores, I. C. Coated capillary electrophoresis tubes and system. 2005.
186. Berne, B. J., *Dynamic light scattering : with applications to chemistry, biology, and physics / Bruce J. Berne and Robert Pecora.* . New York : Wiley: 1976.
187. Jiskoot, W.; Crommelin, D. J., *Methods for Structural Analysis of Protein Pharmaceuticals*. AAPS: Arlington, 2005.

188. Haung, X., Analysis of factors causing peak broadening in capillary zone electrophoresis. *Journal of Chromatography* **1989,** *480,* 95-110.
189. Zholkovskij, E. K.; Masliyah, J. H.; Czarnecki, J., Electroosmotic dispersion in microchannels with a thin double layer. *Anal Chem* **2003,** *75* (4), 901-909.
190. Griffiths, S. K.; Nilson, R. H., Electroosmotic fluid motion and late-time solute transport for large zeta potentials. *Anal Chem* **2000,** *72* (20), 4767-4777.
191. Crow, D. R., *Principles and applications of electrochemistry* fourth ed.; Blackie Academic & Professional,: London, 1994.

Appendices

Appendix A: Effect of capillary diameter on velocity profile

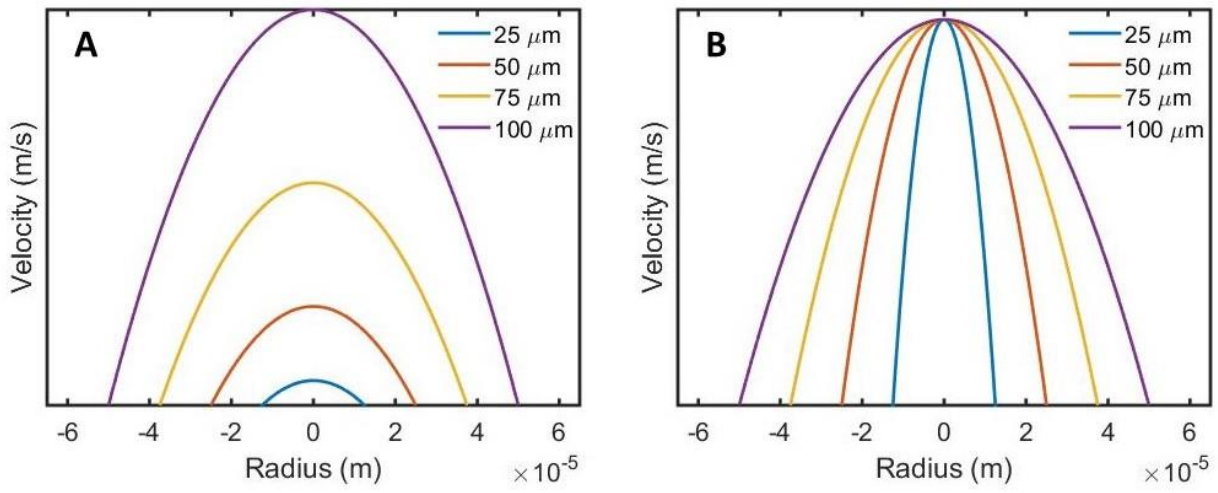

Figure A.1: Effect of capillary diameter on velocity profile at (A) p=80 Pa (B) v=7.8E-4 m/s

In chapter 3, three diameters are chosen for the capillary column: 25, 50, 100 μm. As mentioned in this chapter velocity and pressure are interchangeable if capillary radius and viscosity is constant. In Figure A.1 (A) pressure is kept constant and the velocity profile is plotted for capillaries with different diameters. Comparing to Figure A.1 (B) where maximum velocity is kept constant Figure A.1 (A) shows that the maximum velocity is dependent on the capillary diameter when pressure is constant.

Appendix B: Electropherogram of molecules with different sizes at different voltages

In chapter 6, molecules are run at different voltages. Figure B.1 shows the electropherogram for all voltages for the protein and peptides used in this study.

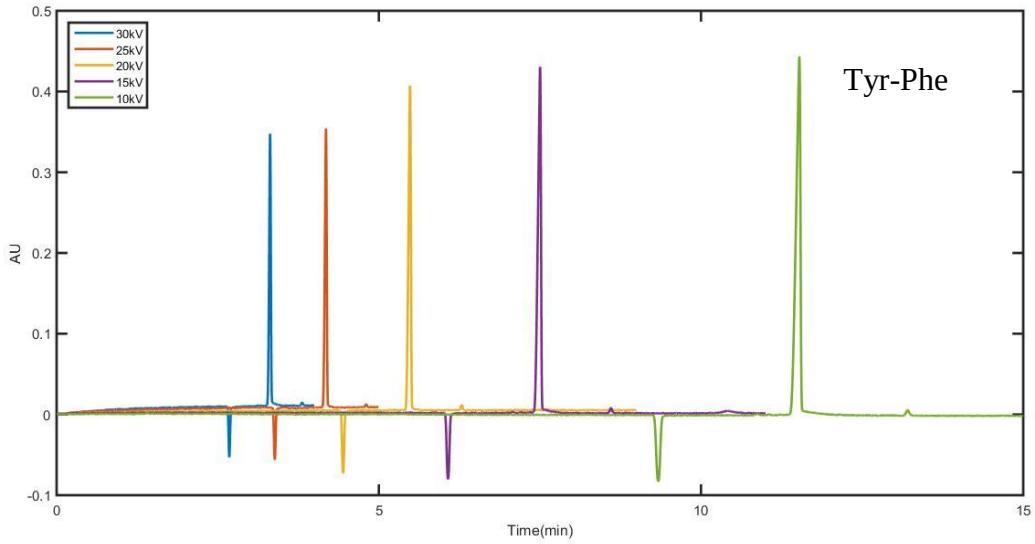

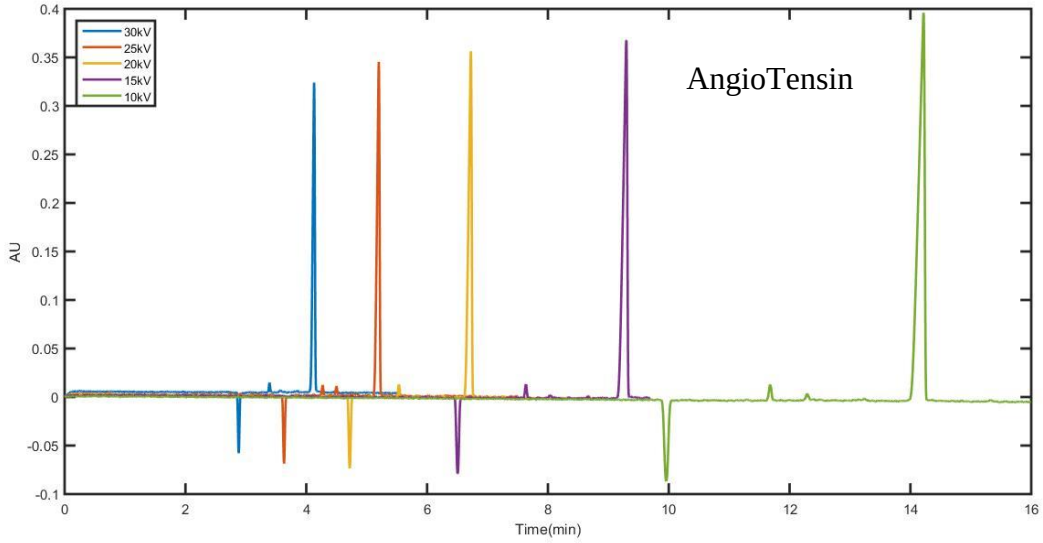

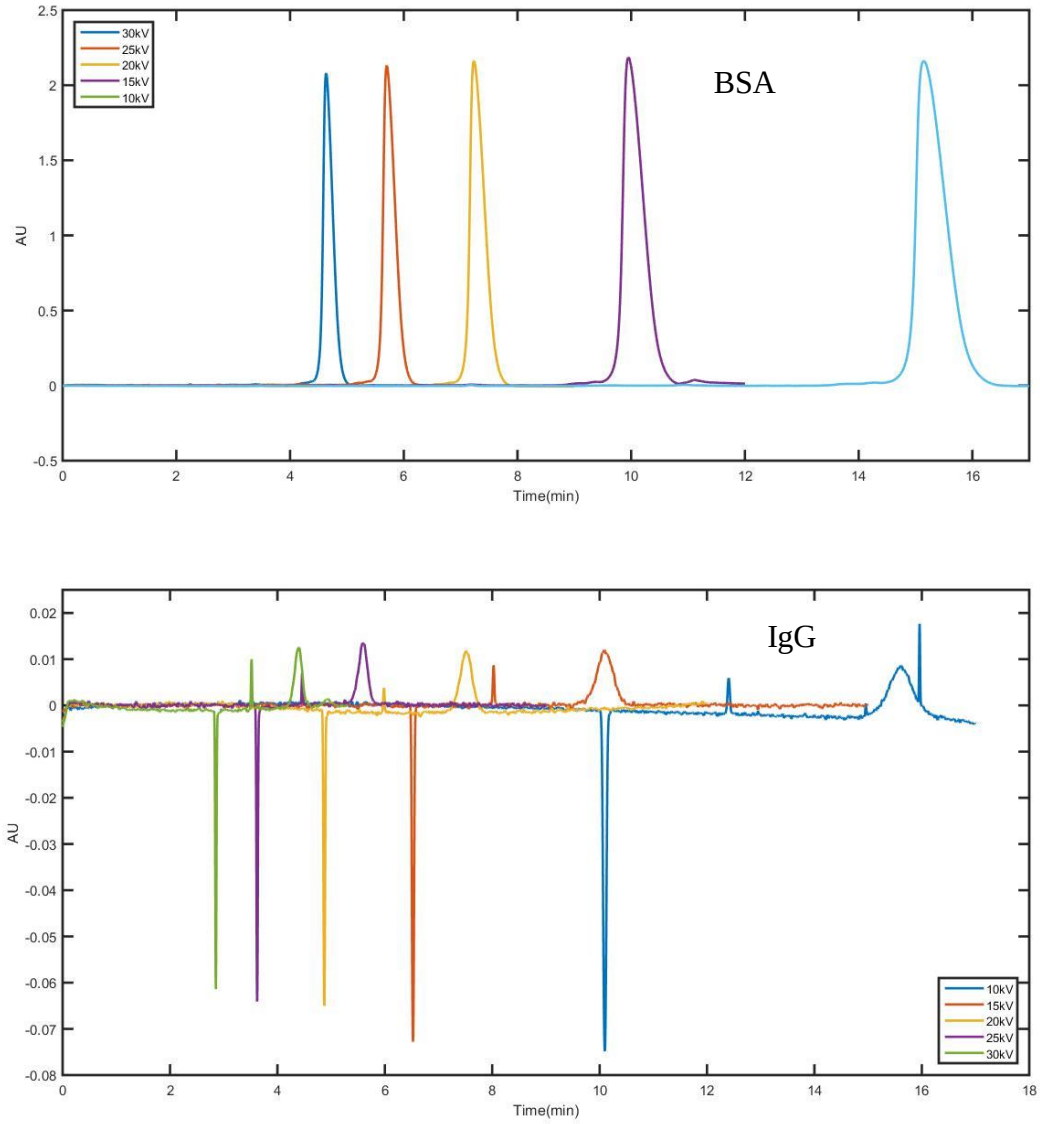

Figure B.1: Electropherogram for Tyr-Phe, AngioTensin, BSA and IgG at different voltages.

Figure B.2 shows the current intensity versus the voltage. As it is shown in the plot, there is no deviation from linearity which is indicative of no joule heating. This eliminates the possibility of band broadening due to joule heating in chapter 6.

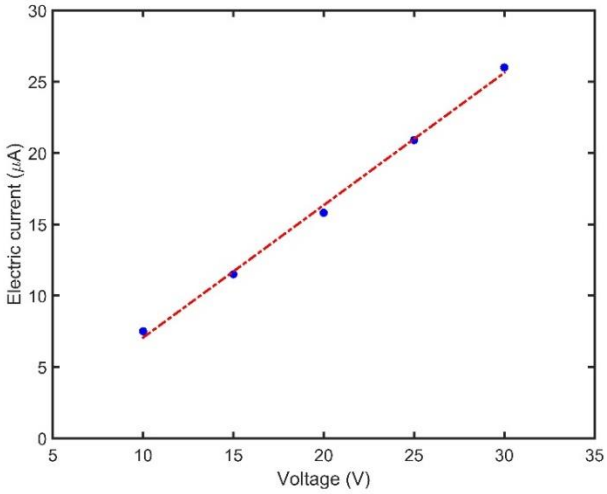

Figure B.2: Electric current through buffer solution at different voltages.

Appendix C: Calculation of zeta potential

In chapter 6 the zeta potential in reported to be 1 V. The below calculations show how this value is calculated.

Calculation of zeta potential:

pKa (Phenol)= 9.8

Phenol is neutral in acidic pH, therefore we used it as EOF marker. We use Helmholtz-Smoluchowski Equation to calculate zeta potential (ζ)

$$\mu_{eo} = \frac{v_{eo}}{E} = \frac{\varepsilon\zeta}{4\pi\eta}$$

$$v_{eo} = \frac{L_{eff}}{t} = \frac{0.5\text{m}}{3.35 * 60\text{ s}} = 2.49 \times 10^{-3}\text{m/s}$$

$$E = \frac{V}{L_{tot}} = \frac{20000\text{ volt}}{0.6\text{ m}} = 3.33 \times 10^{4}\text{ volt/m}$$

$$\mu_{eo} = \frac{v_{eo}}{E} = \frac{2.49 \times 10^{-3}\text{ m/s}}{3.33 \times 10^{4}\text{ V/m}} = 7.47 \times 10^{-8}\text{ m2/V.s}$$

$$\varepsilon = 80 * 8.85 \times 10^{-12}\frac{F}{m}$$

η (25°C) =0.89×10^{-3} Pa. s

$$\mu_{eo} = \frac{\varepsilon\zeta}{4\pi\eta} \rightarrow \quad 7.47 \times 10^{-8} = \frac{80*8.85\times10^{-12}\times\zeta}{4\times3.14\times1.0\times10^{-3}}$$

$$\zeta = \frac{7.47\times10^{-8}\times4\times3.14\times0.89\times10^{-3}}{80*8.85\times10^{-12}} = 1.1\text{ Volt}$$

Appendix D: Gaussian fitting of electropherogram

Figure D.1 shows how the electropherograms where fitted with Gaussian function and the resulting migration time and temporal variance of the peak. BSA used as an example.

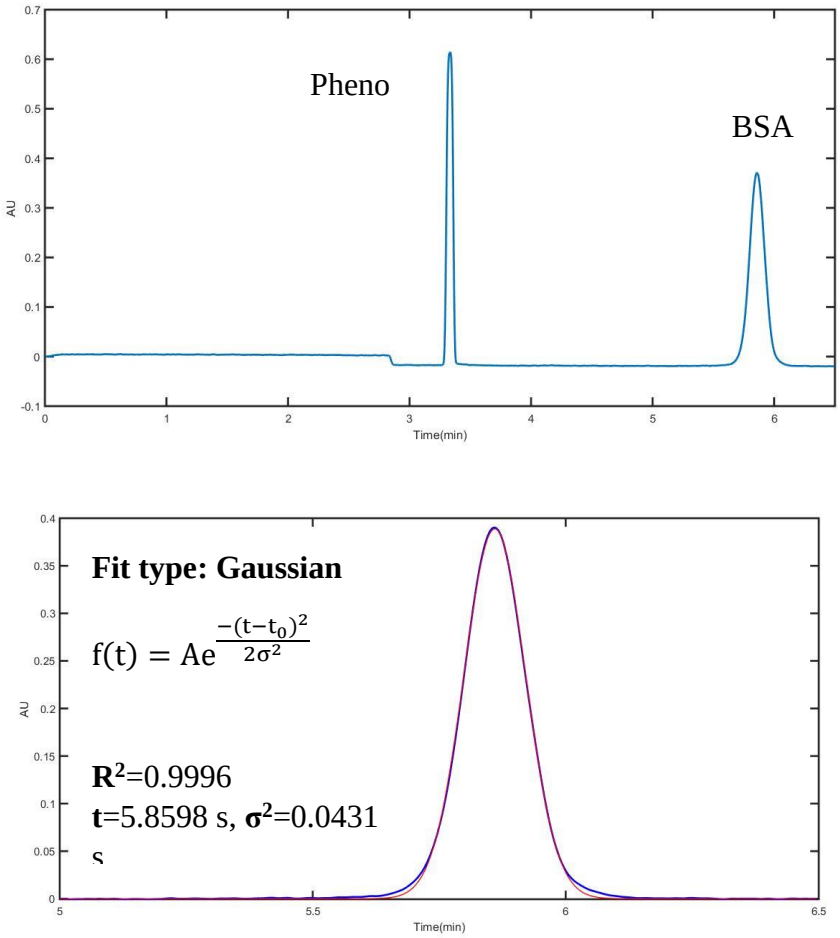

Figure D.1: Electropherogram and data fitting for BSA at 20 kV.